NASA CR-

TECHNICAL REPORT

INVESTIGATION OF THE FRACTURE MECHANICS OF BORIDE COMPOSITES

by

Larry Kaufman, Edward V. Clougherty and Harvey Nesor

MANLABS, INC.

21 Erie Street
Cambridge, Massachusetts 02139

prepared for

NATIONAL AERONAUTICS AND SPACE ADMINISTRATION

July 1971

Contract NASW-2088

NASA Headquarters
Washington, D. C. 20546
James Gangler, Project Manager

NASA CR-

TECHNICAL REPORT

INVESTIGATION OF THE FRACTURE MECHANICS OF BORIDE COMPOSITES

by

Larry Kaufman, Edward V. Clougherty and Harvey Nesor

MANLABS, INC.

21 Erie Street
Cambridge, Massachusetts 02139

prepared for

NATIONAL AERONAUTICS AND SPACE ADMINISTRATION

July 1971

Contract NASW-2088

NASA Headquarters
Washington, D.C. 20546
James Gangler, Project Manager

1.a

FOREWORD

The research described in this report, was conducted by ManLabs, Inc. under NASA Contract NASW-2088. The work was done under the cognizance of the NASA Project Manager, Mr. James Gangler NASA Headquarters, Washington, D.C. 20548, with Drs. Larry Kaufman and Edward V. Clougherty of ManLabs, Inc. serving as Principal Investigators. ManLabs personel who participated in this study included, H. Nesor, L. Gordon, K. Meaney, J. Davis and H. Tushman.

ABSTRACT

Hot pressed zirconium diboride-silicon carbide-graphite composites have demonstrated outstanding characteristics as potential thermal protection components for future lifting reentry applications at temperatures up to 5000°F. Current utilization is limited by a lack of resistance to fracture. Fracture energies of WC-6Co, Boride V (ZrB_2+SiC), Boride VIII (ZrB_2+SiC+C) and Boride VIII-M2 (ZrB_2+SiC+C) were measured by slow bend and impact tests of standard and subscale notched charpy bars. Cobalt bonded tungsten carbide exhibited impact energies of 0.76 ft-lb for standard size notched charpy bars, equivilent to an impact energy per unit area of 73.9 in-lb/in^2 (12950 J/M^2). Boride V and the Boride VIII composites exhibited impact energies which are one third and one quarter respectively of that observed for WC-6Co. These values compare favorably with impact fracture energies measured for SiC and Si_3N_4. Slow bend-notched bar-fracture energies for WC-6Co were near 2.6 in-lb/in^2 (455 J/M^2) or about one twentieth of the impact fracture energies. Slow bend fracture energies for Boride VIII-M2, Boride VIII and Boride V were found to be 58%, 42% and 25% of the value observed for WC-6Co. Fractographic characterization showed distinct differences for the WC-6Co case where slow bend testing resulted in smooth transgranular cleavage while samples broken by impact exhibited intergranular failures. By contrast the boride fractures showed no distinction based on testing method. Fabrication studies were conducted to effect alteration of the boride composites by alloying and introduction of graphite cloth. Graphite cloth has been successfully incorporated in Boride V, however no significant improvement in fracture energy resulted. Addition of nickel to Boride V was unsuccessful due to reaction of nickel with the silicon carbide component of Boride V. However nickel and iron were added successfully to ZrB_2 and hot pressed near 2400°F. This represents a substantial reduction in temperature (1200-1400°F) from the 3600-3800°F normally employed.

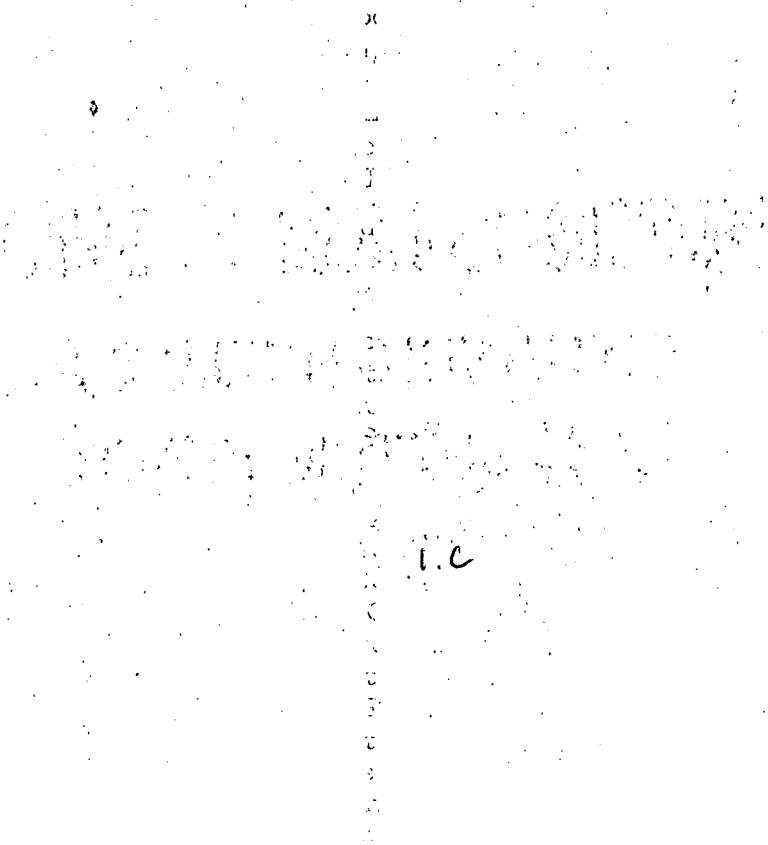

TABLE OF CONTENTS

LIST OF TABLES

LIST OF TABLES (con't)

LIST OF ILLUSTRATIONS

LIST OF ILLUSTRATIONS (Cont)

LIST OF ILLUSTRATIONS (Cont)

LIST OF ILLUSTRATIONS (Cont)

I. SUMMARY OF RESULTS

High temperature oxidation studies and arc plasma reentry simulation tests of hot pressed zirconium diboride-silicon carbide-graphite composites have demonstrated the outstanding characteristics of these materials as potential thermal protection components for long time multi-cycle applications at temperatures up to 5000°F. The relatively high thermal conductivity and strength properties of these composites coupled with their machining characteristics afford additional justification for considering them for future lifting reentry applications. Current utilization of these materials is limited by a lack of resistance to fracture. The present report details the first phase of a study aimed at alleviating the problem by measuring the fracture energy of boride composites and seeking to improve the fracture energy through alloying, compositing and control of structure.

The fracture energies of Boride V (ZrB_2+SiC), Boride VIII (ZrB_2+SiC+C) and Boride VIII-M2 (ZrB_2+SiC+C) were measured by means of slow bend and impact tests of standard and subscale notched charpy bars. Similar measurements were conducted on WC-6Co, a commerically available tool material based on cobalt bonded tungsten carbide. The latter (included to provide a direct basis for comparison exhibited impact energies of 0.76 ft-lb for standard size notched charpy bars. This value is equivilent to an impact energy per unit area of 73.9 in-lb/in^2(12950 J/M^2). By contrast Boride V and the Boride VIII composites exhibited impact energies which are one third and one quarter respectively of that observed for WC-6Co. These values compare favorably with impact fracture energies measured for SiC and Si_3N_4.

Measurement of the fracture energy per unit area for WC-6Co in slow bend tests of notched charpy bars yielded values near 2.6 in-lb/in^2 (455 J/M^2) or about one twentieth of the impact fracture energies. This result is quite surprising since evaluation of ultra high strength steels and titanium alloys usually yields a close correspondence between the slow bend and impact energy values for plane strain fracture in precracked notched bars. Although the precracking technique cannot readily be applied in the present case, differences exceeding a factor of two are quite uncommon. The divergence is all the more difficult to reconcile because plastic or yielding behavior does not occur at room temperature. Similar slow bend fracture energies for Boride VIII-M2, Boride VIII and Boride V were found to be 58%, 42% and 25% of the value observed for WC-6Co. Microstructural and fractographic characterization of the slow bend and impact samples showed distinct differences for the WC-6Co case where slow bend testing resulted in smooth transgranular cleavage while samples broken by impact exhibited intergranular failures. By contrast the boride fractures showed no distinction

based on testing method. However, the Boride V composite (ZrB_2+SiC) exhibited smooth transgranular cleavage in both tests while Boride VIII and VIII-M2 containing graphite as a further addition, was characterized by faceted quasi cleavage surfaces as the result of slow bend and impact testing.

Notwithstanding substantial difference between the impact and slow bend results for WC-6Co and the boride composites, the higher fracture energies exhibited by the former are due to the presence of the cobalt binder phase and the grain size which is 5-10 times smaller than exhibited by the boride composites. Accordingly, fabrication studies were conducted to effect alteration of the boride composites by alloying and introduction of graphite cloth. Graphite cloth has been successfully incorporated in Boride V, however no significant improvement in fracture energy resulted. Addition of nickel to Boride V was unsuccessful due to reaction of nickel with the silicon carbide component of Boride V. However nickel and iron were added successfully to ZrB_2 and hot pressed near 2400°F. This represents a substantial reduction in temperature (1200-1400°F) from the 3600-3800°F normally employed. However, improvement in fracture energy did not result. Initial attempts at adding chromium powder and tantalum wire have been unsuccessful.

II INTRODUCTION

In 1962 ManLabs, Inc. initiated an "Investigation of Borides for High Temperature Applications" under AF33(657)-8635 which identified specific boride composites with outstanding physical and oxidation resistant properties for long-time applications at temperatures above 3500°F. A follow-on program under AF33(615)-3671 devoted to "Development of Refractory Oxidation-Resistant Diborides" has led to a new family of materials with unmatched characteristics of oxidation resistance, strength and thermal shock resistance at temperatures between 3000° and 5000°F. A parallel was initiated in 1966 for "Stability Characterization of Refractory Materials under High Velocity Atmospheric Flight Conditions" under AF33(615)-3859. This study evaluated borides, graphites, carbides, boride-carbide graphite composites, coated refractory metals and alloys, coated graphites and oxide metal composites under conditions simulating long time (up to 25,000 seconds) multi mission conditions characteristic of lifting reentry. Documentation of the results is available in Air Force Material Laboratory reports and related publications (1-18).* The "Stability" program demonstrated the unique advantages of boride composites for long exposure, multi-mission applications under lifting reentry conditions. These results show that the boride composites are outstanding candidates for survival times in the 50,000-150,000 second range at surface temperature between 3000° and 5000°F.

This conclusion can be illustrated by considering Figure 1 which shows the Air Force Flight Dynamic Laboratory FDL-7MC maximum cross range trajectory. This trajectory is typical of high lift/drag ratio lifting reentry vehicles which will be important for future space flight concepts. The central panel shows that the conditions at 600 seconds and 1800 seconds into the flight produce the most severe heating environments. These conditions have been converted to pressure, enthalpy and heat flux based on a three inch body radius. Subsequently, boride composites were exposed to arc plasma tests in air under conditions simulating those shown in Figure 1.**

Sample Boride V (Hf) $HfB_{2.1}$+20%SiC was exposed for thirteen cycles at 0.07 atm (1 psi) stagnation pressure, a stagnation enthalpy of 10,200 BTU/lb (2.39×10^7 J/kg) and a cold wall flux of 495 BTU/ft^2 sec. (5.62×10^6 J/M^{2}sec) Each cycle was about 1800 seconds long with a total exposure time of 22,500 seconds. The surface temperature was observed to be 4650°F. Total material recession was 16 mils (3.81×10^{-4}M) after this extremely long exposure. Figure 2 shows a post exposure section through the sample. Boride VIII(14,30)ZrB_2+SiC+C was exposed at 1.02 atm (15 psi) stagnation pressure, a stagnation enthalpy of 4250 BTU/lb

---

*Underscored numbers in parentheses denote references.

**In view of the current NASA policy of introducing MKS units, the present report employs dual values reflecting English units (BTU, lb (force), ft) which have been commonly employed, up to now, as well MKS units (Joule, Newton, Meter). Table 1 contains the conversion units employed in this report.

(0.99×10^7 J/kg) and a cold wall heat flux of 400 BTU/ft^{2}sec (4.54×10^6 J/M^{2}sec). This test covered twelve cycles of approximately 1800 seconds duration for a total exposure time of 21,600 seconds. Surface temperature held near 4415°F. Figure 3 shows that the recession was 104 mils (2.64×10^{-3}M). Under similar conditions graphite and tungsten would exhibit recessions of 20 to 40 inches. Finally sample Boride V$ZrB_{2.1}$+20% SiC was exposed for four cycles at 1.0 atm (15 psi) stagnation pressure, a stagnation enthalpy of 5000 BTU/lb and a cold wall heat flux of 380 BTU/ft^{2}sec. Each cycle was 1800 seconds long, total exposure time was 7200 seconds. The surface temperatures were near 4550°F. Total material recession was 26 mils. Figure 4 and 5 are post exposure photomicrographs of this sample.

These results illustrate the reuse capability of boride composites for lifting reentry application, since they exceed the range of conditions and flight times characteristic of the FDL-7MC trajectory. This capability is unrivaled by any other materials system.

Relevent physical and mechanical property data for ZrB_2+SiC and ZrB_2+SiC+C are shown in Table 2. Although the hafnium base analogues of these composites are more refractory, the zirconium base composites are one half as dense with raw material costs per per pound which are one tenth of their hafnium base counterparts. Specific grades of the Boride VIII(14,30) material are machineable with carbide tools and have been employed to fabricate nuts and bolts as shown in Figure 6.

A direct illustration of the flexability for designing and fabricating structures which is afforded by the machineability of the Boride VIII(14,30) composites is shown in Figures 7-16 (18). Figures 7 and 8 show a boride male nosetip assembly composed of boride nosetip (on the right) which is connected to a Ta-10W holder coated with Sylvania's R512C (70^w/oSi-20/^{w}/oTi-10^w/oMo) coating connected to a Ta-10W sting (on the left). The sting is held in the arc facility so that the hot air stream impinges on the axis of the boride hemisphere-cone. As indicated in Figure 7, this assembly was exposed at a high heat flux level for 30 minutes in air in a test where the surface temperature was 4555°F with a limited recession. Figure 9 shows post exposure photographs including a destruction of Nosetip HP69 by melting and a successful run of male nosetip HP62 at lower flux levels. Figures 10 and 11 show photographs of a female nosetip which was successfully tested at 4920°F with limited recession.

Arc tests consisting of multiple exposures simulating normal lifting reentry and abort conditions have been performed as illustrated in Figures 12-14. In these tests a male nosetip assembly ran for more than one and one half hours with little recession. Finally, Figures 14-16 shows a leading edge configuration consisting of a Boride composite attached to a coated Ta-10W holder which was successfully tested. Leading Edge HP61 ran to destruction due to melting as shown in Figure 16. Although melting occured no cracking was noted. Leading Edge HP72 survived an 1800 second exposured with a surface temperature of 5090°F with a total oxidation depth of 46 mils as shown in Figure 16.

The boride composites are currently formed by conventional hot pressing-methods with state-of-the-art size limitations in the one half to one foot range. Billets which are ten inches long and four inches by four inches in cross-section (0.254Mx0.102M x 0.102M) are currently being fabricated for a six foot nosetip-leading edge HATS structure (19). However, since the hot pressing technology required to form these composites is identical to that employed in fabricating boron carbide armor and helicopter seats (contoured sizes up to two feet across) present size limitations should be readily overcome.

Measurements of internal temperatures in models exposed in arc plasma tests indicate that significant temperature gradients can be developed across thin oxide scales formed on the surface of metals or intermetallic compounds during oxidation. The gradient results from the formation of an insulating oxide scale on the surface. Temperature gradients up to 1500°F have been measured through 400 mil walls composed of oxide and base material at temperatures between 3000° and 5000°F. Such gradients were found to persist for long time (30 minutes) during oxidation of samples in arc plasma tests.

In spite of the outstanding high temperature strength and resistance to thermal stress and oxidation exhibited by boride composites which have been developed by ManLabs, Inc., utilization is limited by low fracture toughness at room temperature. Several grades of these composites which are based on zirconium diboride with additions of silicon carbide and graphite have been developed in order to optimize high temperature performance and machinability. Elimination of the shortcoming due to low fracture toughness would constitute an important step in expanding the range of applications in which this material can be used.

In order to progress toward elimation of this shortcoming, the current program has been directed toward establishing the fracture characteristics of the present Boride composites and investigation of methods for improvement of the fracture toughness. The present report, which covers the first year of this study, details the results of fabrication, mechanical testing and microstructural investigations.

III FABRICATION AND CHARACTERIZATION OF BORIDE COMPOSITES

A. Introduction

Boride composites based on combinations of ZrB_2, SiC and C have been fabricated by hot pressing to provide the stock used for obtaining suitable mechanical test bars. The basic compositions investigated to date include Boride V ($80^v/oZrB_2$: $20^v/oSiC$) and Boride VIII ($56^v/oZrB_2$: $14^v/oSiC$: $30^v/oC$) as well as several variations reflecting metallic additions. In addition cobalt bonded tungsten carbide was evaluated as a reference material. The latter was procured as tool stock. Table 3 presents the systematic labeling system (10) used at ManLabs to designate billets of hot pressed boride composites.

B. Processing Conditions Employed for Billet Fabrication

The processing conditions employed for billet fabrication are shown in Tables 4 and 5. Most of the billets were hot pressed in ManLabs facility although some composites were hot pressed in the larger sizes in Avco and Norton hot press facilities. More than thirty hot pressings were performed to obtain sufficient materials for testing.

1. Boride V

Boride V is a dense polycrystalline composition of ZrB_2, the principal phase, with $20^v/oSiC$, the secondary phase. This composition is characterized by high modulus ($E = 75 \times 10^6$ psi, $5.1 \times 10^{11} N/M^2$) high strength ($\sigma = 55{,}000$ psi, $3.7 \times 10^8 N/M^2$) and good thermal stress resistance (10). Representative microstructural features are provided in Figure 17.

2. Ni Modified Boride V

Attempts to improve fracture toughness by incorporating a skeletal nickel reinforcing phase were not successful as discussed in the following Section II-C. Specimen stock material obtained from HP34 was employed for slow bend tests. Examination of the microstructural features and X-ray diffraction data show that the nickel additive reacts with silicon carbide under the processing conditions shown in Table 4 to form a nickel silicide phase. The latter would not be expected to provide a reinforcing action and yielded low fracture toughness and strength levels of σ (75^oF) = 35,000 psi or $2.4 \times 10^8 N/M^2$.

3. Boride V - Reinforced by Carbon Cloth

Three billets were successfully hot pressed to full density with 16 mesh carbon cloth in planes parallel to the diametrical plane of the billet. The graphite cloth used in fabricating these billets was an open weone-10 mesh material obtained from Kreha Corp. of America, Gardena California. This square mesh cloth consists of 25 mil ($6.3 \times 10^{-4} M$) thick

fiber threads with 75 mils (1.9×10^{-3}M) between each thread. The first billet, HP80, was fabricated with a one eighth inch separation between the cloth layers. Figure 18; the second billet, HP82, with a one sixteenth inch separation; and the third billet, HP93 with a one thirtysecond inch separation.

X-ray diffraction of these materials provides identification of ZrB_2, SiC and graphite indicating that the carbon graphitizes (at least on the surface of the cloth) during the processing. Microstructural features of these billets are the same. A representative graphite/matrix area is provided in Figures 19 and 20 and microstructural features of the matrix area phase, consisting essentially of ZrB_2 and SiC in the Boride V proportions, are shown in Figure 21.

4. Boride VIII (14,30)

Boride VIII(14,30) is a dense polycrystalline composite of ZrB_2 ($56^v/o$), SiC ($14^v/o$), and C ($30^v/o$). The microstructure and the properties do not show any appreciable anistropy(11 12). The microstructural features are shown in Figure 22. The two billets employed for specimens in this program, D198M for slow bend tests and D201M for impact tests, are equivalent.

5. Boride VIII(14,30)M2

Boride VIII(14,30)M2 is a dense polycrystalline composite of ZrB_2, SiC and C of the same relative proportions as the VIII (14,30) described above. However, Boride VIII (14,30)M2 is processed with a special carbon powder which produces a dense boride material with improved machining characteristics. The VIII(14,30) and VIII(14,30)M2 composites have equivalent oxidation resistance and thermal stability. Microstructural and property anisotropy are significant and some variation in anisotropy has been observed for billets hot pressed by different procedures (19). In particular smaller billets of three inch diameter fabricated at ManLabs are more anisotropic than larger billets pressed at Norton Company. The variation of strength and elastic modulus with billet orientation relative to pressing direction for VIII(14,30)M2 hot pressed by two different methods are shown in Table 6. A comparison of microstructural features is provided in Figure 23. Impact specimens were obtained from billet NP2M2 while slow bend test specimens were taken from billets HP45M2 and billet NP2M2.

6. Metallic Additions to Zirconium Diboride

Stock material for test specimens were obtained for ZrB_2 20 Ni and $ZrB_2$10 Fe. The processing conditions are provided in Table 5. The billets fabricated with ZrB_2 10 Ni, ZrB_2 10 Cr, and ZrB_2 20 Ni-Ta-

wire-reinforced were not employed for test specimens. The latter two compositions produced cracked billets and the former with 10 weight percent Ni was of low relative density. Details of microstructural features and phases identified in the hot pressed billets are provided in Section II-D below.

7. Tungsten Carbide Cermet

The tungsten carbide cermet, WC6Co, was procured as a dense, fine grained material. Microstructural features are provided in Figure 24.

C. Fabrication Studies of ZrB_2+SiC Compositions with Ni Additive

Conventional hot pressing experiments were attempled using nickel additions of 9.5 ^{w}/o and 18 ^{w}/o to a base Boride V composition. Processing conditions, resulting billet densities, and a list of tests performed on the processed billets are provided in Table 5. In view of the low densities observed in the two processing runs at 2620^{o} and 2810^{o}F, HP20 and HP22 respectively, it was concluded that no additional tests would be performed on these billets. The magnitude of the absolute density for Boride V is 5.50 g/cc; the addition of nickel as a non-reacting material would raise the density of the 9.5 and 18.5 ^{w}/o Ni compositions to a higher value.

The last three processing runs performed at temperatures of 3000^{o}, 3200^{o}, and 3050^{o}F revealed some difficulties inherent in the composition selected for study. Representative microstructures for HP25, HP34 and HP83 and results of X-ray diffraction and electron microprobe analyses are provided in Figures 25,26 and 27, respectively. These micrographs reveal that liquid phases were present during processing and, in fact, a significantly large quantity of molten material extruded from the hot pressing mold during run HP83. The extruded material was principally nickel which contained a needle-like precipitate of ZrO_2. Microprobe data indicated a high zirconium content for the precipitate and X-ray data identified monoclinic ZrO_2.

Analysis of the processing results in Table 5 and the billet characterization data in Figures 25,26 and 27 shows that at temperatures in the range of 2800^{o} to 3000^{o}F reaction of nickel with silicon is detrimental to the formation of a metal reinforced carbide ZrB_2+SiC composition. Nickel silicide phases are produced and silicon carbide is removed from the matrix. Liquid phase formation which is desireable for a processing and infiltrating to form skeletal phases definately occurred but the resulting solidfied grain boundary phase is not metallic, but rather intermetallic and hence does not provide strength reinforcement.

D. Fabrication Studies of ZrB_2 Compositions with Metal Additions

Hot pressing experiments were carried out for the ZrB_2 compositions with 10 and 20 weight percent Ni, 10 weight percent Fe, 10 weight percent Cr, and 20 weight percent Ni with Ta wire reinforcement shown in Table 5.

The 20 weight percent nickel composition was the most successful from the point of lowering processing temperature. Temperatures of 2420°F were employed to produce dense microstructures Figure 28. Higher processing temperatures of 3020°F, HP88 resulted in loss of Ni with densification of the remaining ZrB_2, Figure 29. Processing with 10 weight percent Ni was not successful since a slow density billet was produced. The nickel phase in ZrB_2 20Ni billets occurs in the grain boundary and is Ni_3B_4 as identified by X-ray diffraction.

Processing runs using 10 weight percent Fe produced dense materials, HP98 and HP101. In both cases the resulting billets are ferromagnetic indicating that iron boride was not formed. X-ray analysis identified bcc iron and iron was found in the grain boundaries. A representative microstructure is provided in Figure 30. The processing temperature of 3000°F is considerably less than the 3600°F and higher temperatures needed to fabricate dense bodies of ZrB_2.

Processing runs with 10 weight percent Cr produced a low density billet, HP99 and a cracked billet, HP103. The somewhat higher processing temperature employed for HP103 is not considered responsible for the cracking. The microstructural features of the dense ZrB_2 10Cr billet is provided in Figure 31.

Attempts to incorporate Ta wire reinforcement in a ZrB_2 20 Ni matrix were unsuccessful. The resulting billet, HP102, was cracked and there was reaction of the Ta with the matrix composition. The gross features of a cross section showing the 0.040 in. Ta filaments in place are shown in Figure 16. The microstructural features of the ZrB_2 20 Ni matrix interface with the Ta wire are shown in Figure 32.

IV MECHANICAL TESTING OF BORIDE COMPOSITES

A. Introduction

The thermal stress and oxidation resistance of Boride V and Boride VIII composites described in Section II are unrivaled by any known material system. The major obstacle to wider utilization of these attractive features is the low resistance to fracture exhibited by these composites. The objective of the activities described in this section was characterization of the fracture energy of current boride composites and evaluation of variations in composition and structure.

B. Additional Measurements of Bend Strength and Modulus of Boride Composites

The discussions of properties and fabrication presented in Sections II and III provide backround information on engineering mechanical property data for Boride V and Boride VIII (Table 2) and the anisotropy in the bending strength and modulus of Boride VIII-M2 rising from alteration of billet size and processing conditions. Tables 8-10 provide additional data on bend strength and modulus for boride composites. Table 8 summarizes the results of three point bending tests of Boride V, Boride VIII-M2 and Boride V plus nickel. These tests were conducted with bars which were 2.25 inches long (0.0672M), 0.200 inches thick (0.0051M) and 0.200 inches high (0.0051M). The three point bending test bars did not have any notches. The span length of the bars was cut from 3 inch diameter (0.0762M) x 3 inch high (0.0762M) billets in a plane parallel to the diametral face (i.e. in the plane of the billet). The values for bend strength and modulus of Boride V are in general agreement with the values shown in Table 2 at room temperature although the bend strength is higher for Billet V07FR31L of Boride V than the engineering property value shown in Table 2.

Similarly, the bend strength for Boride VIII-M2 given in Table 8 is in keeping with the results shown for this material (cut from Billet HP74M2) in the parallel orientation in Table 6. However the modulus is substantially below that observed by sonic methods. The results of bend tests of Boride V plus nickel yielded substantially lower strength and modulus values than Boride V as shown in Table 8. This finding is in keeping with the results presented in Section III-C. Thus, reaction of the nickel additive with the silicon carbide component of Boride V during processing prevented full densification and lead to a low density product which exhibits a lower strength than Boride V.

Table 9 contains the results of "four point bending" tests of Boride VIII and Boride VIII-M2 conducted over a wide range of temperatures. Although the bend strengths obtained from these tests are not directly comparable the general level of agreement is quite tolerable. Thus, the

bend strength values shown in Table 9 for Boride VIII indicate nearly constant strength levels for samples taken parallel to the billet plane between room temperature and 3730°R (2073°K). Although the strength levels are below those shown in Table 2 for Boride VIII the latter were obtained in 3-point bending tests. Moreover, the moduli shown in Table 9 for Boride VIII are about 30% larger than those given in Table 2. These differences are also attributable to the testing method (4-point vs 3-point bending).

Comparison of the bend strength and modulus values reported in Tables 5 and 8 for samples of Boride VIII-M2 (in the parallel orientation) measured in 3-point bending with similar samples measured at room temperature by 4-point bending yields a relatively good comparison for the moduli but lower strengths (25% lower) for the 4-point bending samples.

Table 10 summarizes the results of room temperature, 4-point bending tests conducted on samples of graphite reinforced Boride V. Billets HP80 and HP82 were prepared with graphite cloth loadings corresponding to layers of square weave cloth at spacings of 1/8" (3.18×10^{-3}M) and 1/16" (1.59×10^{-3}M) respectively as indicated in Section III-B-2. The measurements shown in Table 10 for the bend strength of HP80 in 4-point bending determined on samples which were oriented parallel and perpendicular to the plane of the billet are comparable to the bend strength of Boride V. Thus introduction of graphite cloth at the low level characteristic of the 1/8" spacing does not materially alter the strength. However, HP82 which has a higher graphite cloth loading, exhibits lower bend strengths.

C. Measurement of the Fracture Energy of Boride Composites

The fracture energy of boride composites and cobalt bonded tungsten carbide bars was measured by means of slow bend and impact tests of bars similar to that shown in Figure 34. The length of the notched charpy bar configuration is 2.25 inches (0.0572M) while the overall height is 0.394 inches (0.010M). The notch is a groove with a 0.001 inch (2.54×10^{-5}M) radius root which was electrical discharge machined. The first series of slow bend tests were performed on bars of Boride V (80 v/o ZrB_2-20 v/o SiC) of variable thickness as reported in Table 11. Figures 35-38 summarize the results and illustrate the fracture characteristics.

The slow bend tests were conducted in three point bending with a span length of 1.75 inches (0.0444M). The loading rate was 100/lbs minute (7.41N/Sec) with simultaneous recording of load and deflection on an x-y recorder. Table 11 and Figure 35 indicate that the (W/A) values obtained for 0.125 inch (0.00318M) thick bars are slightly higher than the (W/A) values obtained with 0.200 (0.00508M) and 0.394 inch (0.010M) bars. The energy W is the area under the load-deflection curve while A, the fracture area, is the product of h (see Figure 35) and the thickness, t.

Charpy impact tests were conducted on ManLabs Model CIM-1 (24 ft-lb) (32.54J) impact tester which has a read-out accuracy of 0.01 in-lbs (0.00113J). The test bar configuration employed in these tests was that shown in Figures 34 and 35 with t = 0.394 inches (0.010M) which is the standard ASTM size. Pendulum height and velocity were varied during the testing program in order to minimize tossing of the samples and thus insure reproducible results. Test data generated during the impact tests in terms of in-lbs (or Joules) was converted into energy per unit volume i.e. in-lbs/in^2 or J/M^2 by dividing the energy read-out by the cross-sectional area of the sample which is the product of h (height) and t (thickness). Tables 11-18 contain all of the results of fracture energy measurements obtained during the current program.

Figure 39 shows typical Load-Deflection Curves for samples of Boride VIII, Boride VIII-M2 and WC-6Co. These curves form the basis of the slow bend data contained in Tables 11-18 and were employed to construct the average values of the fracture energy (W/A) determined for several boride composites and WC-6Co. Figures 41-45 show photographs of the initial series of slow-bend test bars after fracture. This initial series of results as well as subsequent slow bend test data given in Tables 11-17 and summarized in Table 18 indicate that WC-6Co has the highest fracture energy. The cobalt bonded tungsten carbide material exhibits (W/A) values near 2.6 in-lb/in^2 or 455 J/M^2. By comparison Boride VIII-M2 yielded values near 1.5 in-lb/in^2, (i.e. 263 J/M^2) or 58% of the WC-6Co values. Lower fracture energies of 1.1 in-lb/in^2 or 193 J/M^2 were observed for Boride VIII, while Boride V which contains no graphite exhibited the lowest slow bend fracture energies corresponding to (W/A) = 0.65 in-lb/in^2, (114 J/M^2). Reference to Figures 44 and 45 provides a clue to the different fracture energies of the boride composites as disclosed by the slow bend tests. Thus, the Boride VIII-M2 bars exhibit stepped or irregular fractures while the other bars exhibit relatively smooth straight fractures. The improvement in (W/A) afforded by the graphite additions shown by Boride VIII and VIII-M2 in the slow bend tests may be due to the fact that the low modulus graphite phase present in the former composites absorbs a substantial amount of energy. This phase is not present in the Boride V composite. The latter contains ZrB_2 and SiC alone which have moduli 20 to 30 times higher than graphite. It should be noted that the relatively high (W/A) value exhibited by the WC-6Co ($90^v/oWC-10^v/oCo$) tool materials is due partly to the cobalt binder phase and partly to the small grain size. Comparison of Figures 17, 22, 23 and 24 indicate that WC-6Co has a grain size which is 5-10 times smaller than that exhibited by the boride composites.

Turning to a discussion of the impact test results, Figures 46-51 show photographs of a number of full sized impact bars after fracture. In most cases, the fracture surfaces were relatively smooth, although Boride VIII-M2 shown in Figure 50 exhibited some surface faceting.

Nevertheless, the result differs considerably from that displayed in the slow bend tests illustrated in Figure 45. The impact test data provided in Tables 12-17 and summarized in Table 18 disclose two essential features. First, the WC-6Co material exhibits impact energy values near 0.76 ft-lb. This translates to 73.9 in-lb/in^2 or 12950 J/M^2 on a unit area basis. The boride composites exhibit impact energies which are one quarter to one third the values measured for WC-6Co. Moreover, the Boride VIII and Boride VIII-M2 composites which exhibited higher slow bend fracture energies than Boride V (see Figure 40) exhibit lower impact fracture energies (see Table 18). What is most surprizing however, is the extremely large difference between the slow-bend and impact fracture energies observed for all of the materials tested. In contrast to the results summarized in Table 18 where the impact energies are 17 to 40 times larger than the slow bend fracture energies, experience with a range of ultra high strength steels and titanium alloys in our laboratory (20) usually yields a close correspondence between the two values with the impact energies exceeding the slow bend fracture energies by no more than a factor or two. Although the latter results have been obtained under plane strain fracture conditions using precracked samples (which cannot be readily employed in the present situation) the current results are still surprising in view of our earlier experience (20). The divergence is all the more difficult to reconcile because no plastic or yielding behavior occurs in these materials at room temperature.

In order to gain additional confidence in the present data additional tests will be conducted during the next phase of this program using impact test samples which have smaller thickness dimensions. The current test sample size (t = 0.394 inches or 0.01M) was selected because it corresponds to the standard impact size. However tests of smaller samples would provide a means of checking the impact fracture energy of (W/A) values.

At present, the boride composites exhibit fracture energies which are one third to two thirds of the fracture energies exhibited by cobalt bonded tungsten carbide in impact and slow bend tests. Studies of alloying additions, compositing and grain size refinement will be conducted in order to achieve boride fracture energies which are comparable to those of cobalt bonded tungsten carbide without degradation of the thermal or oxidation resistance.

Unfortunately, there are limited opportunities for comparing slow bend and impact fracture energies of other ceramic type materials reported in the literature with the present results for boride composites. However a recent NASA sponsored study of silicon carbide and silicon nitride composites (21) provides some data for comparison. Investigation of the impact energy of 1/4" x 1/4": unnotched specimens at room temperature yielded impact energies of 8 in-lbs/in^2, (1402 J/M^2) for hot pressed SiC (21). Higher values, 16 in-lb/in^2, (2803 J/M^2) were noted for Si_3N_4. Improvement of the impact energy of SiC to a level of 18 in-lbs/in^2, (3154 J/M^2) was obtained by incorporation of carbon cloth. The best values, corresponding to 25 in-lbs/in^2, (4380 J/M^2) were attained by incorporating the SiC whiskers in SiC.

V MICROSTRUCTURAL CHARACTERIZATION OF FRACTURE SURFACES

Microstructural characterization of all of the slow bend and impact test samples was carried out by means of light microscopy and electron fractography employing a two stage carbon replica technique with chromium shadowing at 30°. The gross features which distinguish the fracture surfaces noted earlier in Section IV and displayed in Figures 36-51 were investigated further by microstructural examination. Electron fractography proved to be most expeditious technique for displaying the surface characteristics. Figures 52-75 show typical fractographs of the samples of boride composites and WC-6Co broken in impact and slow bend tests.

With the exception of the WC-6Co material, the fracture surfaces for a given material generated by impact do not appear to differ significantly from those obtained in the slow bend tests. However differences were observed for various composites. Figures 52-55 show typical fractographs of Boride V after slow bend and impact failure. Both sets of fractographs exhibit smooth transgranular cleavage. Little change was effected by inclusion of nickel in Boride V as evidenced by Figures 56-57 or by the incorporation of graphite cloth as shown in Figures 58-61.

A qualitative change in the fracture surface characteristics is illustrated in Figures 62-63 for Boride VIII samples broken in slow bend and impact tests. In both cases the fractographs exhibit rumpled quasi cleavage features which is probably due to the distribution of graphite with the structure (See Figure 22). Similar characteristics are displayed by the slow bend and impact surfaces of Boride VIII-M2 shown in Figures 66-71.

In all of the forgoing examples the fracture characteristics resulting from slow bend and and impact failures are virtually undistinguishable. However in the case of WC-6Co, shown in Figures 68-71 distinct differences are apparent. Thus, samples of this material broken in slow bend tests exhibit smooth transgranular cleavage while samples which were broken by impact exhibit intergranular failures.

REFERENCES

1. Kaufman, L. and Nesor, H., "Stability Characterization of Refractory Materials under High Velocity Atmospheric Flight Conditions" AFMF-TR-69-84, Part I Volume I: Summary, ManLabs, Inc. Cambridge, Mass. (March 1970).

2. Kaufman, L. and Nesor, H., "Stability Characterization of Refractory Materials under High Velocity Atmospheric Flight Conditions," AFML-TR-69-84, Part II Volume I: Facilities and Techniques Employed for Characterization of Candidate Materials, ManLabs, Inc., Cambridge, Mass. (December 1969).

3. Kaufman, L. and Nesor, H., "Stability Characterization of Refractory Materials under High Velocity Atmospheric Flight Conditions", AFML-TR-69-84, Part II, VolumeII: Facilities and Techniques Employed for Cold Gas/Hot Wall Tests, ManLabs, Inc., Cambridge, Mass. (December 1969).

4. Kaufman, L. and Nesor, H., "Stability Characterization of Refractory Materials under High Velocity Atmospheric Flight Conditions", AFML-TR-69-84, Part II Volume III: Facilities and Techniques Employed for Hot Gas/Cold Wall Tests, ManLabs, Inc., Cambridge, Mass. (December 1969).

5. Kaufman, L. and Nesor, H., "Stability Characterization of Refractory Materials under High Velocity Atmospheric Flight Conditions", AFML-TR-69-84, Part III Volume I: Experimental Results of Low Velocity Cold Gas/Hot Wall Tests, ManLabs, Inc., Cambridge, Mass. (December 1969).

6. Perkins, R., Kaufman, L. and Nesor, H., "Stability Characterization of Refractory Materials under High Velocity Atmospheric Flight Conditions", AFML-TR-69-84, Part III Volume II: Experimental Results of High Velocity Cold Gas/Hot Wall Tests, ManLabs, Inc., Cambridge, Mass. (December 1969).

7. Kaufman, L. and Nesor, H., "Stability Characterization of Refractory Materials under High Velocity Atmospheric Flight Conditions", AFML-TR-69-84, Part III Volume III: Experimental Results of High Velocity Hot Gas/Cold Wall Tests, ManLabs, Inc., Cambridge, Mass. (February 1970).

8. Kaufman, L., Nesor, H., Bernstein, H. and Baron, J.R., "Stability Characterization of Refractory Materials under High Velocity Atmospheric Flight Conditions", AFML-TR-69-84, Part IV Volume I: Theoretical Correlation of Material Performance with Stream Conditions, ManLabs, Inc., Cambridge Mass. (December 1969).

9. Bernstein, H. and Baron, J.R., "Stability Characterization of Refractory Materials under High Velocity Atmospheric Flight Conditions", AFML-TR-69-84, Part IV Volume II: Calculation of the General Surface Reaction Problem, ManLabs, Inc., Cambridge, Mass. (December 1969).

10. Clougherty, E.V., "Research and Development of Refractory Oxidation-Resistant Diborides, Part II Volume I: Summary," AFML-TR-68-190, Part II Volume I, July 1970.

11. Clougherty, E.V., Hill, R.H., Rhodes, W.R., and Peters, E.T., "Research and Development of Refractory Oxidation-Resistant Diborides, Part II Volume II: Processing and Characterization", AFML-TR-68-190, Part II Volume II, January 1970.

12. Clougherty, E.V. and Peters, E.T., "Research and Development of Refractory Oxidation-Resistant Diborides, Part II Volume III: Thermochemical Stability Characteristics", AFML-TR-68-190, Part II Volume III, January 1970.

13. Rhodes, W.H., Clougherty, E.V., and Kalish, D., "Research and Development of Refractory Oxidation-Resistant Diborides, Part II Volume IV: Mechanical Properties", AFML-TR-68-190, Part II Volume IV, January 1970.

14. Clougherty, E.V., Wilkes, K.E., and Tye, R.P., "Research and Development of Refractory Oxidation-Resistant Diborides Part II Volume V: Physical Thermal, Electrical and Optical Properties", AFML-TR-68-190, Part II Volume V, November 1969.

15. Clougherty, E.V., Niesz, D.E., Mistretta, A.L., "Research and Development of Refractory Oxidation-Resistant Diborides, Part II Volume VI: Thermal Stress Resistance", AFML-TR-68-190, Part II Volume VI, December 1969.

16. Clougherty, E.V., "Research and Development of Refractory Oxidation-Resistant Diborides, Part II Volume VIII: Application Evaluations and Design Considerations", AFML-TR-68-190, Part II Volume VIII, July 1970.

17. Kaufman, L. "Boride Composites A New Generation of Nose Cap and Leading Edge Materials for Reusable Lifting Re-entry Systems" AIAA paper No. 70-278, AIAA Advanced Space Transportation Meeting, Cocoa Beach, Florida February 1970. (published in SAMPE Quarterly) (1970) 2 46.

18. Kaufman, L., and Nesor, H., "Stability Characterization of Refractory Materials under High Velocity Atmospheric Flight Conditions", AFML-TR-69-84, Part V Additional Studies, ManLabs, Inc. Cambridge, Mass. April 1971.

19. Clougherty, E. "Diboride Technology and Fabrication" Subcontract RCO446120 for the Martin-Marietta Corp. "Ceramic Nose Cap and Leading Edge Program" Air Force Contract No. F33615-70-C-1179.

20. Kalish, D. and Kulin, S.A. "Thermomechanical Treatments Applied to Ultrahigh Strength Steels" Final Report Contract NOw 66-0142-c. Naval Air Systems Command, November 1966.

21. Cannon, R.M. and Hill, R.J. "High Temperature Compounds for Turbine Vanes" NASA CR-7294 Avco Corp. (AVSD-0629-70-RR) 31 August 1970.

TABLE 1

CONVERSION UNITS EMPLOYED IN THIS REPORT

1 inch = 0.0254 meters

1 lb (force) = 4.448 Newtons

1 ft-lb (energy) = 1.356 Joules

1 in-lb = 0.113 Joules

1 in-lb/in^2 = 175.2 J/M^2

1 lb (force)/in^2 (pressure) = 6894 N/M^2

1 BTU = 1054.4 Joules

1 BTU/lb = 2324 J/kg

1 BTU/ft^2 sec = 11350 J/M^2 sec

1 lb (mass)/ft^3 = 16.02 kg/M^3

1 BTU/lb ^oR = 4184 J/kg ^oK

1 BTU/ft sec ^oR = 6227 J/M sec ^oK

TABLE 2

ENGINEERING PROPERTY DATA FOR BORIDE COMPOSITES

Boride V ($80^{v}/o ZrB_2$-$20^{v}/o SiC$)

Temp.	Density	Heat Capacity	Thermal Conductivity	Modulus	Bend Strength
^{o}R	lbs/ft^3	BTU/lb ^{o}R	$BTU/ft.sec^{o}R \times 10^{-2}$	$10^6 lbs/in^2$	$10^3 lbs/in^2$
540	342	0.100	1.67	76	50
1080	340	0.150	0.85	74	51
1620	337	0.160	0.80	72	52
2160	335	0.170	0.77	70	53
2700	333	0.176	0.73	67	48
3240	331	0.184	0.70	64	43
3780	329	0.189	0.67		
4320	326	0.194	0.65		
4860	324	0.199			

Room temperature compressive strength: 500,000 lbs/in^2

Coefficient of thermal expansion: $3.3 \times 10^{-6}/^{o}R$ (540^{o} to $3000^{o}R$)

Boride VIII ($56^{v}/o ZrB_2$-$14^{v}/o SiC$-$30^{v}/o C$)

Temp.	Density	Heat Capacity	Thermal Conductivity	Modulus	Bend Strength
^{o}R	lbs/ft^3	BTU/lb ^{o}R	$BTU/ft.sec^{o}R \times 10^{-2}$	$10^6 lbs/in^2$	$10^3 lbs/in^2$
540	280	0.108	0.75	31	41
1080	279	0.178	0.68	31	42
1620	277	0.195	0.62	31	43
2160	276	0.216	0.57	31	44
2700	274	0.227	0.53	31	45
3240	273	0.238	0.50	31	46
3780	272	0.247	0.48		
4320	270	0.256	0.46		
4860	269	0.264			

Coefficient of thermal expansion: $3.6 \times 10^{-6}/^{o}R$ (540^{o} to $3000^{o}R$)

TABLE 2 (MKS)

ENGINEERING PROPERTY DATA FOR BORIDE COMPOSITES

Boride V ($80^{v}/oZrB_2$-$20^{v}/oSiC$)

Temp.	Density	Heat Capacity	Thermal Conductivity	Modulus	Bend Strength
^{o}K	$10^3 kg/M^3$	$J/kg^{o}K$	$J/Msec^{o}K$	$10^{11} N/M^2$	$10^8 N/M^2$
300	5.48	418	104	5.2	3.4
600	5.45	628	53	5.1	3.5
900	5.40	669	50	5.0	3.6
1200	5.37	711	48	4.8	3.7
1500	5.33	736	45	4.6	3.3
1800	5.30	770	44	4.4	3.0
2100	5.27	791	42		
2400	5.22	812	40		
2700	5.19	833			

Room temperature compressive strength: $34.5 \times 10^8 N/M^2$

Coefficient of thermal expansion: $5.9 \times 10^{-6}/^{o}K$ (300^{o} to $1665^{o}K$)

Boride VIII ($56^{v}/oZrB_2$-$14^{v}/oSiC$-$30^{v}/oC$)

Temp.	Density	Heat Capacity	Thermal Conductivity	Modulus	Bend Strength
^{o}K	$10^3 kg/M^3$	$J/kg^{o}K$	$J/Msec^{o}K$	$10^{11} N/M^2$	$10^8 N/M^2$
300	4.49	452	47	2.1	2.8
600	4.47	744	42	2.1	2.9
900	4.44	816	39	2.1	3.0
1200	4.42	904	35	2.1	3.0
1500	4.39	950	33	2.1	3.1
1800	4.37	996	31	2.1	3.2
2100	4.36	1033	30		
2400	4.33	1071	29		
2700	4.31	1105			

Coefficient of thermal expansion $6.5 \times 10^{-6}/^{o}K$ (300^{o} to $1665^{o}K$)

TABLE 3

MATERIAL IDENTIFICATION SYSTEM

Billet Identification No.	Components and Composition
Material V	**80 ^{v}/oZrB$_2$: 20 ^{v}/oSiC**
V07F R31L	Material V, ZrB$_2$ Lot 07F, Billet No. R31L
V10 HP28	Material V, ZrB$_2$ Lot 10, Billet No. HP28
V (Ni) HP34	Material V, Ni powder added, Billet No. HP34
V (Carbon reinforced 1/8" sep.)	Material V layers of 1/8" thickness between layers of carbon cloth mesh
Material VIII(14,30)	**56 ^{v}/oZrB$_2$: 14 ^{v}/oSiC: 30 ^{v}/oC**
VIII (14,30) 11 D198M	Material VIII(14,30), ZrB$_2$ Lot 11, Regal Carbon Powder, Billet No. D198M
VIII (14,30) HP45M2	Material VIII(14,30), Billet No. HP45, M2 designates a special carbon additive
Tungsten Carbide Cermet	**94 ^{w}/oWC: 6 ^{w}/oCo**
WC 6 Co	Dense, high strength tungsten carbide cermet tool material consisting of two phase structure with 90 ^{v}/o WC-10 ^{v}/o Co.
ZrB$_2$ Additive Systems	
ZrB$_2$ 20 Ni	80 ^{w}/oZrB$_2$: 20 ^{w}/oNi

TABLE 4

PROCUREMENT SOURCE AND PROCESSING CONDITIONS*

FOR BORIDE V, BORIDE VIII (14,30) AND TUNGSTEN CARBIDE

Billet Identification No.	Press Facility	Temp.	Pressure	Time	Density	Ref.
Billet Size		°F	psi ($10^4 N/M^2$)	min	g/cc ($10^{-3} kg/M^3$)	
Material V						
V07FR31L 6 in x 6 in x 2 in	A	3705	3000 (2068)	90	5.53 (5.53)	(11)
V10HP28 3 in dia x 1 in high	ML	3650	3000 (2068)	40	5.48 (5.48)	
Material (VIII (14,30)						
VIII(14,30) 11 D198M 6 in dia x 3 in high	A	3920	3000 (2068)	300	4.58 (4.58)	(12)
VIII (14,30) 11 D201M 6 in dia x 4 in high	A	3920	3000 (2068)	240	4.58 (4.58)	(12)
Material VIII (14,30)M2						
VIII (14,30) HP45M2 3 in dia x in high	ML	3750	3000 (2068)	120	4.5 (4.5)	(19)
VIII (14,30) NP2M2 6 in x 6 in x 2 in	N	3990	2200 (1517)	--	4.58 (4.58)	
Tungsten Carbide Cermet						
WC 6 Co		Procured as Dense Square Stock				

*The quantities tabulated as Temperature, Pressure and Time refer to the conditions at the maximum fabricating temperature (optical). The press facilities identified as ML, N, and A refer to fabrication equipment at ManLabs, Norton Company and Avco.

TABLE 5

PROCESSING CONDITION FOR Boride V-Ni COMPOSITES

Composition: Base boride composition is 88 $^{w}/_{o}ZrB_2$ and 12 $^{w}/_{o}$ SiC (Material V, 20 $^{v}/_{o}$SiC) with addition of Ni in amounts of 9.5 and 18 $^{w}/_{o}$ of base boride.

Billet Size: 3 in. diameter x 1 in. high

Billet No. Ni Content	Pressure psi	Temp ^{o}F	Time min.	Density g/cc	Billet Disposition
HP20 9.5 $^{w}/_{o}$	3000	2620	90	3.76	Billet repressed for HP22
HP22 9.5 $^{w}/_{o}$	3000	2810	135	4.05	Low density, no fur- tests
HP25 18 $^{w}/_{o}$	3000	3000	190	5.29	X-ray, Metallography Electron Microprobe Bend Strength
HP34 18 $^{w}/_{o}$	3000	3200	135	5.32	X-ray, Metallography Bend Strength
HP83 18 $^{w}/_{o}$	3000	3050	200	4.93	X-ray, Metallography Electron Microprobe Bend Strength

TABLE 6

VARIATION OF ANISOTROPY FOR MATERIAL VIII (14, 30) M2

(Room Temperature Data)

(Four Point Bending)

Billet Ident.	Orientation**	Sonic Modulus	Static Modulus	Strength	Strength/Av. Modulus
		10^6psi(10^{11}N/M^2)	10^6psi(10^{11}N/M^2)	10^3psi(10^8N/M^2)	$\times 10^{-3}$
No. NP2M2	Perpendicular	22.1 (1.52)	22.9 (1.58)	28.9 (1.99)	1.28
D = 4.58g/cc	Parallel	36.7 (2.53)	36.4 (2.51)	49.5 (3.41)	1.35
No. HP74M2	Perpendicular	18.1 (1.25)	ND	25.1 (1.73)	1.39
d = 4.51g/cc	Parallel	43.4 (2.99)	ND	66.0 (4.55)	1.52

*The fabrication procedures at ManLabs employ a loose powder mold filling operation with no temporary binders added to the component powders. Norton Company employs its own proprietary procedures for hot pressing which include the use of preforms as opposed to loose powder fills.

***Specimen span orientations tabulated are relative to the plane of the hot pressed billet which is perpendicular to the applied pressing direction.

TABLE 7

PROCESSING CONDITIONS FOR ZrB_2-METAL ADDITIVE COMPOSITES

Composition*	Billet No.	Processing Conditions**			Density
		Press	Temp.	Time	g/cc
		psi	°F	min.	
~~$ZrB_2$20Ni~~	~~HP88~~	~~3000~~	~~3000~~	~~270~~	~~6.14~~
$ZrB_2$20Ni°	HP90	3000	2425	245	5.96av.
$ZrB_2$20Ni	HP91	3000	2475	165	6.04
$ZrB_2$10Ni°°	HP96	3000	2460	255	4.94
$ZrB_2$10Ni	HP97	3000 300	2600 2800	135 75	5.12
$ZrB_2$20Ni with Ta wire°°°	HP102	3000	2460	280	6.11
$ZrB_2$10Fe	HP98	3000 3000	2800 2900	115 200	5.84
$ZrB_2$10Fe	HP101	3000	2900	240	6.03
$ZrB_2$10Cr	HP99	3000 3000	2900 3000	105 180	4.47
$ZrB_2$10Cr	HP103	3000	3200	150	5.57

*See Table 3 for significance of formula designations

**Tabulated values are the times at the maximum fabricating pressures and temperatures.

°Center Section 6.46 g/cc

°°Repressed HP97

°°°Cracked

TABLE 8

RESULTS OF THREE POINT BENDING TESTS OF RECTANGULAR BARS FOR SAMPLE MATERIALS

$\sigma = \frac{1.5Pl}{th^2}$ (maximum Stress) : $E = \frac{Pl^3}{4th^3\delta}$ (Youngs modulus)

l = span length = 1.75 inches

Material	P (lbs)	t (in)	h (in)	σ (ksi)	E (10^3ksi)
Boride V	213	0.2045	0.2005	68.0	78.1
($80^v/_o ZrB_2$-$20^v/_o SiC$	201	0.2045	0.2005	64.2	72.2
Billet V07FR31L	194	0.2045	0.2005	61.9	84.2
Average	203			64.7	78.2
Boride VIII-M2	202	0.200	0.200	66.1	33.9
($56^v/_o ZrB_2$-$14^v/_o SiC$	189	0.200	0.200	62.0	33.7
-$30^v/_o C$)	192	0.200	0.200	63.0	31.9
Average	194			63.7	33.2
Boride V plus	127	0.200	0.200	41.5	31.8
Nickel	115	0.200	0.200	37.5	30.8
($70^v/_o ZrB_2$-$20^v/_o SiC$	117	0.200	0.200	38.2	30.9
$10^v/_o Ni$)					
Average	120			39.1	31.2

TABLE 8 (MKS)

RESULTS OF THREE POINT BENDING TESTS OF RECTANGULAR BARS FOR SAMPLE MATERIALS

$\sigma = \frac{1.5Pl}{th^2}$ (maximum stress): $E = \frac{Pl^3}{4th^3\delta}$ (Youngs Modulus)

l = span length = 0.0429M

Material	P (N)	t 10^{-2}M	h 10^{-2}M	σ $10^8 N/M^2$	E $10^{11} N/M^2$
Boride V	947	0.501	0.491	4.69	5.38
($80^V/oZrB_2$-$20^V/oSiC$)	894	0.501	0.491	4.43	4.98
Billet V07FR31L	862	0.501	0.491	4.27	5.80
Average	901			4.46	5.39
Boride VIII-M2	898	0.490	0.490	4.56	2.34
($56^V/oZrB_2$-$14^V/oSiC$	841	0.490	0.490	4.27	2.32
-$30^V/oC$)	854	0.490	0.490	4.34	2.20
Average	864			4.39	2.29
Boride V plus	565	0.490	0.490	2.86	2.19
Nickel	512	0.490	0.490	2.59	2.12
($70^V/oZrB_2$ $20^V/oSiC$ $10^V/oNi$)	520	0.490	0.490	2.63	2.13
Average	532			2.69	2.15

TABLE 9

ADDITIONAL MECHANICAL PROPERTY DATA FOR BORIDE VIII($56^{v}/oZrB_2$-$14^{v}/oSiC$-$30^{v}/oC$) COMPOSITES

(Four Point Bending)

Material Density gms/cm^3	Billet Size (Sample Span Billet Diam. Orientation)	Bend Strength (ksi) 540^oR	1930^oR	3010^oR	3730^oR
Boride VIII $\rho = 4.58$	6" Diam x 4" High (parallel)	35± 3		37± 3	33± 3
	6" Diam x 4" High (Perpendicular)	30± 2		24± 1	23± 1
Boride VIII $\rho = 4.66$	3" Diam x 1" High (parallel)	27± 3	32± 3	30± 3	27± 2
Boride VIII-M2 $\rho = 4.54$	3" Diam x 1" High (parallel)	48± 3	60± 5	28± 3	23± 2
	3" Diam x 1" High (Perpendicular) (1 inch span)	45± 2	57± 1	29± 2	20± 1
		Youngs Modulus (10^3Ksi)			
Boride VIII $\rho = 4.58$	6" Diam x 4" High (parallel)	43± 1	40± 1		
Boride VIII $\rho = 4.66$	3" Diam x 1" High (parallel)	40	41		
Boride VIII-M2 $\rho = 4.54$	3" Diam x 1" High (parallel)	33± 1	29± 1		

Compressive Strength

Boride VIII, $\rho = 4.6 = 191$ Ksi
Boride VIII-M2, $\rho = 4.55 = 154$ Ksi

TABLE 9 (MKS)

ADDITIONAL MECHANICAL PROPERTY DATA FOR

BORIDE VIII ($56^{v}/oZrB_2$-$14^{v}/oSiC$-$30^{v}/oC$) COMPOSITES

(Four Point Bending)

Material Density $10^{-3}kg/M^3$	Billet Size (Sample Span-Billet Diam Orientation)	Bend Strength $10^8 N/M^2$ 300°K	1073°K	1673°K	2073°K
Boride VIII $\rho = 4.58$	0.152M Diam. x 0.102M High (parallel)	2.4± 0.2		2.6± 0.2	2.3± 0.2
	0.152M Diam. x 0.102M High (perpendicular)	2.1± 0.1		1.7± 0.1	1.6± 0.1
Boride VIII $\rho = 4.66$	0.076M Diam x 0.025M High (parallel)	1.9± 0.2	2.2± 0.2	2.1± 0.2	1.9± 0.1
Boride VIII-M2 $\rho = 4.54$	0.076M Diam x 0.025M High (parallel)	3.3±0.2	4.1± 0.4	1.9± 0.4	1.6± 0.1
	0.076M Diam x 0.025M High (perpendicular)	3.1± 0.1	3.9± 0.1	2.0± 0.1	1.4± 0.1
	(0.025Mspan)	Youngs Modulus $10^{11} N/M^2$			
Boride VIII $\rho = 4.58$	0.152M Diam x 0.102M High (parallel)	3.0± 0.1	2.8± 0.1		
Boride VIII $\rho = 4.66$	0.076M Diam x 0.025M High (parallel)	2.8	2.8		
Boride VIII-M2 $\rho = 4.54$	0.076M Diam x 0.025M High (parallel)	2.3± 0.1	2.0± 0.1		

Compressive Strength Boride VIII, $\rho = 4.6 \times 10^{-3} kg/M^3 = 13.2 \times 10^8 N/M^2$

Boride VIII-M2, $\rho = 4.55 \times 10^{-3} kg/M^3 = 10.6 \times 10^8 N/M^2$

TABLE 10

BEND STRENGTH OF BORIDE V AND BORIDE V REINFORCED WITH GRAPHITE CLOTH

(Room Temperature, 4-point bending)*

(Height = 0.500 inches, Thickness = 0.150 inches, Length = 1.00 inches)

(Span distance 0.720 inches, load distance = 0.375 inches)

		Bending Strength (Ksi)
Boride V HP28	No Reinforcement	60.3 61.0 60.7 Average
Boride V (Reinforced) HP20 (1/8" Spacing)	Graphite Cloth lies in the Length-Thickness plane	75.4 77.2 76.3 Average
Boride V (Reinforced) HP80 (1/8" Spacing)	Graphite Cloth lies in the length-Height plane	62.0 72.0 61.0 64.3 Average
Boride V (Reinforced) HP82 (1/16" Spacing)	Graphite Cloth lies in the length-Thickness plane	46.8 48.7 45.8 47.1 Average
Boride V Reinforced HP82 (1/16" Spacing)	Graphite Cloth lies in the length-Height plane	39.3 37.3 38.1 38.2 Average

* Bending of Length-Thickness planes occurs about the Thickness Axis

TABLE 10 (MKS)

BEND STRENGTH OF BORIDE V AND BORIDE V REINFORCED WITH GRAPHITE CLOTH

(Room Temperature, 4-point bending)*

(Height = 0.00127M, Thickness = 0.00381M, Length = 0.0254M)

(Span distance 0.0183M, load distance = 0.0095M)

		Bending Strength ($10^8 N/M^2$)
Boride V HP28	No Reinforcement	4.16
		4.21
		4.19 Average
Boride V (Reinforced) HP28 (3.18×10^{-3}M Spacing)	Graphite Cloth lies in the length-Thickness plane	5.20
		5.32
		5.26 Average
Boride V (Reinforced) HP80 (3.18×10^{-3}M Spacing)	Graphite Cloth lies in the length-Height plane	4.27
		4.96
		4.21
		4.43 Average
Boride V (Reinforced) HP82 (1.59×10^{-3}M Spacing)	Graphite Cloth lies in the length-Thickness plane	3.23
		3.36
		3.16
		3.25 Average
Boride V Reinforced HP82 (1.59×10^{-3}M Spacing)	Graphite Cloth lies in the length-Height plane	2.71
		2.57
		2.63
		2.64 Average

* Bending of Length-Thickness planes occurs about the Thickness Axis

TABLE 11

SUMMARY OF NOTCHED BAR SLOW BEND AND IMPACT TESTS OF BORIDE V ($80^{v}/oZrB_2$-$20^{v}/oSiC$)

SLOW BEND TESTS

l = span length = 1.75 inches

Number	h (in)	t (in)	P(max) (lbs)	W (in-lbs)	A (in^2)	Slow Bend Fracture Energy (W/A) (in-lbs/in^2)
3-13-4	0.319	0.390	225	0.0844	0.1243	0.679
5-28-1	0.317	0.394	221	0.0774	0.1249	0.620
5-28-2	0.317	0.394	231	0.0832	0.1249	0.666
5-28-3	0.315	0.394	230	0.0771	0.1241	0.621
3-13-5	0.313	0.202	99	0.0386	0.0632	0.611
3-13-6	0.313	0.201	106	0.0445	0.0629	0.707
5-28-4	0.315	0.200	114	0.0345	0.0630	0.548
5-28-5	0.318	0.200	116	0.0394	0.0636	0.619
5-28-6	0.317	0.200	116	0.0348	0.0634	0.549
3-13-7	0.314	0.127	68	0.0275	0.0397	0.693
5-28-7	0.317	0.125	70	0.0311	0.0396	0.785
5-28-8	0.316	0.125	68	0.0278	0.0395	0.704
5-28-9	0.317	0.125	68	0.0269	0.0396	0.679
Boride V + Nickel ($70^{v}/oZrB_2$-$20^{v}/oSiC$-$10^{v}/oNi$)						
8-6-1	0.322	0.201	85	0.0298	0.0647	0.461
8-6-2	0.324	0.201	74	0.0377	0.0651	0.579
8-6-3	0.324	0.201	69	0.0417	0.0651	0.641
8-6-4	0.319	0.201	78	0.0384	0.0641	0.599
Boride V + Graphite Cloth - 1/8" Spacing						
HP80-4	0.314	0.394	206	0.0847	0.124	0.683
Boride V + Graphite Cloth - 1/16" Spacing						
HP82-3	0.314	0.394	164	0.0822	0.124	0.663
HP82-4	0.314	0.394	164	0.0644	0.124	0.519
Boride V + Graphite Cloth - 1/32" Spacing						
HP93-55	0.316	0.395	169	0.0862	0.125	0.691
HP93-65	0.315	0.395	170	0.0731	0.125	0.587
HP93-75	0.316	0.395	165	0.0743	0.125	0.595
HP93-85	0.316	0.395	169	0.0794	0.125	0.636

TABLE 11 (MKS)

SUMMARY OF NOTCHED BAR SLOW BEND AND IMPACT TESTS OF BORIDE V ($80^{v}/_{o}ZrB_2$-$20^{v}/_{o}SiC$)

SLOW BEND TESTS

l= span length = 0.0445M

Number	h (10^{-3}M)	t (10^{-3}M)	P(max) (N)	W (10^{-3}J)	A ($10^{-5}M^2$)	Slow Bend Fracture Energy (W/A) (J/M^2)
3-13-4	8.10	9.91	1001	9.54	8.02	120
5-28-1	8.05	10.00	983	8.75	8.06	109
5-28-2	8.05	10.00	1027	9.40	8.06	117
5-28-3	8.00	10.00	1023	8.71	8.00	109
3-13-5	7.95	5.13	440	4.36	4.08	107
3-13-6	7.95	5.11	471	5.03	4.06	124
5-28-4	8.00	5.08	507	3.90	4.06	96
5-28-5	8.08	5.08	516	4.45	4.10	108
5-28-6	8.05	5.08	516	3.93	4.09	96
3-13-7	7.98	3.23	302	3.11	2.56	121
5-28-7	9.05	3.18	311	3.51	2.55	138
5-28-8	8.03	3.18	302	3.14	2.55	123
5-28-9	8.05	3.18	302	3.04	2.55	119
Boride V + Nickel ($70^{v}/_{o}ZrB_2$-$20^{v}/_{o}Ni$)						
8-6-1	8.18	5.11	378	3.37	4.17	81
8-6-2	8.23	5.11	329	4.26	4.20	101
8-6-3	8.23	5.11	307	4.71	4.20	112
8-6-4	8.10	5.11	347	4.34	4.13	105
Boride V + Graphite Cloth - $18x10^{-3}$M Spacing						
HP80-4	7.98	10.00	916	9.57	8.00	120
Boride V + Graphite Cloth - $9x10^{-3}$M Spacing						
HP82-3	7.98	10.00	729	9.29	8.00	116
HP82-4	7.98	10.00	729	7.28	8.00	91
Boride V + Graphite Cloth - $0.80x10^{-3}$M Spacing						
HP93-55	8.03	10.03	752	9.74	8.06	121
HP93-65	8.00	10.03	756	8.26	8.06	103
HP93-75	8.03	10.03	734	8.40	8.06	104
HP93-85	8.03	10.03	752	8.97	8.06	111

TABLE 12

SUMMARY OF NOTCHED BAR IMPACT TESTS OF

BORIDE V ($80^{v}/o ZrB_2$-$20^{v}/o SiC$)

Number	h (in)	t (in)	IMPACT TESTS ft-lbs = Impact Energy	= (in-lbs/in^2)
HP-28-1	0.315	0.393	0.222	21.5
HP-28-2	0.317	0.393	0.225	21.7
31-L1C	0.317	0.394	0.203	19.6
31-L2C	0.311	0.393	0.382	37.5
31-L3C	0.317	0.394	0.241	23.2
31-L4C	0.316	0.394	0.223	21.5
31-L5C	0.315	0.394	0.277	26.8
31-L6C	0.315	0.394	0.229	22.2
Boride V + Graphite Cloth - 1/8" Spacing				
HP80-1	0.316	0.393	0.272	26.3
HP80-2	0.314	0.393	0.294	28.6
Boride V + Graphite - 1/16" Spacing				
HP82-1	0.312	0.393	0.255	25.0
HP82-2	0.312	0.393	0.262	25.6
Boride V + Graphite - 1/32" Spacing				
HP93-1C	0.315	0.390	0.270	26.4
HP93-2C	0.318	0.390	0.218	21.1
HP93-3C	0.316	0.391	0.230	22.4
HP93-4C	0.314	0.391	0.233	22.8

TABLE 12 (MKS)

SUMMARY OF NOTCHED BAR IMPACT TESTS OF

BORIDE V ($80^{v}/o ZrB_2$-$20^{v}/o SiC$)

Number	h ($10^{-3}M$)	t ($10^{-3}M$)	IMPACT TESTS (J) = Impact Energy	(J/M^2)
HP-28-1	8.00	9.98	0.301	3770
HP-28-2	8.05	9.98	0.305	3800
31-L1C	8.05	10.00	0.275	3430
31-L2C	7.90	9.98	0.518	6570
31-L3C	8.05	10.00	0.327	4060
31-L4C	8.03	10.00	0.302	3770
31-L5C	8.00	10.00	0.376	4690
31-L6C	8.00	10.00	0.311	3890
Boride V + Graphite Cloth-$3.18 \times 10^{-3}M$ Spacing				
HP80-1	8.03	9.98	0.369	4610
HP80-2	7.98	9.98	0.399	5010
Boride V + Graphite - $1.59 \times 10^{-3}M$ Spacing				
HP82-1	7.92	9.98	0.346	4380
HP82-2	7.92	9.98	0.355	4480
Boride V + Graphite - $0.80 \times 10^{-3}M$ Spacing				
HP93-1C	8.00	9.91	0.366	4620
HP93-2C	8.08	9.91	0.296	3700
HP93-3C	8.03	9.93	0.312	3920
HP93-4C	7.98	9.93	0.316	3990

TABLE 13

SUMMARY OF NOTCHED BAR SLOW BEND AND IMPACT TESTS
OF TUNGSTEN CARBIDE - 6^{W}poCo (90^{V}/oWC-10^{V}/oCo)

SLOW BEND TESTS

l = span length = 1.75 inches

Number	h (in)	t (in)	P(max) (lbs)	W (in-lbs)	A_2 (in^2)	Slow Bend Fracture Energy $(W/A)_2$ (in-lbs/in^2)
10-6-5	0.316	0.203	270	0.1431	0.0641	2.23
10-6-6	0.317	0.202	268	0.1675	0.0640	2.62
10-6-7	0.317	0.202	282	0.1720	0.0643	2.68
10-6-8	0.317	0.202	254	0.1600	0.0640	2.50
4S	0.309	0.394	482	0.2076	0.1217	1.71
9S	0.322	0.395	562	0.3934	0.1272	3.09
10S	0.316	0.394	530	0.3551	0.1243	2.86
11S	0.317	0.395	535	0.3478	0.1252	2.78
12S	0.319	0.395	558	0.3794	0.1260	3.01

IMPACT TESTS

			ft-lbs = Impact Energy	= (in-lbs/in^2)
1C	0.318	0.394	0.608	58.2
2C	0.313	0.394	0.700	68.1
6C	0.314	0.395	0.916	88.9
7C	0.311	0.395	0.754	73.8
8C	0.312	0.395	0.778	76.0
13C	0.316	0.395	0.878	85.5
14C	0.320	0.395	0.706	67.1

TABLE 13 (MKS)

SUMMARY OF NOTCHED BAR SLOW BEND AND IMPACT TESTS

OF TUNGSTEN CARBIDE - $6^{w}/_{o}Co$ ($90^{v}/_{o}WC$-$10^{v}/_{o}Co$)

SLOW BEND TESTS

l = span length = 0.0445M

Number	h ($10^{-3}M$)	t ($10^{-3}M$)	P(max) (N)	W ($10^{-3}J$)	A ($10^{-5}M^2$)	Slow Bend Fracture Energy (W/A) (J/M^2)
10-6-5	8.03	5.16	1210	16.17	4.13	391
10-6-6	8.05	5.13	1201	18.93	4.13	459
10-6-7	8.05	5.13	1263	19.44	4.15	470
10-6-8	8.05	5.13	1138	18.08	4.13	438
4S	7.85	10.00	2159	23.46	7.85	300
9S	8.18	10.03	2518	44.45	8.20	541
10S	8.03	10.00	2374	40.13	8.02	501
11S	8.05	10.03	2397	39.30	8.08	487
12S	8.10	10.03	2500	42.87	8.13	527

IMPACT TESTS

			(J) = Impact Energy =	(J/M^2)
1C	8.08	10.00	0.824	10,200
2C	7.95	10.00	0.949	11,930
6C	7.98	10.03	1.242	15,580
7C	7.90	10.03	1.022	12,930
8C	7.92	10.03	1.055	13,320
13C	8.03	10.03	1.191	14,980
14C	8.13	10.03	0.957	11,760

TABLE 14

SUMMARY OF NOTCHED BAR SLOW BEND AND IMPACT TESTS
OF BORIDE VIII ($56^{v}/oZrB_2$-$14^{v}/oSiC$-$30^{v}/oC$)

SLOW BEND TESTS

l = span length = 1.75 inches

Number	h (in)	t (in)	P(max) (lbs)	W (in-lbs)	A (in^2)	Slow Bend Fracture Energy (W/A) (in-lbs/in^2)
D198						
10-6-1	0.318	0.202	112	0.0689	0.0641	1.08
10-6-2	0.317	0.201	111	0.0705	0.0636	1.11
10-6-3	0.321	0.200	115	0.0661	0.0642	1.03
D201M						
3S	0.314	0.394	190	0.1101	0.1240	0.89
4S	0.314	0.394	180	0.1074	0.1240	0.87
11S	0.321	0.393	212	0.1717	0.1260	1.36
12S	0.318	0.393	203	0.1543	0.1248	1.24
13S	0.313	0.393	206	0.1751	0.1230	1.42
14S	0.314	0.393	205	0.1579	0.1234	1.28
15S	0.317	0.393	201	0.1387	0.1244	1.12
16S	0.315	0.393	206	0.1318	0.1238	1.07

IMPACT TESTS

			ft-lbs = Impact Energy =	(in-lbs/in^2)
D201M				
5C	0.318	0.393	0.169	16.3
6C	0.314	0.393	0.173	16.8
7C	0.316	0.393	0.196	19.0
8C	0.318	0.394	0.200	19.2
9C	0.316	0.394	0.193	18.7
10C	0.319	0.393	0.172	16.5
1C	0.310	0.394	0.181	17.8
2C	0.311	0.394	0.172	17.5

TABLE 14(MKS)

SUMMARY OF NOTCHED BAR SLOW BEND AND IMPACT TESTS

OF BORIDE VIII ($56^{v}/oZrB_2$-$14^{v}/oSiC$-$30^{v}/oC$)

SLOW BEND TESTS

l = span length = 0.0445M

Number	h (10^{-3}M)	t (10^{-3}M)	P(max) (N)	W (10^{-3}J)	A ($10^{-5}M^2$)	Slow Bend Fracture Energy (W/A) (J/M^2)
D198						
10-6-1	8.08	5.13	498	7.79	4.13	189
10-6-2	8.05	5.11	494	7.97	4.10	194
10-6-3	8.15	5.08	512	7.47	4.03	180
D201M						
3S	7.98	10.00	845	12.44	8.00	156
4S	7.98	10.00	801	12.14	8.00	152
11S	8.15	9.98	943	19.40	8.13	238
12S	8.08	9.98	903	17.44	8.05	217
13S	7.95	9.98	916	19.79	7.93	249
14S	7.98	9.98	912	17.84	7.96	224
15S	8.05	9.98	894	15.67	8.02	196
16S	8.00	9.98	916	14.89	7.99	187

IMPACT TESTS

			(J) = Impact Energy=	(J/M^2)
D201M				
5C	8.08	9.98	0.229	2860
6C	7.98	9.98	0.235	2940
7C	8.03	9.98	0.266	3330
8C	8.08	10.00	0.271	3360
9C	8.03	10.00	0.262	3280
10C	8.10	9.98	0.233	2890
1C	7.87	10.00	0.245	3120
2C	7.90	10.00	0.233	3070

TABLE 15

SUMMARY OF NOTCHED BAR SLOW BEND AND IMPACT TESTS

OF BORIDE VIII ($56^{v}/oZrB_2$-$14^{v}/oSiC$-$30^{v}/oC$)M2

SLOW BEND TESTS

l = span length = 1.75 inches

Number	h (in)	t (in)	P(max) (lbs)	W (in-lbs)	A (in^2)	Slow Bend Fracture Energy W/A (in-lbs/in^2)
HP45						
8-31-1	0.316	0.200	120	0.1140	0.0632	1.80
8-31-2	0.321	0.200	123	0.0836	0.0642	1.30
8-31-3	0.317	0.200	122	0.0970	0.0632	1.53
8-31-4	0.318	0.200	147	0.1169	0.0635	1.84
NP 2						
3S	0.314	0.394	224	0.1668	0.1240	1.36
4S	0.314	0.394	179	0.1250	0.1240	1.01
11S	0.317	0.394	208	0.1726	0.1249	1.38
12S	0.317	0.394	176	0.1584	0.1249	1.27
13S	0.315	0.394	198	0.1841	0.1241	1.48
14S	0.314	0.394	181	0.1620	0.1237	1.31
15S	0.315	0.394	178	0.1566	0.1241	1.26
16S	0.313	0.394	179	0.1593	0.1233	1.29

IMPACT TESTS

		ft-lbs	= Impact Energy = (in-lbs/in^2)
NP 2			
1C	0.318	3.393	0.168 16.1
2C	0.314	0.393	0.186 18.1
5C	0.315	0.394	0.183 17.7
6C	0.317	0.394	0.170 16.3
7C	0.314	0.394	0.169 16.4
8C	0.318	0.394	0.172 16.5
9C	0.315	0.394	0.213 20.6
10C	0.310	0.394	0.173 17.0

TABLE 15 (MKS)

SUMMARY OF NOTCHED BAR SLOW BEND AND IMPACT TESTS

OF BORIDE VIII ($56^{v}/oZrB_2$-$14^{v}/oSiC$-$30^{v}/oC$)M2

SLOW BEND TESTS

l = span length = 0.0445

Number	h (10^{-3}M)	t (10^{-3}M)	P(max) (N)	W (10^{-3}J)	A ($10^{-5}M^2$)	Slow Bend Fracture Energy (W/A) (J/M^2)
HP45						
8-31-1	8.03	5.08	534	12.88	4.08	315
8-31-2	8.15	5.08	547	9.45	4.14	228
8-31-3	8.05	5.08	543	10.96	4.08	268
8-31-4	8.08	5.08	654	13.21	4.10	322
NP 2						
3S	7.98	10.00	996	18.85	8.00	238
4S	7.98	10.00	796	14.13	8.00	177
11S	8.05	10.00	925	19.50	8.06	242
12S	8.05	10.00	783	17.90	8.06	223
13S	8.00	10.00	881	20.80	8.00	259
14S	7.98	10.00	805	18.31	8.00	230
15S	8.00	10.00	792	17.70	8.00	221
16S	7.95	10.00	796	18.00	7.95	226

IMPACT TESTS

			(J) = Impact Energy =			(J/M^2)
NP2						
1C	8.08	9.98	0.228			2820
2C	7.98	9.98	0.252			3170
5C	8.00	10.00	0.248			3100
6C	8.05	10.00	0.231			2850
7C	7.98	10.00	0.229			2870
8C	8.08	10.00	0.233			2890
9C	8.00	10.00	0.289			3610
10C	7.87	10.00	0.235			2980

TABLE 16

SUMMARY OF NOTCHED BAR IMPACT TESTS

OF 80^{w}/oZrB_2-20^{w}/o NICKEL

Number	h (in)	t (in)	ft-lbs ≡ Impact Energy ≡	(in-lbs/in^2)
HP901C	0.317	0.394	0.266	25.6
HP902C	0.316	0.394	0.286	27.6
HP911C	0.317	0.394	0.239	23.0
HP912C	0.318	0.394	0.252	24.2

TABLE 16 (MKS)

SUMMARY OF NOTCHED BAR IMPACT TESTS

OF 80w/oZrB$_2$-20w/o NICKEL

Number	h (10^{-3}M)	t (10^{-3}M)	(J) = Impact Energy =	(J/M^2)
HP901C	8.05	10.00	0.361	4490
HP902C	8.03	10.00	0.388	4840
HP911C	8.05	10.00	0.324	4030
HP912C	8.08	10.00	0.342	4240

TABLE 17

SUMMARY OF NOTCHED BAR SLOW BEND AND IMPACT TESTS

OF $90^{w}/oZrB_2$-$10^{w}/o$ IRON

SLOW BEND TESTS

l = span length = 1.75 inches

Number	h (in)	t (in)	P(max) (lbs)	W (in-lbs)	A (in^2)	Slow Bend Fracture Energy (W/A) (in-lbs/in^2)
HP98-4S	0.313	0.394	126	0.0451	0.1233	0.368
HP98-5S	0.317	0.395	128	0.0512	0.1251	0.409
(ρ=5.84 gms/cm^3)						
HP101-4S	0.315	0.392	124	0.0645	0.1233	0.523
HP101-5S	0.314	0.390	133	0.0532	0.1226	0.434
HP101-6S	0.318	0.391	147	0.0588	0.1244	0.473
(ρ=6.03 gms/cm^3)						

IMPACT TESTS

			ft-lbs = Impact Energy	=(in-lbs/in^2)
HP98-1C	0.318	0.395	0.231	22.1
HP98-2C	0.319	0.395	0.228	21.8
HP98-3C	0.320	0.395	0.226	21.5
(ρ=5.84 gms/cm^3)				
HP101-1C	0.321	0.391	0.230	22.0
HP101-2C	0.318	0.392	0.232	22.4
HP101-3C	0.319	0.391	0.253	24.3
(ρ=6.03 gms/cm^3)				

TABLE 17 (MKS)

SUMMARY OF NOTCHED BAR SLOW BEND AND IMPACT TESTS OF $90^{w}/oZrB_2$-$10^{w}/o$ IRON

SLOW BEND TESTS

l = span length = 0.0445M

Number	h (10^{-3}M)	t (10^{-3}M)	P(max) (N)	W (10^{-3}J)	A ($10^{-5}M^2$)	Slow Bend Fracture Energy (W/A) (J/M^2)
HP98-4S	7.95	10.00	560	5.10	7.95	64.5
HP98-5S	8.05	10.03	569	5.79	8.07	71.7
($\rho = 5.84 \times 10^{-3} kg/M^3$)						
HP101-4S	8.00	9.96	552	7.29	7.95	91.6
HP101-5S	7.98	9.91	592	6.01	7.91	76.0
HP101-6S	8.08	9.93	654	6.64	8.02	82.9
($\rho = 6.03 \times 10^{-3} kg/M^3$)						

IMPACT TESTS

(J) ≡ Impact Energy = (J/M^2)

HP98-1C	8.08	10.03	0.313	3870
HP98-2C	8.10	10.03	0.309	3820
HP98-3C	8.13	10.03	0.306	3770
($\rho = 5.84 \times 10^{-3} kg/M^3$)				
HP101-1C	8.15	9.93	0.312	3850
HP101-2C	8.08	9.96	0.315	3920
HP101-3C	8.10	9.93	0.343	4260
($\rho = 6.03 \times 10^{-3} kg/M^3$)				

TABLE 18

SUMMARY OF NOTCHED BAR SLOW BEND AND IMPACT TEST DATA

(height under notch, h = 0.312-0.324 inches)

Material	Bar Thickness t(in)	Average Slow Bend Fracture Energy (in-lbs/in^2)	Average Impact Fracture Energy (in-lbs/in^2)
Boride V	0.394	0.65	24.3
Boride V	0.200	0.61	-
Boride V	0.125	0.72	-
Boride V + Nickel	0.201	0.57	-
Boride V + Graphite Cloth (1/8" Spacing)	0.394	0.68	27.5
Boride V + Graphite Cloth (1/16" Spacing)	0.394	0.59	25.3
Boride V + Graphite Cloth (1/32" Spacing)	0.395	0.63	23.2
90^v/oWC-10^v/oCo	0.202	2.51	-
90^v/oWC-10^v/oCo	0.394	2.69	73.9
Boride VIII	0.202	1.07	-
Boride VIII	0.394	1.16	17.7
Boride VIII M2	0.200	1.62	-
Boride VIII M2	0.394	1.30	17.3
ZrB_2 + Nickel	0.394	-	25.1
ZrB_2 + Iron $\rho = 5.84$ gm/cm^3	0.395	0.40	21.8
ZrB_2 + Iron $\rho = 6.03$ gm/cm^3	0.395	0.48	22.9

TABLE 18 (MKS)

SUMMARY OF NOTCHED BAR SLOW BEND AND IMPACT TEST DATA

(height under notch, $h = 7.42\text{-}8.23 \times 10^{-3}$M)

Material	Bar Thickness $t\ (10^{-3}M)$	Average Slow Bend Fracture Energy (J/M^2)	Average Impact Fracture Energy (J/M^2)
Boride V	10.00	114	4260
Boride V	5.08	107	--
Boride V	3.18	126	--
Boride V + Nickel	5.11	100	--
Boride V + Graphite Cloth (3.18×10^{-3}M Spacing)	10.00	119	4820
Boride V + Graphite Cloth (1.59×10^{-3}M Spacing)	10.00	103	4430
Boride V + Graphite Cloth (0.80×10^{-3}M Spacing)	10.03	110	4060
90 v/o WC - 10 v/o Co	5.13	440	--
90 v/o WC - 10 v/o Co	10.00	471	12950
Boride VIII	5.13	187	--
Boride VIII	10.00	203	3100
Boride VIII M2	5.08	284	--
Boride VIII M2	10.00	228	3030
ZrB_2 + Nickel	10.00	--	4400
ZrB_2 + Iron $\rho = 5.84 \times 10^{-3} kg/M^3$	10.03	70	3820
ZrB_2 + Iron $\rho = 6.03 \times 10^{-3} kg/M^3$	10.03	84	4010

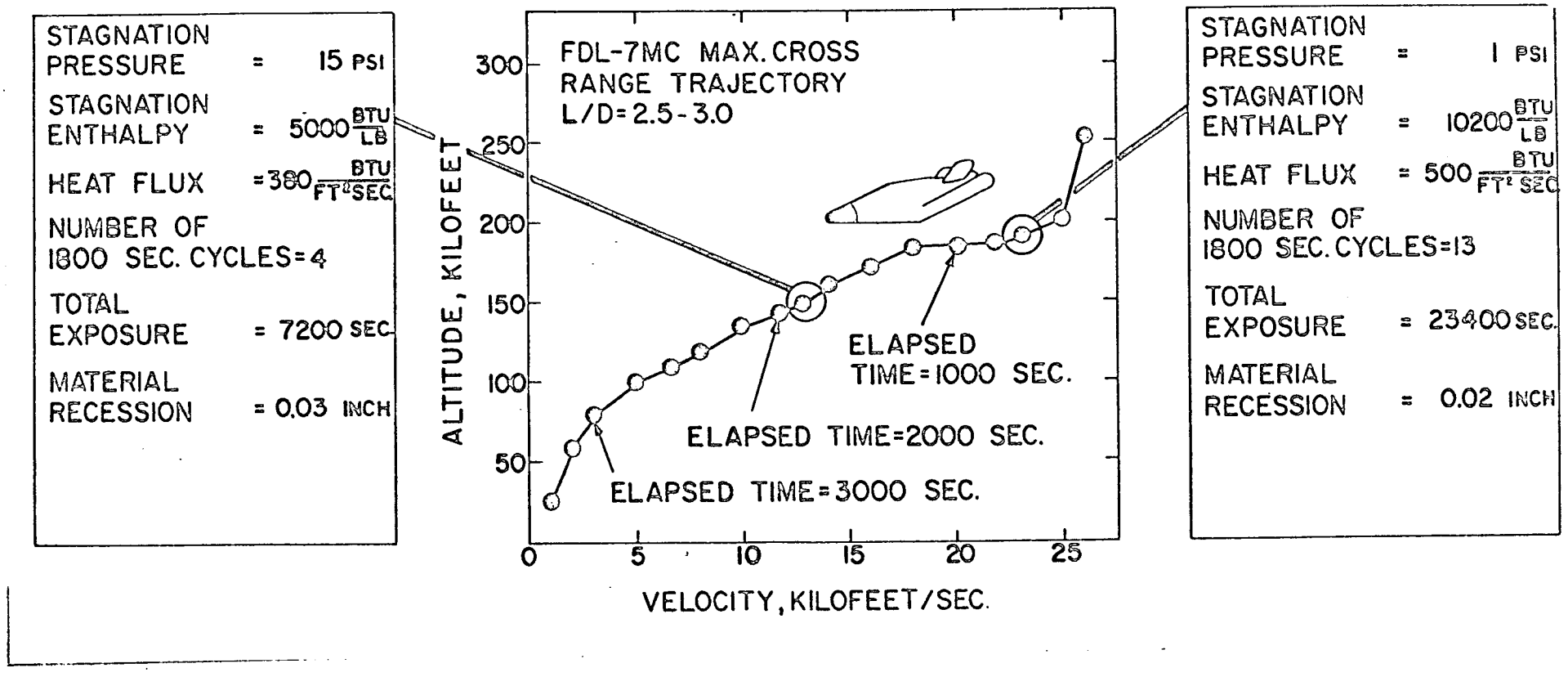

Figure 1. Schematic Representation of Reuse Capabilities of Boride Composites.

15 PSI	= 1.02 atm.	1 PSI	= 0.068 atm
5000 BTU/lb	= 1.16×10^{7} J/kg	10200 BTU/lb	= 2.37×10^{7} J/kg
380 BTU/ft^{2}sec	= 4.31×10^{6} J/M^{2}sec	500 BTU/ft^{2}sec	= 5.68×10^{6} J/M^{2}sec
0.03 in.	= 7.62×10^{-4} M	0.02 in.	= 5.08×10^{-4} M

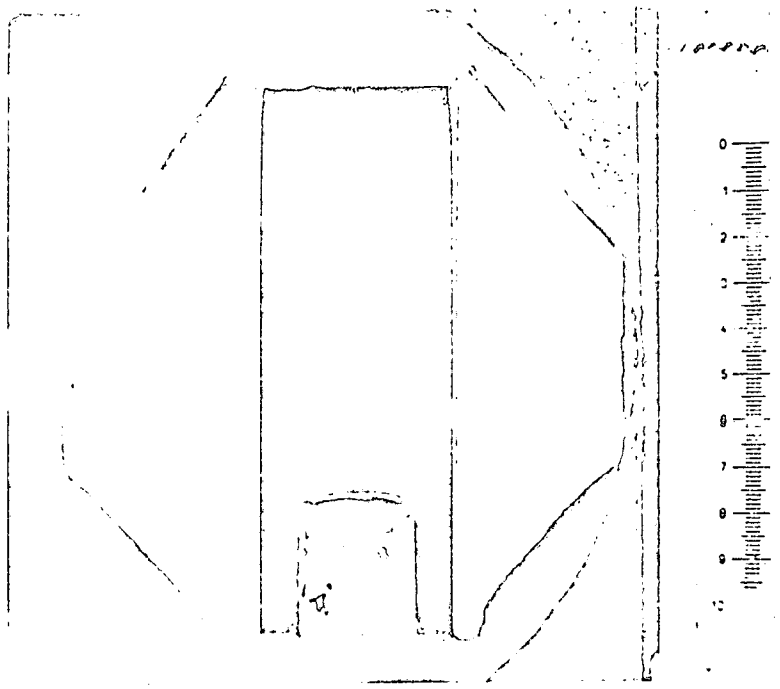

Plate No. 2-0675

10300 BTU/lb = 2.39×10^{7} J/kg

495 BTU/ft^2sec = 5.62×10^{6} J/M^2sec

15 mils = 3.81×10^{-4} M

X2.38

Figure 2. Arc Plasma Test Boride V (Hf)$HfB_{2.1}$+20% SiC Average Surface Temperature 4650°F, Exposure Time 22,400 Seconds (13 cyclic exposures each of approximately 1800 seconds), Stagnation Pressure 0.07 Atm., Stagnation Enthalpy 10,300 BTU/lb, Cold Wall Heat Flux 495 BTU/ft^2Sec. 15 Mils Recession, Hot Face Up. One Inch Scale.

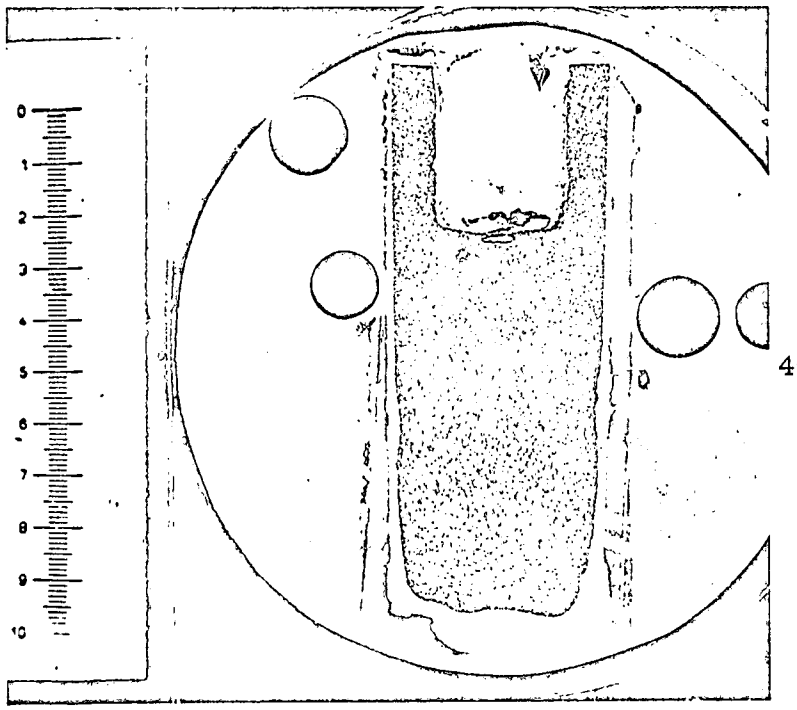

Plate No. 2-0595

4250 BTU/lb = 0.99×10^{7} J/kg

400 BTU/ft^2sec = 4.54×10^{6} J/M^2sec

104 Mils = 2.64×10^{-3} M

X2.69

Figure 3. Arc Plasma Test Boride VIII(14,30)ZrB_2+SiC+C Average Surface Temperature 4415°F, Exposure Time 21,600 Seconds (12 cyclic exposures each of 1800 seconds), Stagnation Pressure 1.02 Atm., Stagnation Enthalpy 4250 BTU/lb, Cold Wall Heat Flux 400 BTU/ft^2sec, 104 Mils Recession, Hot Face Down. One Inch Scale.

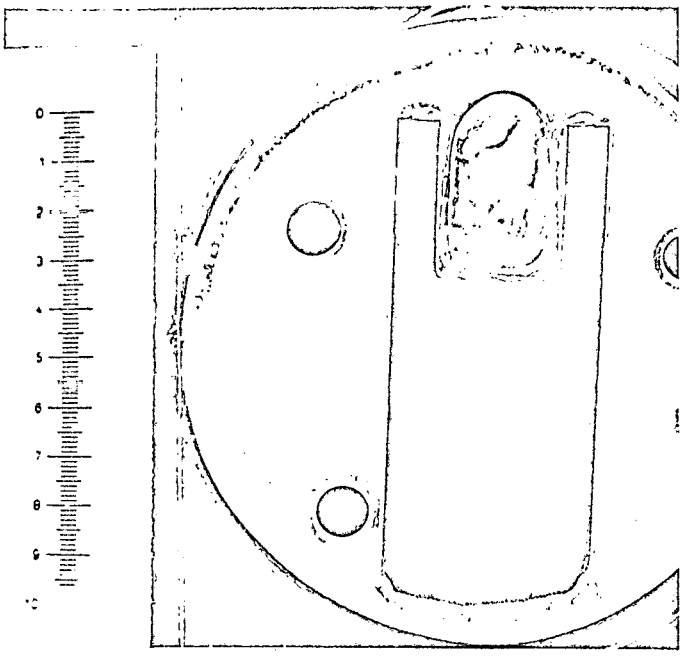

Plate No. 2-0222

5000BTU/lb = 1.16×10^{7} J/kg

385 BTU/ft^2sec = 4.37×10^{6} J/M^2sec

26 Mils = 6.6×10^{-4} M

X2.50

Figure 4. Arc Plasma Test Boride V, $ZrB_{2.1}$+20%SiC Average Surface Temperature 4550°F, Exposure Time 7200 Seconds (4 cyclic exposures each of 1800 seconds), Stagnation Pressure 1.00 Atm., Stagnation Enthalpy 5000 BTU/lb, Cold Wall Heat Flux 385 BTU/ft^2-sec. 26 Mils Recession, Hot Face Down. One Inch Scale.

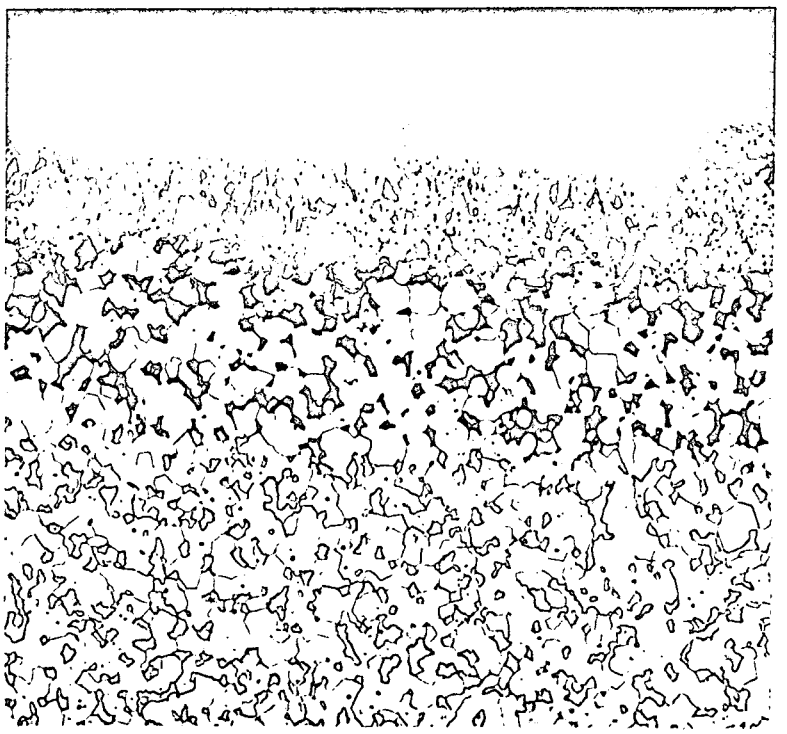

Plate No. 2-0223

Etched X2 50

Figure 5. Arc Plasma Test Boride V, $ZrB_{2.1}$+20%SiC, Hot Surface.

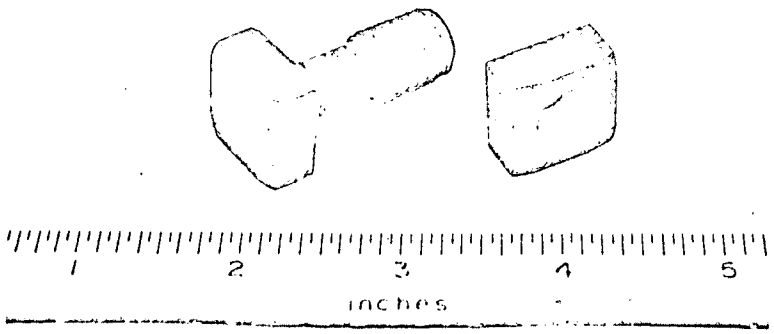

Figure 6. Nut and Bolt Machined from Boride VIII(14,30)-M2 Using Carbide Tooling.

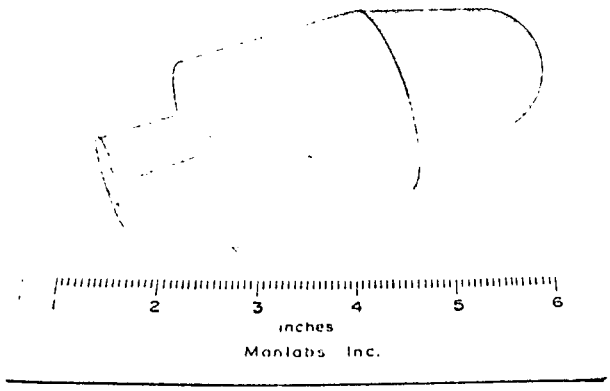

Plate No. 6029

8500 BTU/lb = 1.98×10^{7} J/kg

548 BTU/ft^2sec = 6.21×10^{6} J/M^2sec

29 Mils = 7.37×10^{-4} M

Figure 7. Boride Male Nosetip Assembly for Arc Plasma Testing Showing Boride Nosetip in R512C coated Ta-10W Holder attached to Ta-10W sting. This assembly was run at 4555°F in air at 0.071 atm. in the Avco Rovers Arc at Mach 3.2 for 30 minutes with a recession of 29 mils. The Heat Flux was 548 BTU/ft^2sec at an enthalpy level of 8500 BTU/lb. No cracks were observed during or after testing.

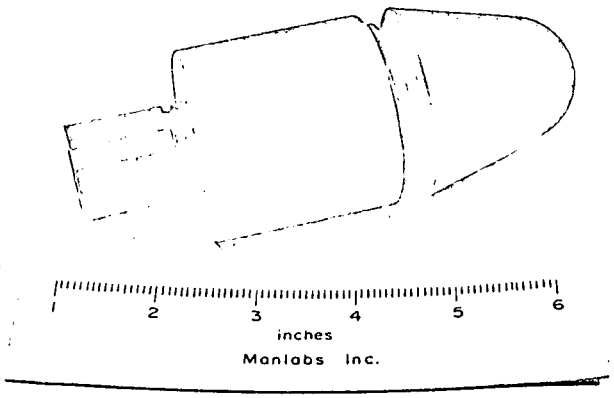

Plate No. 6030

Figure 8. Partial Disassembly of Boride Male Nosetip Assembly showing threaded joints. The nosetip was fabricated from ManLabs Boride VIII-M2 (ZrB_2+SiC+C) Composite.

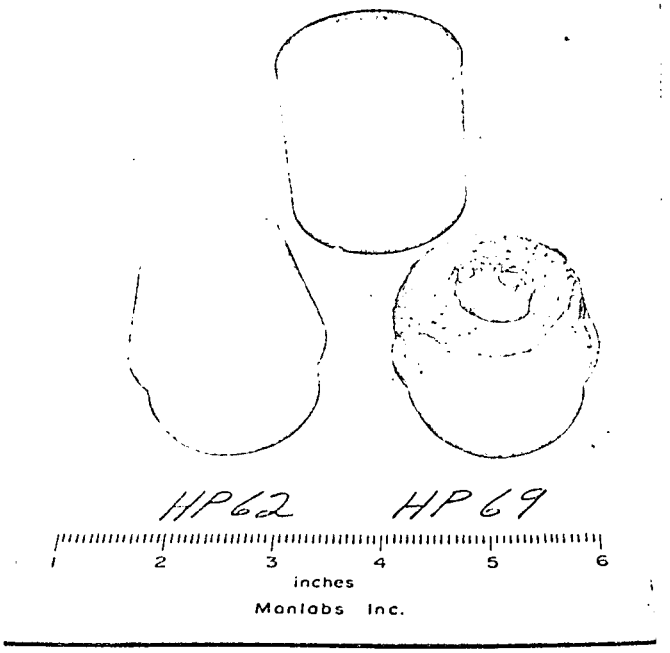

Plate No.
6114

8900 BTU/lb = 2.07×10^{7} J/kg

500 BTU/ft^2sec = 5.68×10^{6} J/M^2sec

29 Mils = 7.36×10^{-4} M

Figure 9. Post Exposure Photographs of Boride VIII-M2 Male Nosetips. HP69 ran to destruction at Mach 3.2 under ascending conditions at Stagnation Pressures near 0.07 Atm. Little degradation was observed after 277 seconds at 289 BTU/ft^2sec, 5400 BTU/lb, 2440°F, 349 seconds at 381 BTU/ft^2sec, 6700 BTU/lb, 2595°F, 390 seconds at 500 BTU/ft^2sec, 8900 BTU/lb, 3110°F. Exposure at 708 BTU/ft^2sec and 9400 BTU/lb resulted in surface temperatures near 5100°F and resulted in thermal shock failure and melting. HP62 ran for 1800 seconds at a Stagnation Pressure of 0.071 Atm., Stagnation Enthalpy of 8500 BTU/lb, Cold Wall Heat Flux of 548 BTU/ft^2sec and a surface temperature of 4555°F. Total oxidation depth after exposure was 29 mils. Subsequent to exposure, HP62 was easily unscrewed from the Ta-10W holder.

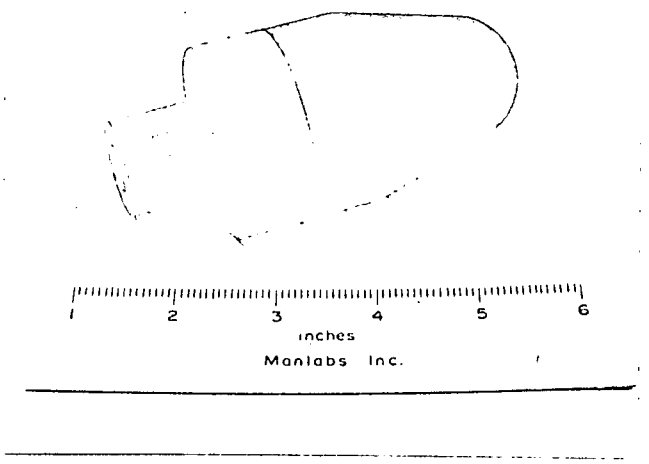

Plate No. 6024

8550 BTU/lb = 1.99×10^{7} J/kg

520 BTU/ft^2 sec = 5.90×10^{6} J/M^2sec

36 Mils = 9.1×10^{-4} M

Figure 10. Boride Female Nosetip Assembly for Arc Plasma Testing, showing Boride Nosetip in R512C coated Ta-10W Holder attached to Ta-10W sting. This assembly was run at 4920°F in air at 0.063 atm. in the Avco Rovers Arc at Mach 3.2 for 30 minutes with a recession of 36 mils. The Heat Flux was 520 BTU/ft^2sec at an enthalpy level of 8550 BTU/lb. No cracks were observed during or after testing.

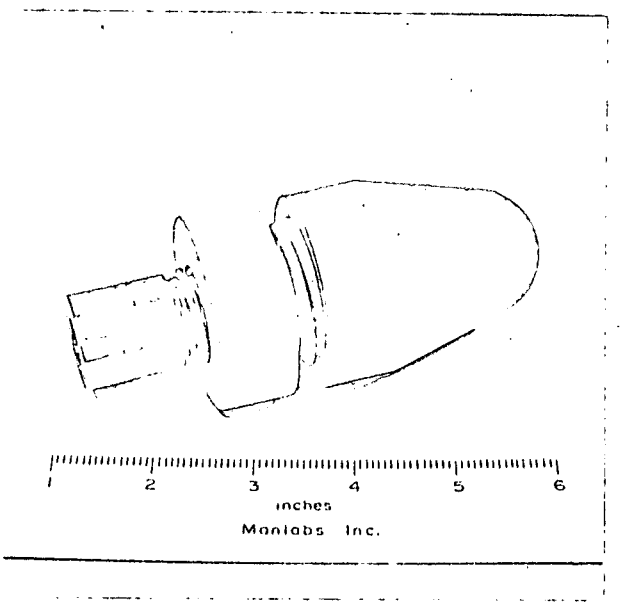

Plate No. 6025

Figure 11. Partial Disassembly of Boride Female Nosetip Assembly showing threaded joints. The nosetip was fabricated from ManLabs Boride VIII-M2 (ZrB_2+SiC+C) Composite.

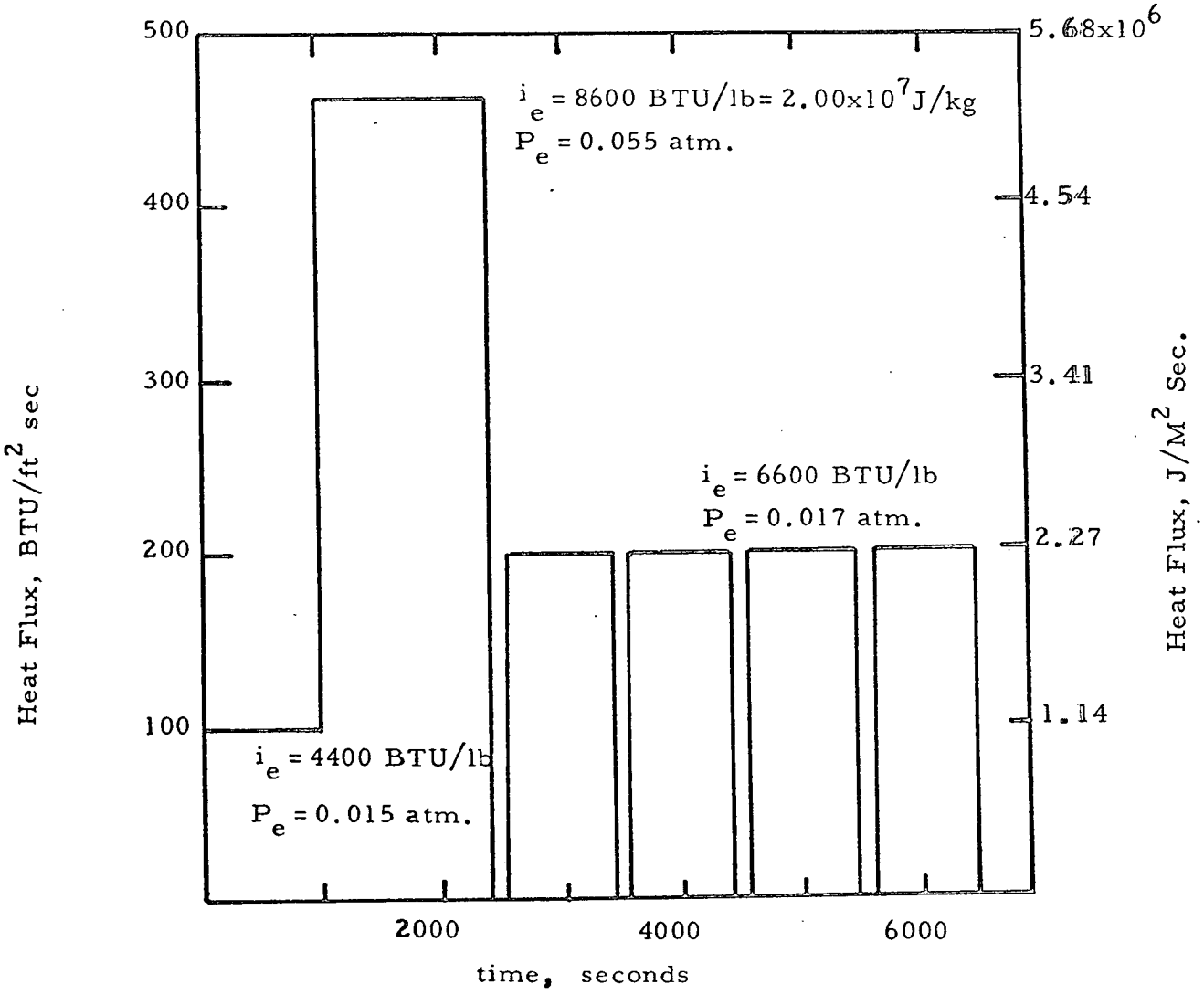

Figure 12 . Exposure history for Boride Male Nosetip Boride VIII-M2-9X

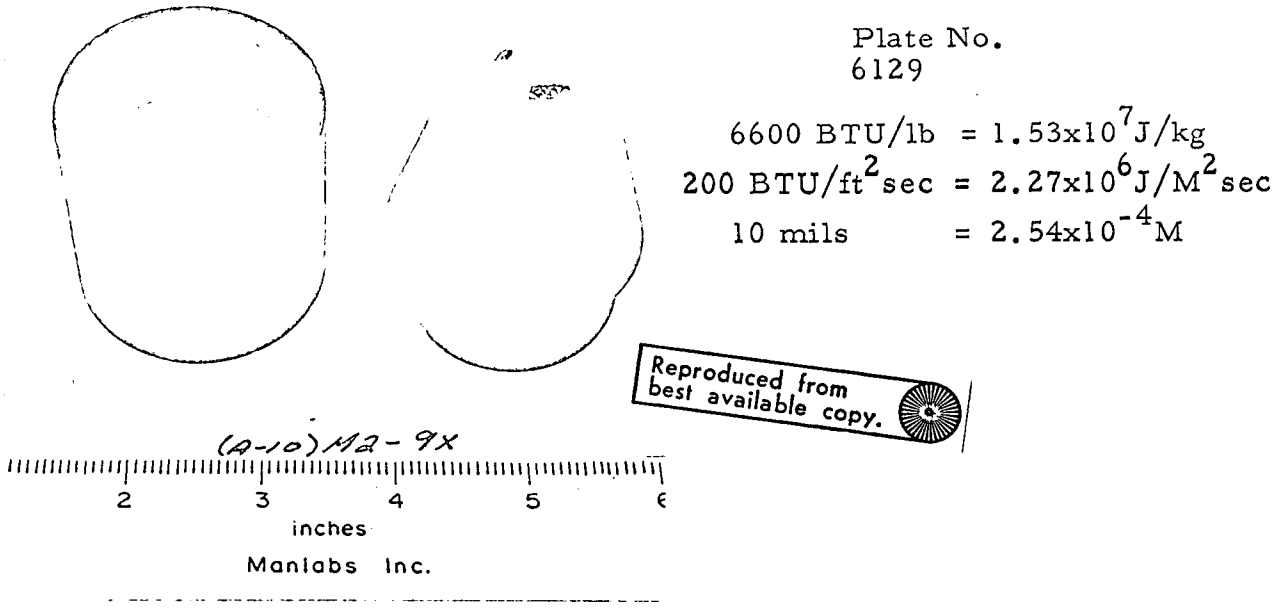

Figure 13. Post Exposure Photographs of Boride VIII-M2 Male Nosetip HP9X following exposure illustrated in Figure 12. The sequence consisted of a 1000 second hold at 0.015 Atm, 112 BTU/ft^{2}sec, 4400 BTU/lb, 1662°F followed by direct heating for 1500 seconds at 0.055 atm., 464 BTU/ft^{2}sec, 8600 BTU/lb, 3790°F. After exposure the model was cooled for 50 seconds by removal from the stream. Subsequently it was reinserted four separate times for 1000 second holds at 200 BTU/ft^{2}sec, 6600 BTU/lb and 0.017 Atm interupted by 50 second removals from the stream. Surface temperatures of 3110°F, 3130°F, 3220°F and 3290°F were observed during these holds. Total oxidation depth was 10 mils. Nosetip HP9X was easily unscrewed from the holder after test.

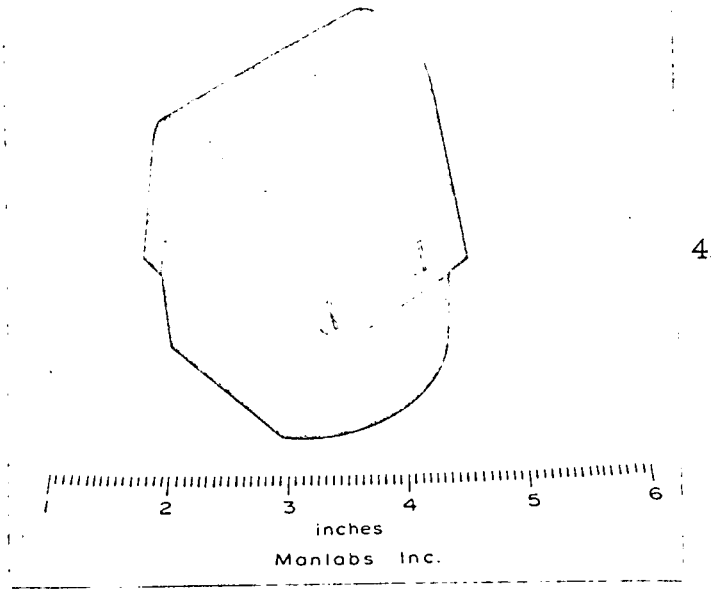

Plate No. 6047

10,800 BTU/lb = 2.5×10^{7} J/kg

452 BTU/ft^2sec = 5.13×10^{6} J/M^2sec

46 mils = 1.16×10^{-3} M

Figure 14. Boride Female Leading Edge Assembly for Arc Plasma Testing showing Boride Leading Edge in R512C coated Ta-10W Holder at Ta-10W Bolts in place. This assembly was run at 5090°F in air at 0.062 atm in the Avco Rovers arc for 30 minutes at Mach 3.2 with a recession of 46 mils. The Heat Flux was 452 BTU/ft^2sec at an enthalpy level of 10,800 BTU/lb. No cracks were observed during or after the test.

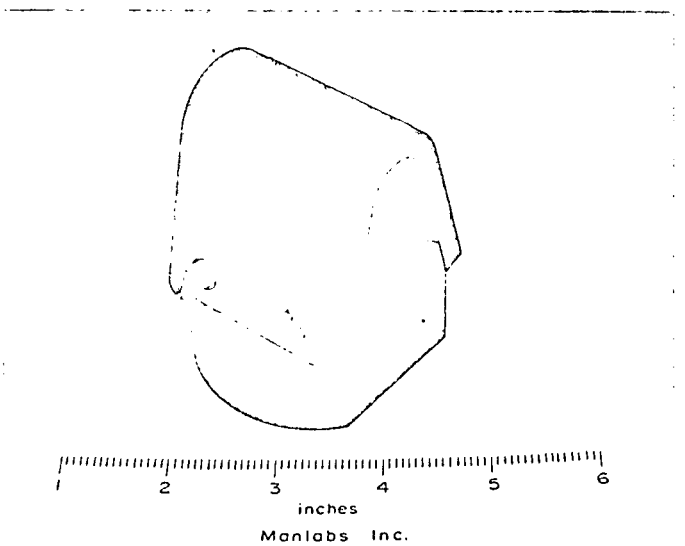

Plate No. 6049

Figure 15. Boride Female Leading Edge Assembly showing one of the Ta-10W bolts removed. The Leading Edge component was fabricated from ManLabs Boride VIII-M2 (ZrB_2+SiC+C) Composite.

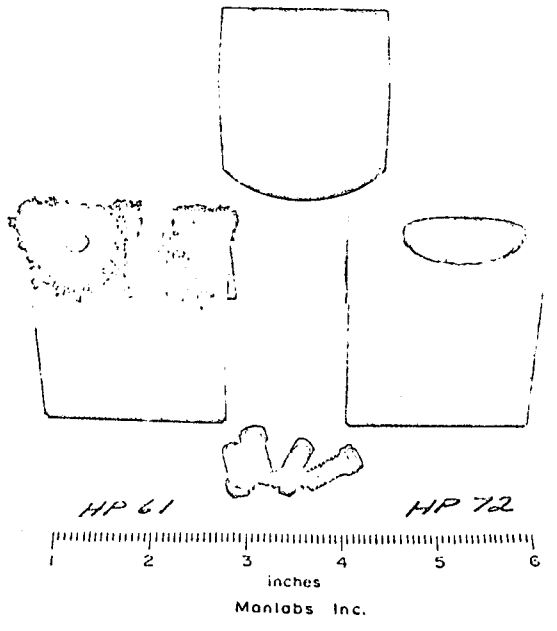

Plate No.
6126

8600 BTU/lb = 2.00×10^{7} J/kg

408 BTU/ft^2sec = 4.63×10^{6} J/M^2sec

46 Mils = 1.16×10^{-3} M

Figure 16. Post Exposure Photographs of Boride VIII-M2 Female Leading Edges. HP61 ran to destruction at Mach 3.2 under ascending conditions at Stagnation Pressures near 0.07 Atm. Little degradation was observed after 435 seconds at 160 BTU/ft^2sec, 4750 BTU/lb, 2180°F; 335 seconds at 242 BTU/ft^2sec., 6500 BTU/lb, 2440°F, 407 seconds at 322 BTU/ft^2sec. 8000 BTU/lb, 2595°F and 474 seconds at 408 BTU/ft^2 sec. 8600 BTU/lb and 2910°F. During the subsequent exposure for 58 seconds at 617 BTU/ft^2sec, 10500 BTU/lb and 0.085 atm, the stream developed non uniformities and burn-through occurred on the left side of HP61 shown above. No cracks were formed. HP72 ran at a Stagnation Pressure of 0.062 atm, Stagnation Enthalpy of 10800 BTU/lb, Cold Wall Heat Flux of 452 BTU/ft^2sec and a surface temperature of 5090°F for 1800 seconds. Total oxidation depth was 46 mils. The tantalum bolts employed in Tests HP61 and HP72 are shown above.

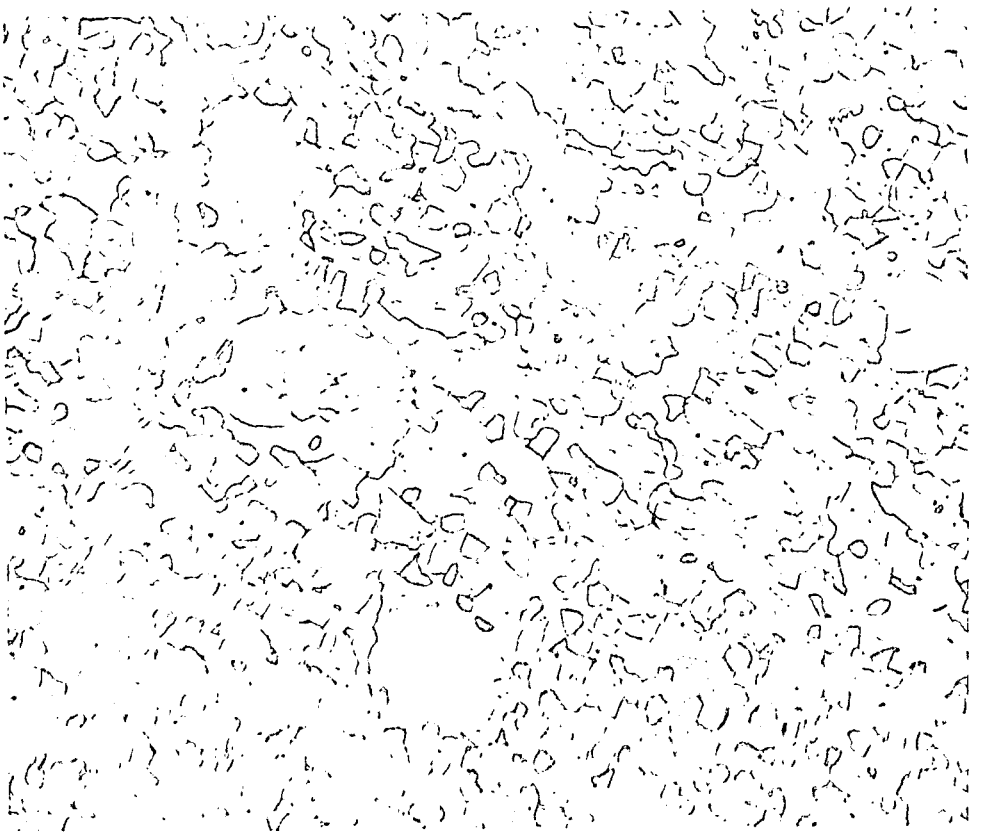

Plate No.
5775

Etched with 10 Gylcerine 5HNO_3:HF X500

Figure 17. Microstructural Characteristics of Boride V (80^V/oZrB_2-20^V/oSiC)

Plate No.
6164

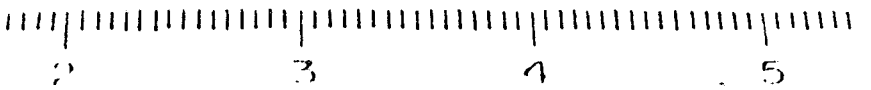

Figure 18. Macrophotograph of Graphite Reinforced Material V, HP80

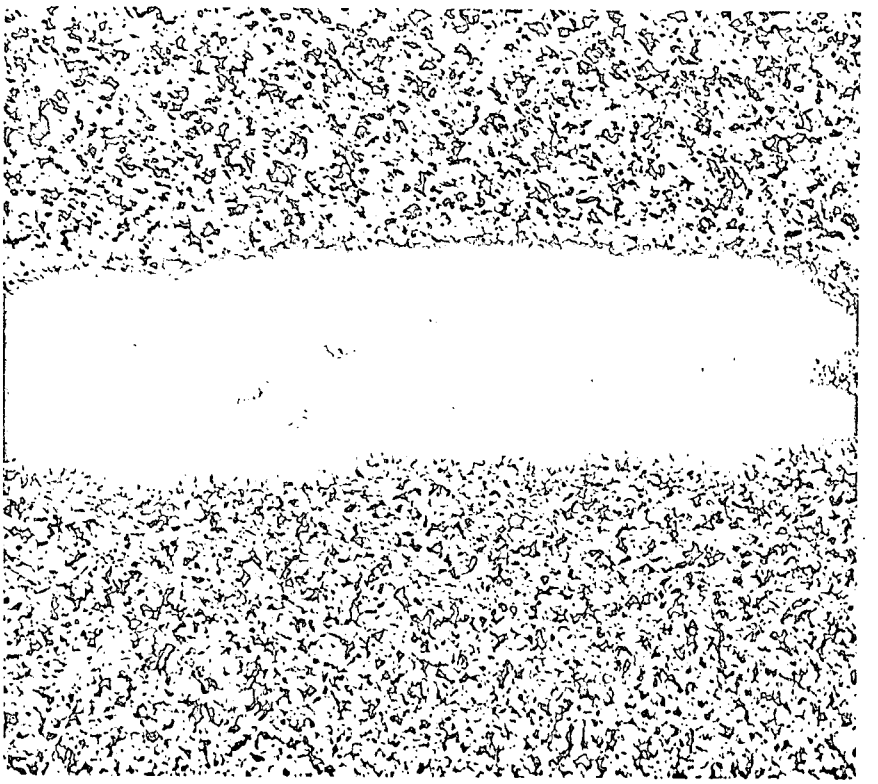

Plate No.
6171

As Polished 100X

Figure 19. Macrophotograph of Graphite Reinforced Material V, HP80, Perpendicular Orientations.

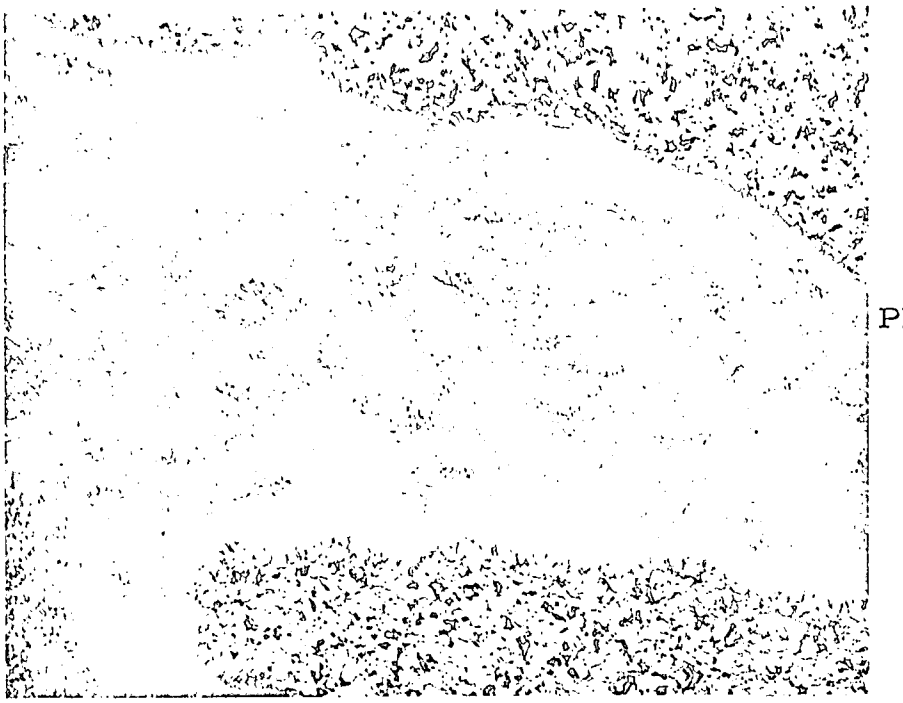

Plate No. 6173

As Polished 100X

Figure 20. Macrophotographs of Parallel Orientations of Graphite Reinforced Material V, HP80.

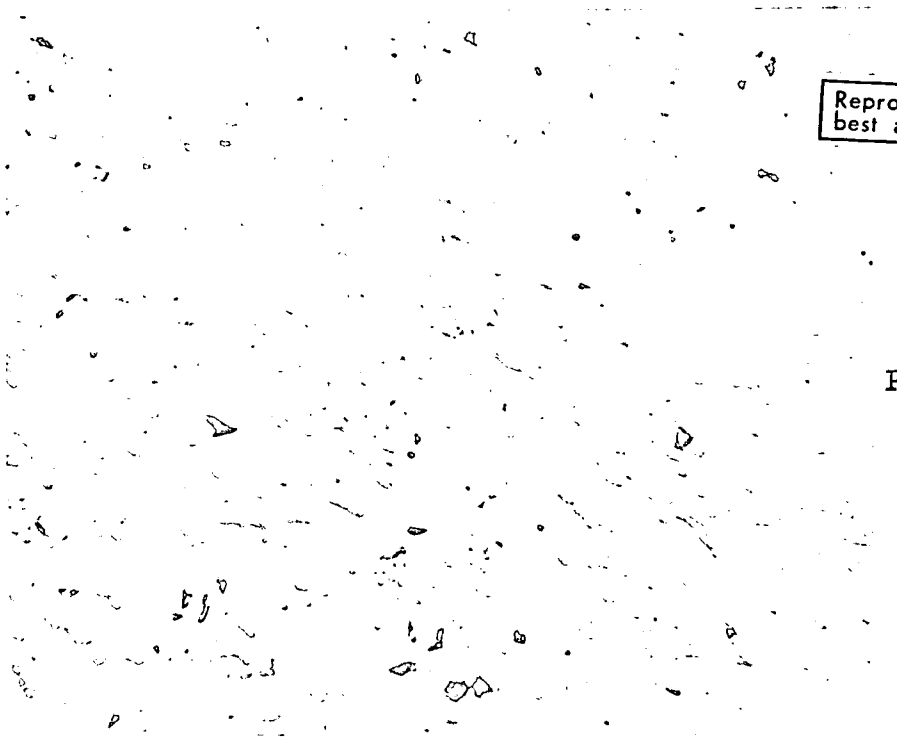

Plate No. 6175

As Polished 500X

Figure 21. Microstructural Features of Material V Matrix in Graphite Reinforced Material V, HP80.

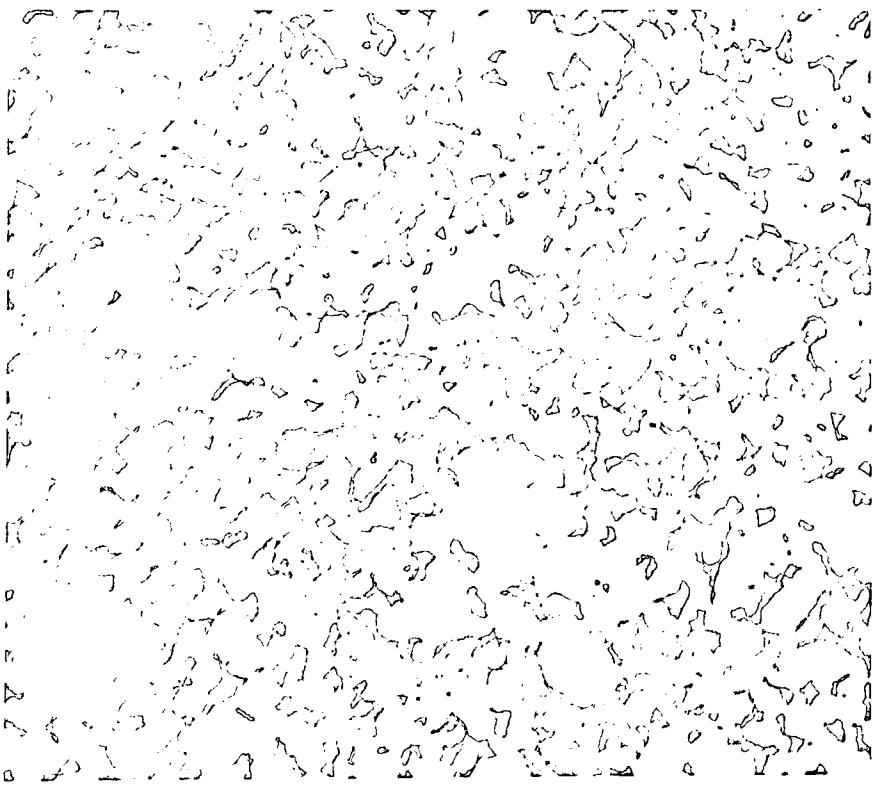

Plate No. 5930

UnEtched X500

Figure 22. Microstructural Characteristics of Boride VIII ($56^{v}/oZrB_2$-$14^{v}/oSiC$-$30^{v}/oC$) Carbon added in the form of 50Å-200Å particles which tend to agglomerate during mixing and hot pressing.

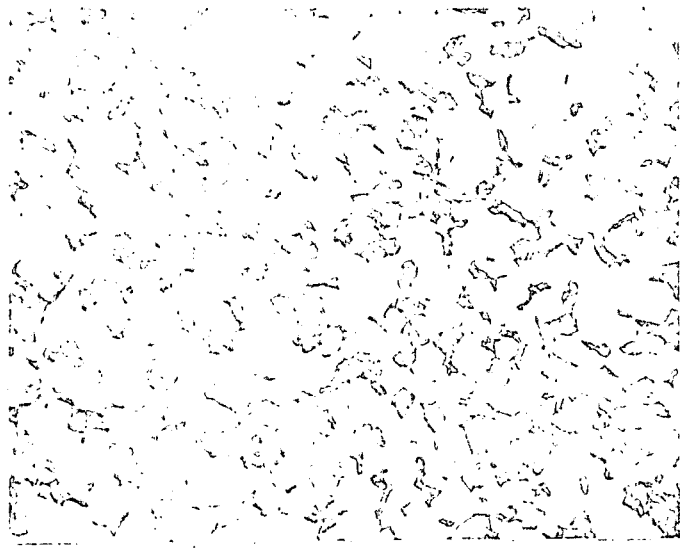

Unetched X500

Plate No. 6168

HP70, Parallel

Unetched X500

Plate No. 6169

HP70, Perpendicular

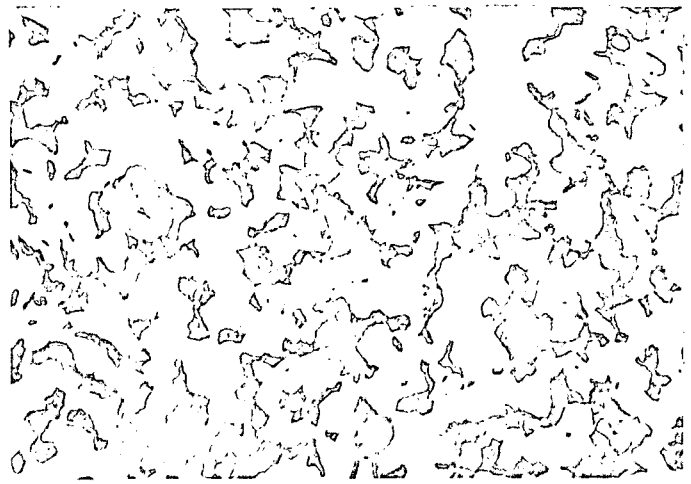

Unetched X500

Plate No. 6122

NP2M2, Parallel

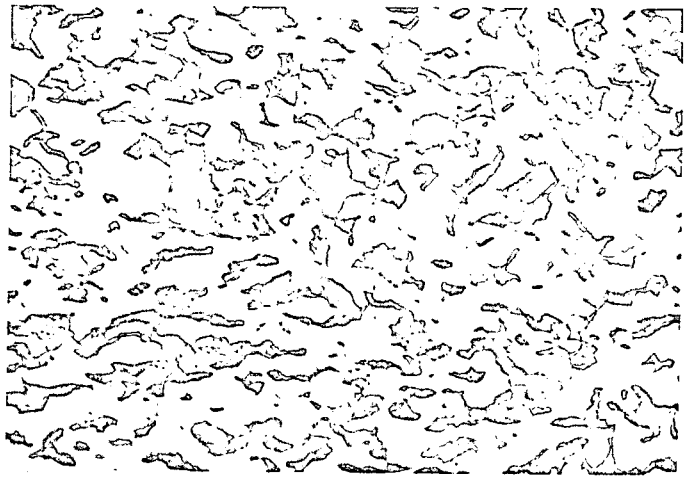

Unetched X500

Plate No. 6123

NP2M2, Perpendicular

Figure 23. Microstructural Features of Variations in Material VIII(14,30) M2 with Processing.

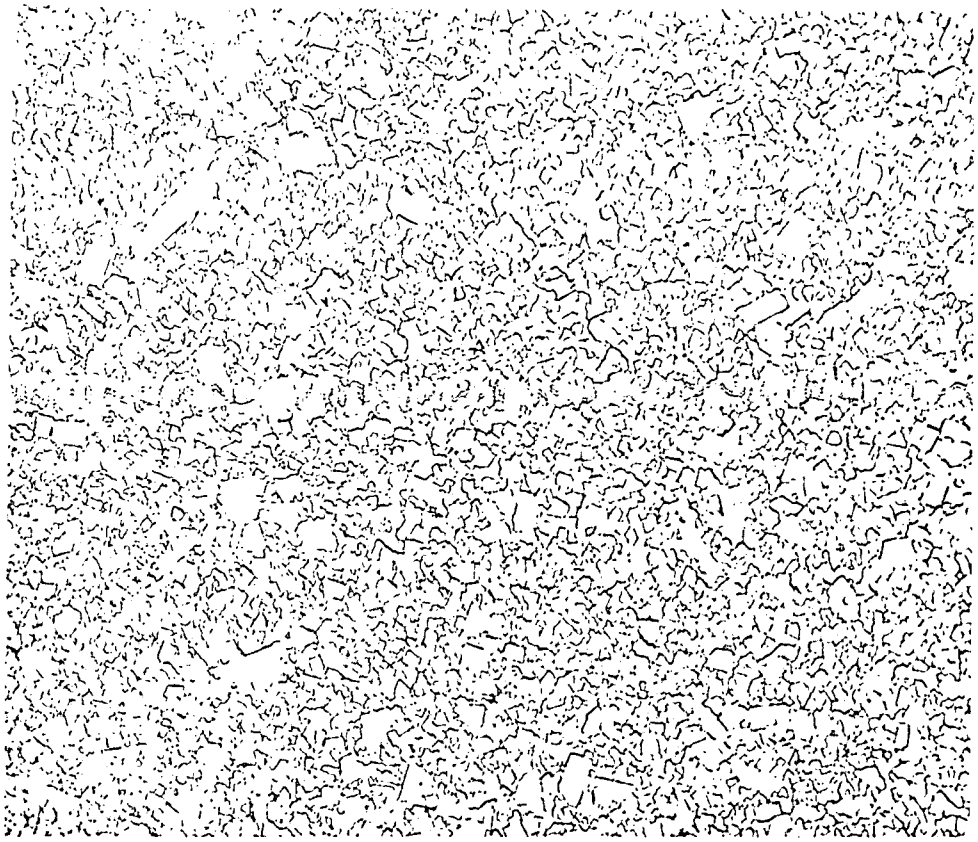

Plate No. 6176

Etched 1500X

Figure 24. Microstructural Features of Tungsten Carbide Cermet, WC6Co

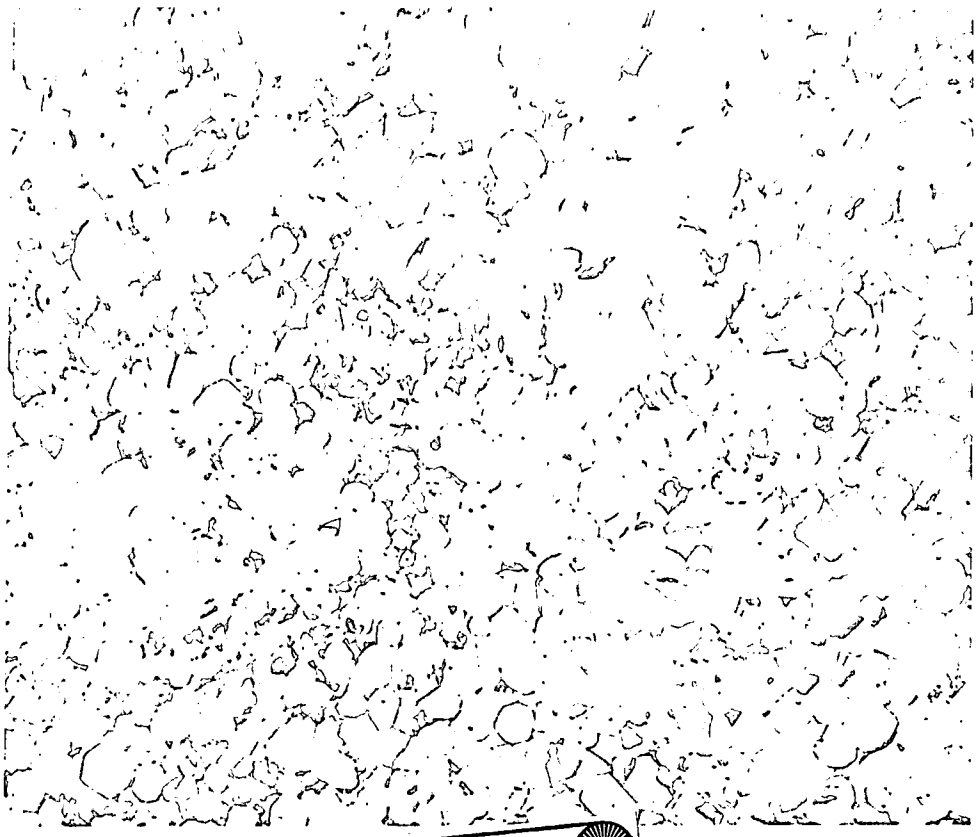

Plate No.
5773

As Polished

500X

Characterization Data:

Density:	5.29 g/cc
Strength:	36,500 psi at room temperature, 3 point bending
X-Ray Diffraction:	ZrB_2 identified, SiC absent, Ni absent, Ni B suggested
Electron Microprobe Analysis:	Ni containing phase at Zr containing pl.
Elemental distribution scan:	no positive identification of Ni-Si phase, some indication of Zr-Si phase: grain boundary phase probably below detection limit
Point counting:	White phase rich in Zr Grain boundary phase contains Si and Ni Grey phase rich in Si

Figure 25. Microstructural Features and Characterization Data for Hot Pressed Material V-Ni Compositions, HP25

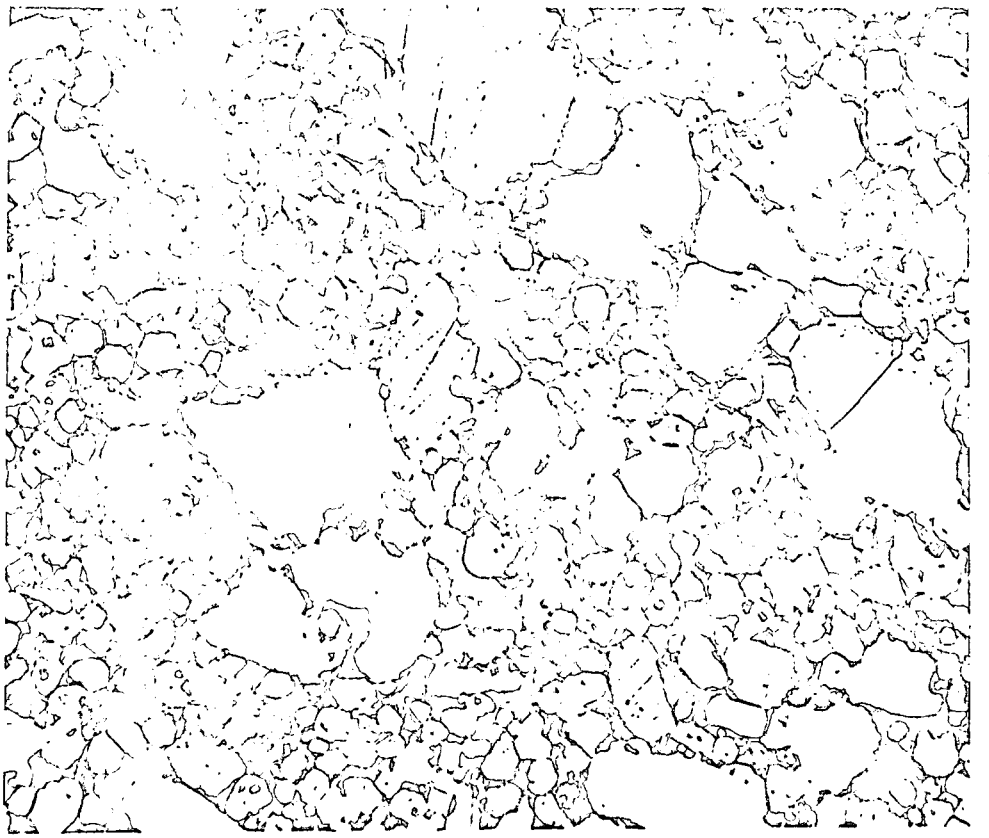

Plate No.
5899

Etched 500X

Characterization Data:

Density:	5.32 g/cc
Strength:	35,000 psi at room temperature, 3 point loading
X-ray Diffraction:	ZrB_2 identified, SiC absent, Ni absent,
	Extra lines same as HP25 but of weaker intensity

Figure 26. Microstructural Features and Characterization Data for Hot Pressed Material V-Ni Compositions, HP34

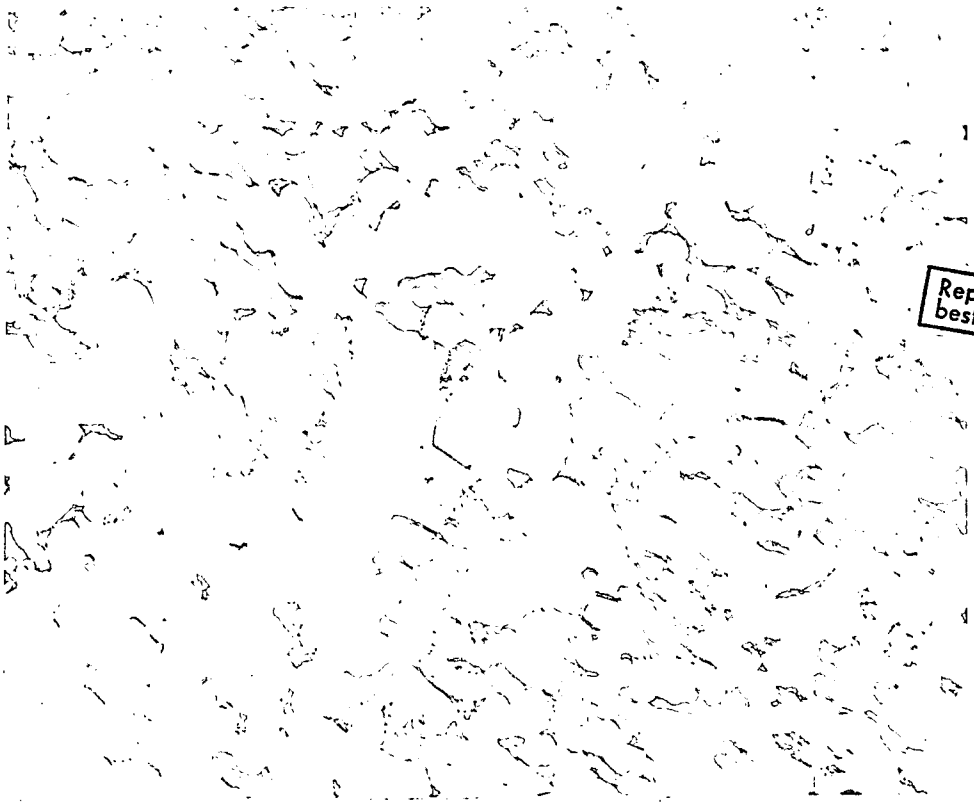

Plate No.
6136

As Polished 500X

Characterization Data:

Density:	4.93 g/cc
Electron Microprobe Analysis:	Scanning display technique: Areas deficient in Zr are rich in either Si or Ni or both.

Figure 27. Microstructural Features and Characterization Data for Hot Pressed Material V-Ni Compositions, HP83

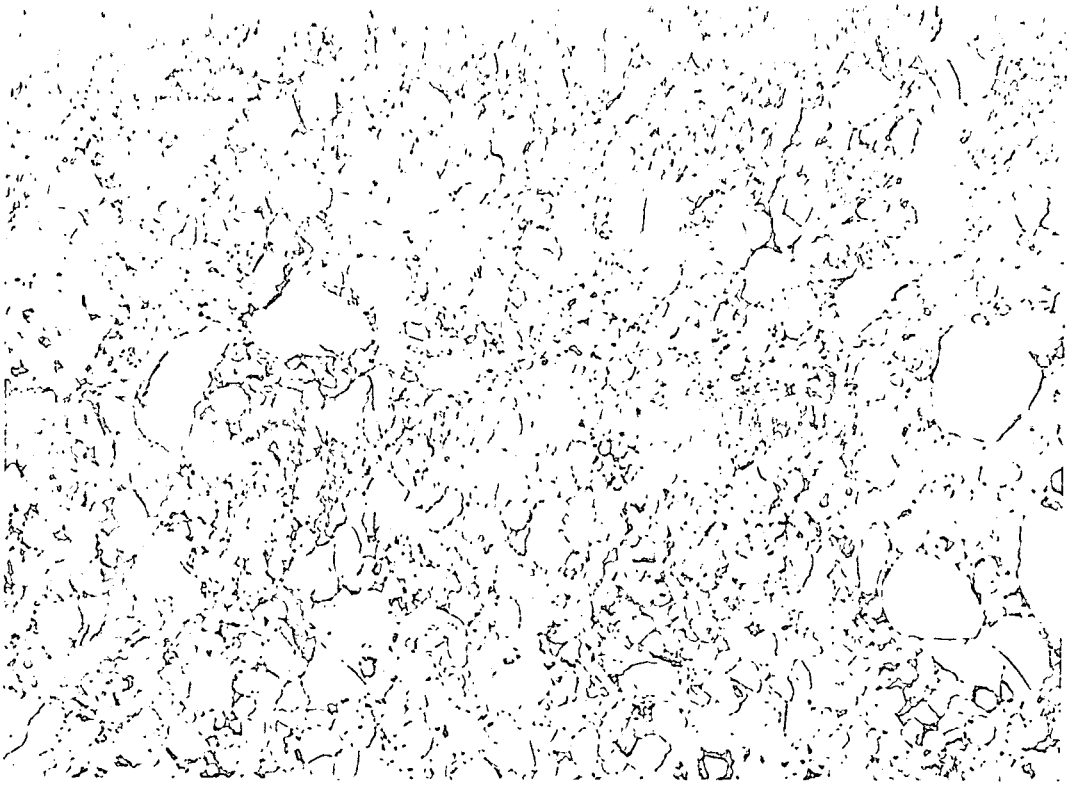

ManLabs
Plate No.
6221

Etched 500X

Figure 28. Microstructural Features of ZrB_2-Ni Composition Processed at 2420°F Maximum, HP90

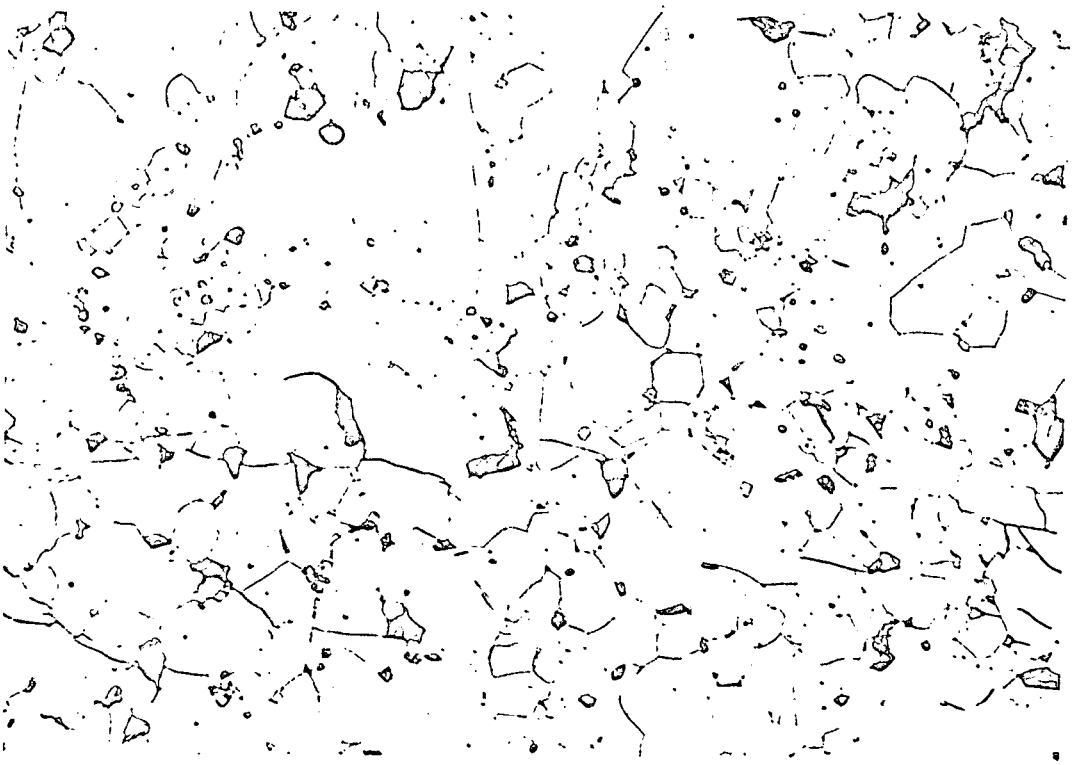

ManLabs
Plate No.
6189

Etched 500X

Figure 29. Microstructural Features of ZrB_2-Ni Composition Processed at 3020°F Maximum, HP88

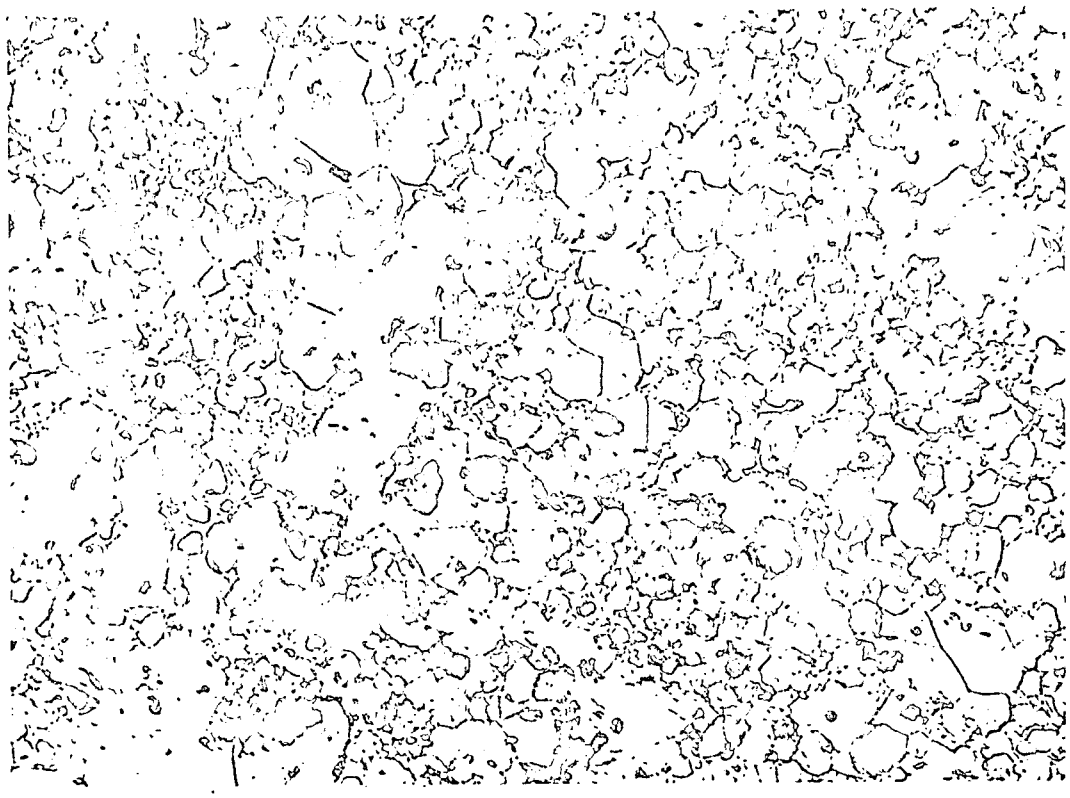

Plate No.
6278

Etched X500X

Figure 30. Microstructural Features of $ZrB_2$10Fe, HP101

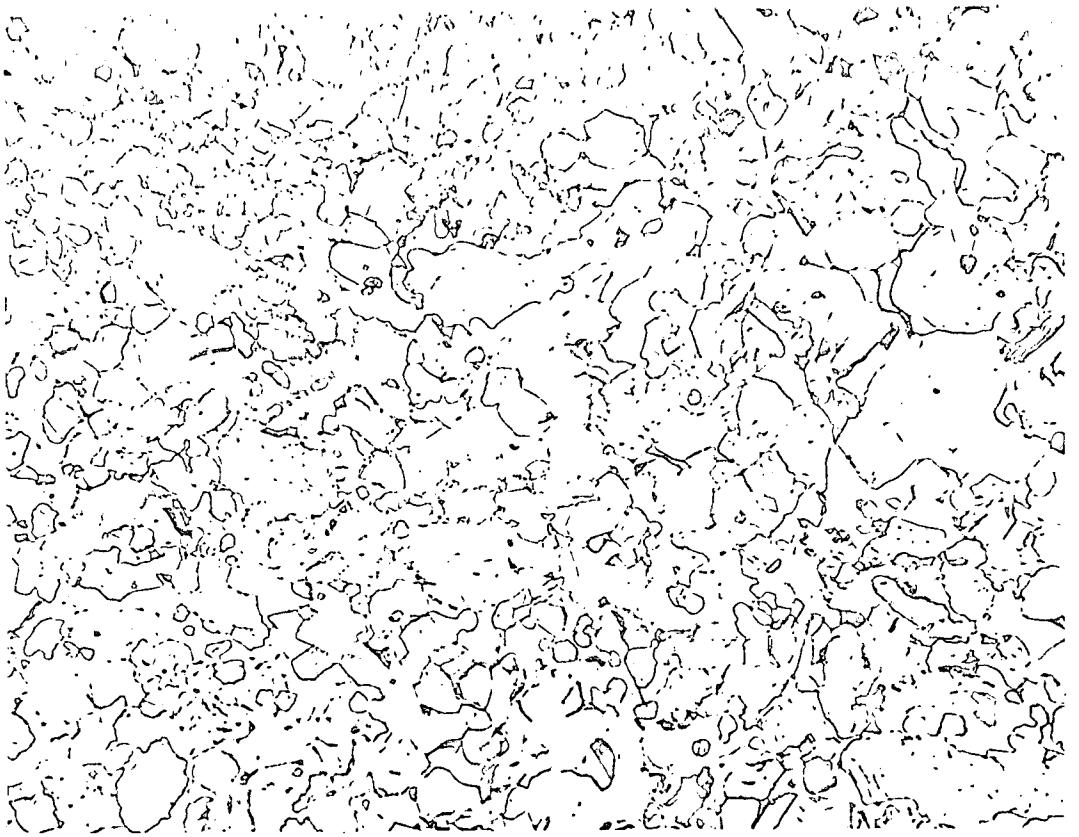

Plate No.
6272

Etched X500

Figure 31. Microstructural Features of $ZrB_2$10Cr, HP103

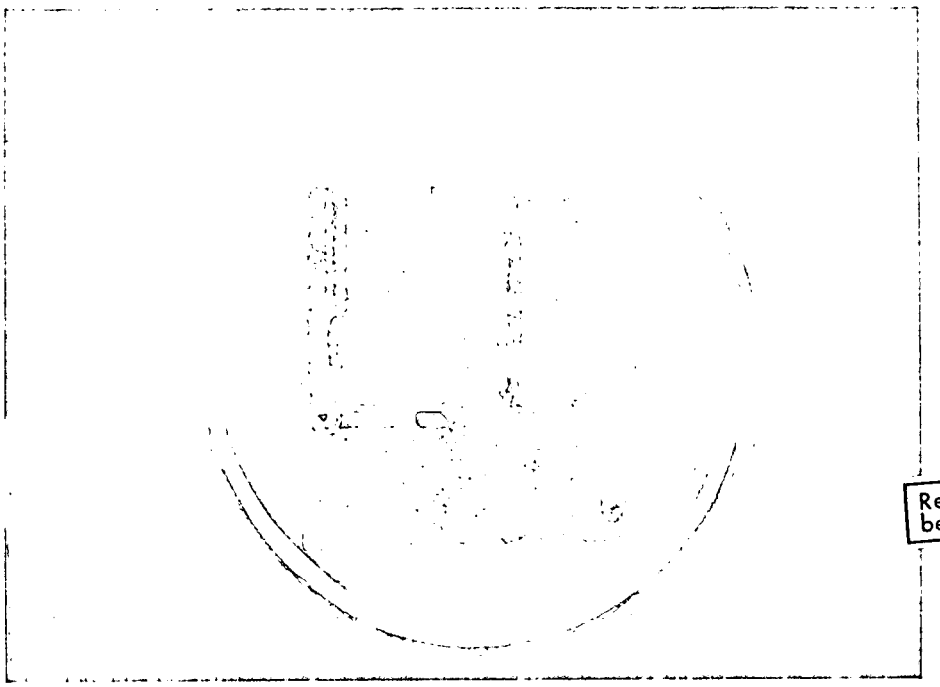

Plate No.
6275

As Polished 2.25X

Figure 32. Photomacrograph of Attempted Fabrication of Ta Reinforced $ZrB_2$20Ni, HP102

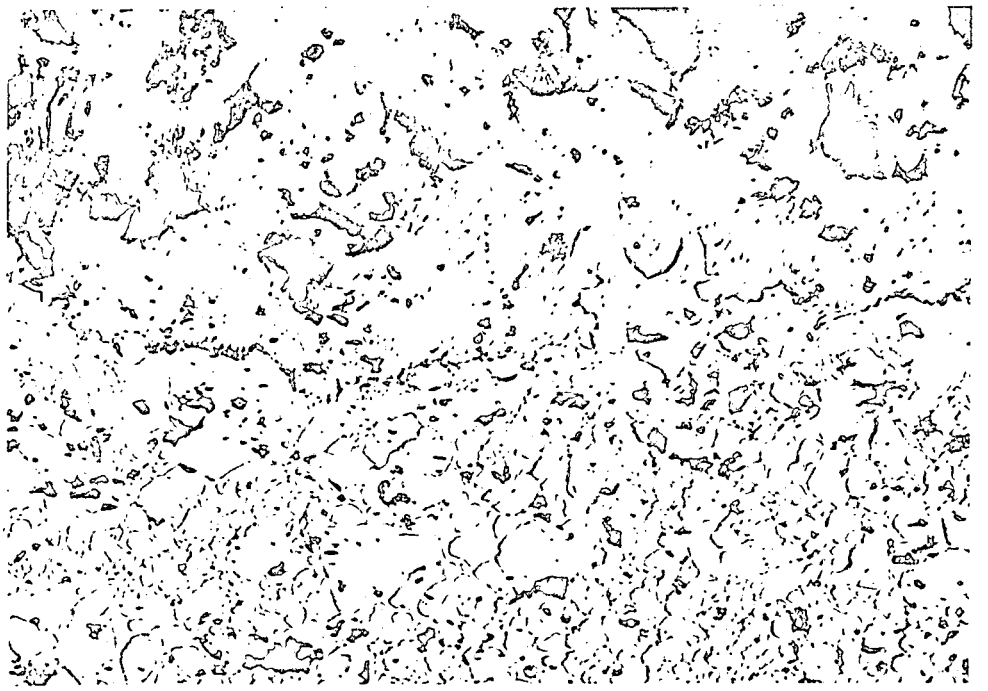

Plate No.
6277

As Polished 500X

Figure 33. Microstructural Features of Ta Wire and $ZrB_2$20Ni Matrix Interface (Longitudinal Direction), HP102

Plate No. 5832

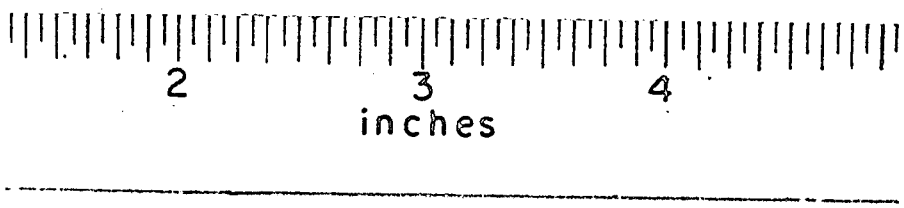

Figure 34. Photograph of Notched Charpy Bar with 0.077 inch (0.00196M) notch, interior angle 45°. Electrical Discharge Machined root radius equals 0.001 inches(2.54×10^{-5}M).

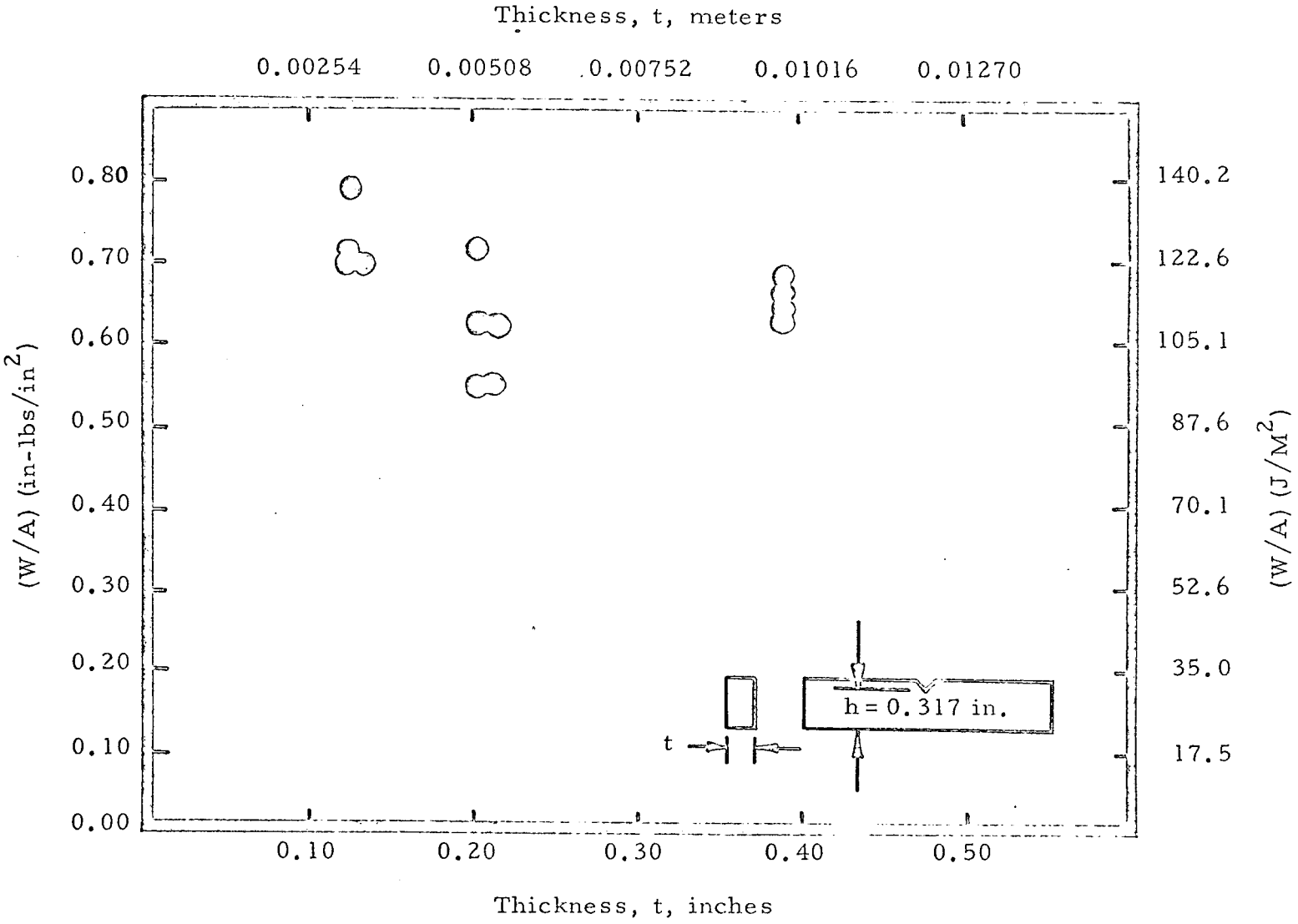

Figure 35. Variation of (W/A) with Sample thickness for Boride V (ZrB_2+SiC) (0.317 in = 0.00805M)

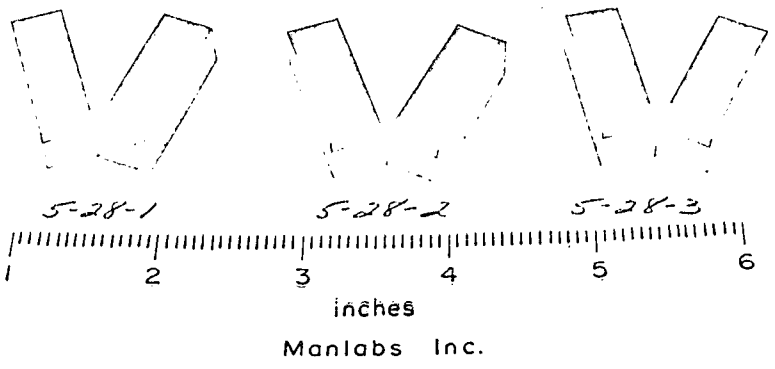

Plate No. 6076

NOT REPRODUCIBLE

Figure 36. Photograph of Boride V ($80^{v}/oZrB_2$-$20^{v}/oSiC$) Notched Charpy Bars run to fracture in Slow Bend test. Thickness equals 0.394 inches (0.010M). Average maximum load, 25 lbs. (1000N): average (W/A) = 0.65 (in-lbs/in^2) = 114 (J/M^2).

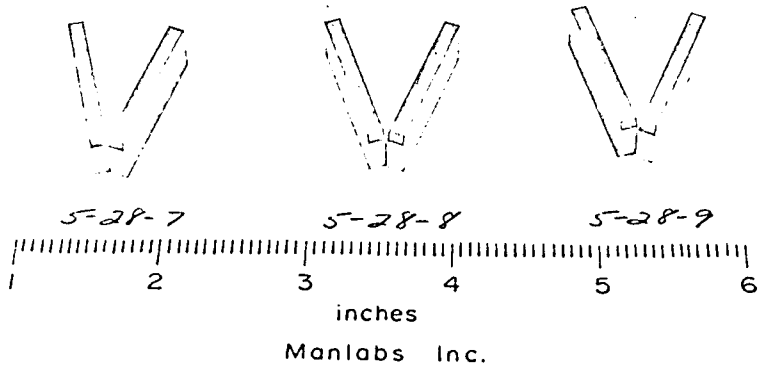

Plate No. 6078

Figure 37. Photograph of Notched Boride V ($80^{v}/oZrB_2$-$20^{v}/oSiC$) Charpy Bars run to fracture in Slow Bend test. Thickness equals 0.125 inches (0.00318M). Average maximum load, 68 lbs (302 N): average (W/A) = 0.72 (in-lbs/

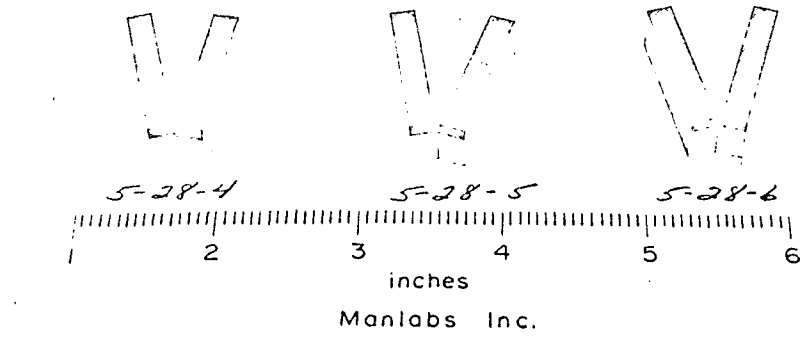

Plate No. 6077

Figure 38. Photograph of Boride V ($80^{v}/oZrB_2$-$20^{v}/oSiC$) Notched Charpy Bars run to fracture in Slow Bend test. Thickness equals 0.200 inches (0.00508M). Average maximum load, 110 lbs. (489N): average (W/A) = 0.61 (in-lbs/in^2) = 107 (J/M^2).

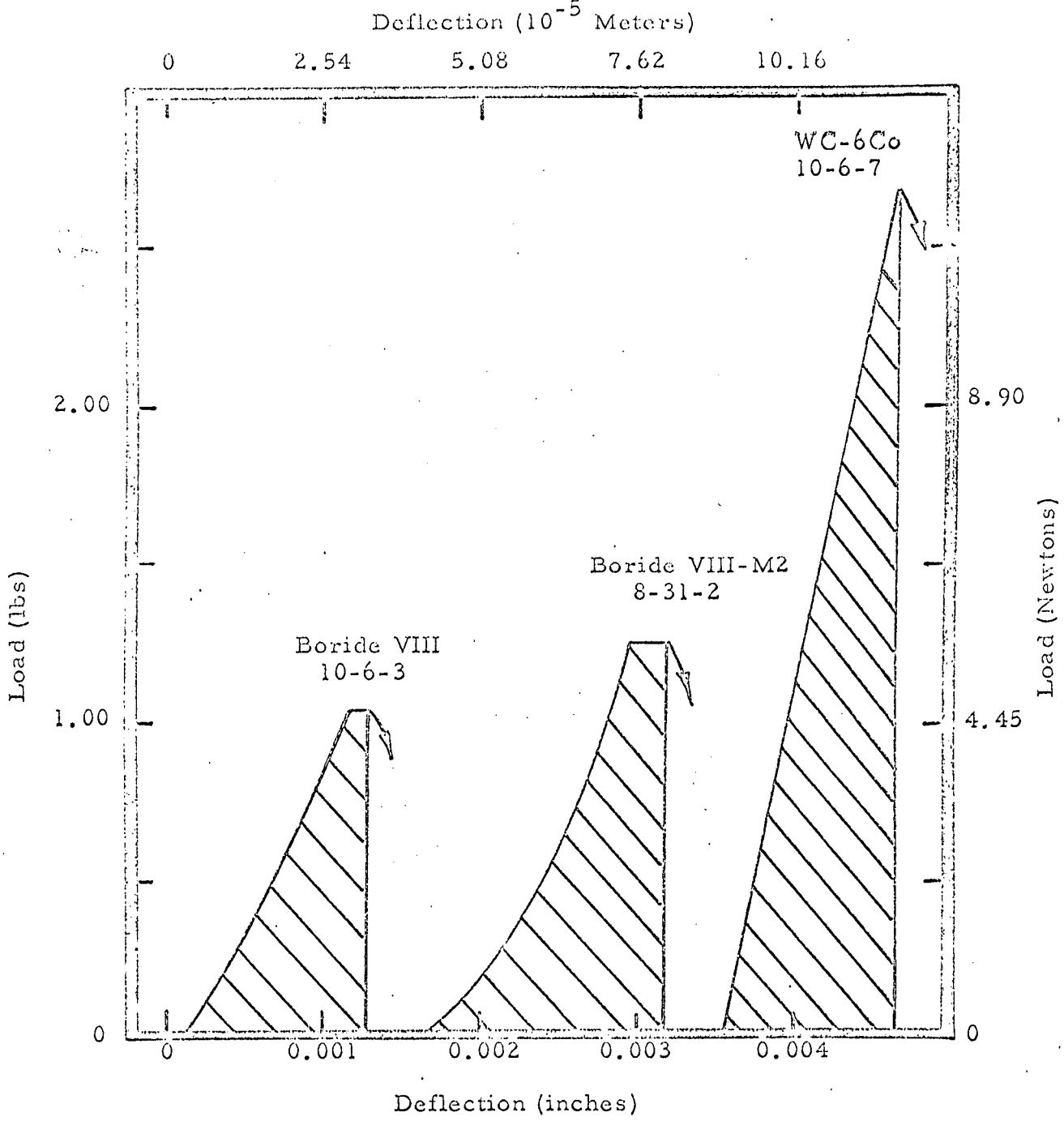

Figure 39. Typical Slow Bend Load-Deflection Curves for Notched Bars.

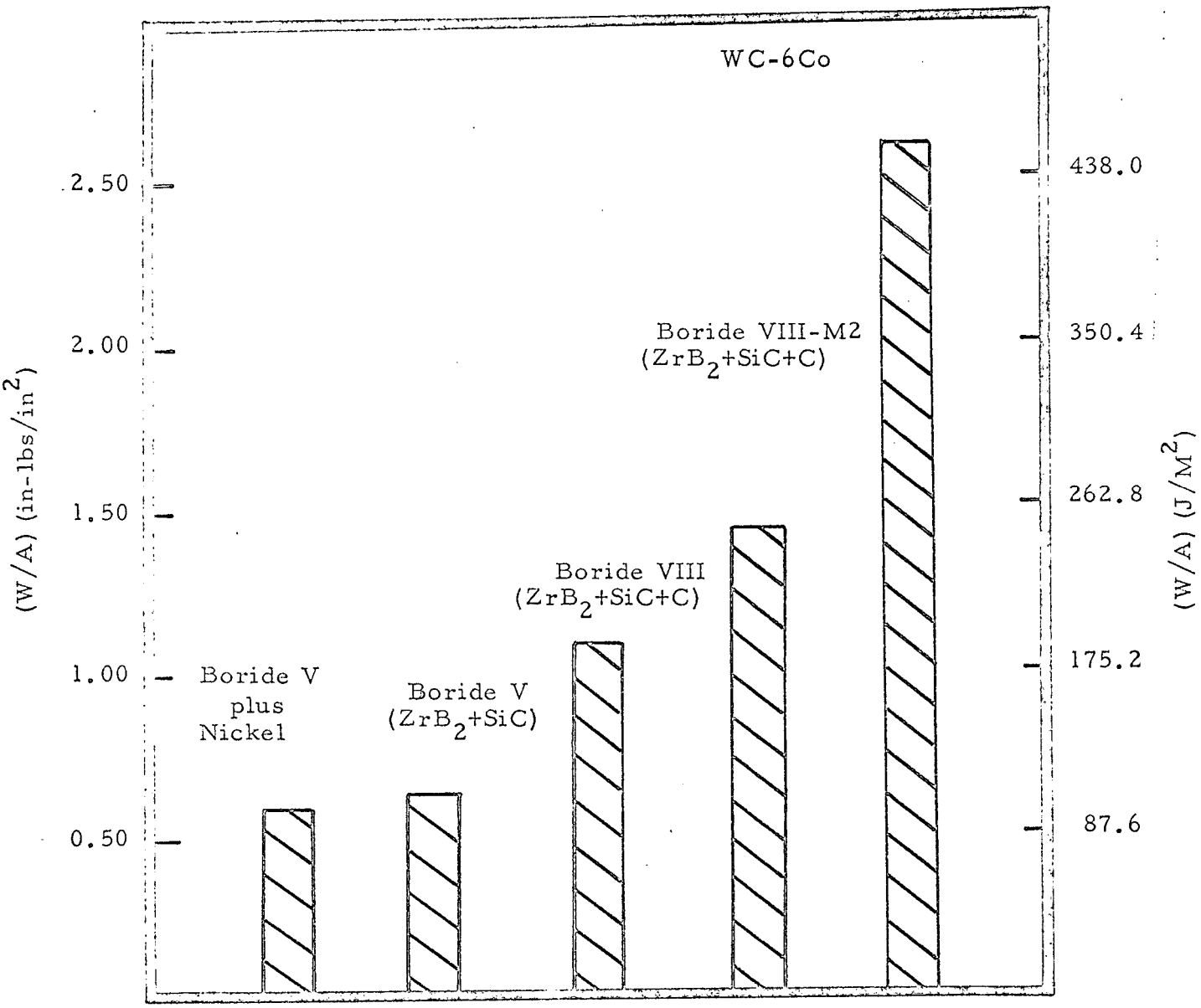

Figure 40. Average Values of (W/A) Determined from Slow Bend Tests of Notched Bars.

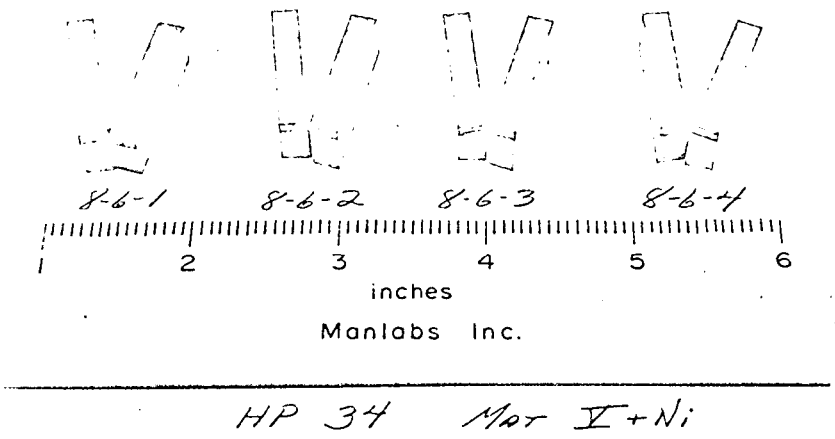

Plate No. 6081

Figure 41. Photograph of Boride V plus Ni ($70^{v}/oZrB_2$-$20^{v}/oSiC$-$10^{v}/oNi$) Notched Charpy Bars run to fracture in Slow Bend test. Thickness equals 0.200 inches, (5.11×10^{-3}M). Average maximum load, 77 lbs, (342N): average (W/A); 0.57 (in-lbs/in^2), (100J/M^2)

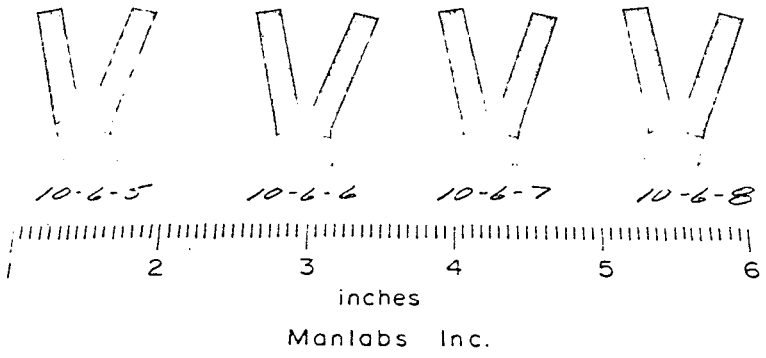

Plate No. 6079

Figure 42. Photograph of Boride VIII($56^{v}/oZrB_2$-$14^{v}/oSiC$-$30^{v}/oC$) Notched Charpy Bars run to fracture in Slow Bend test. Thickness equals 0.200 inches,(5.08×10^{-3}M). Average maximum load, 113 lbs, (503N): average (W/A), 1.07 (in-lbs/in^2),(187 J/M^2).

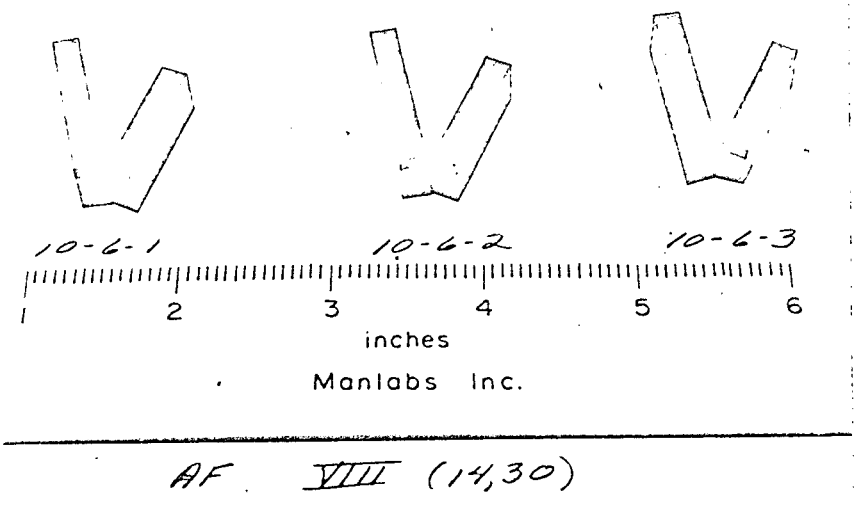

Plate No. 6080

Figure 43. Photograph of Tungsten Carbide plus $6^{w}/oCo$($90^{v}/oWC$-$10^{v}/oCo$) Notched Charpy Bars run to fracture in Slow Bend test. Thickness equals 0.200 inches,(5.08×10^{-3}M). Average maximum load, 269 lbs, (1197N):average (W/A), 2.51 (in-lbs/in^2),(440 J/M^2).

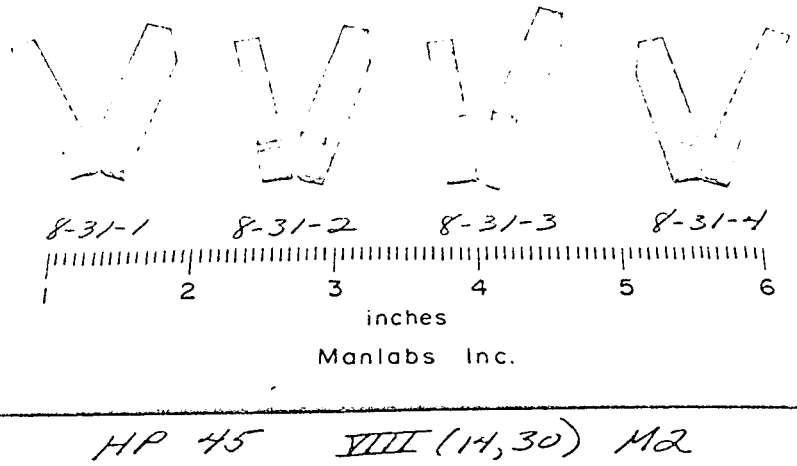

Plate No. 6082

Figure 44. Photograph of Boride VIII-M2 ($56^{v}/oZrB_2$-$14^{v}/oSiC$-$30^{v}/oC$) Notched Charpy Bars run to fracture in Slow Bend test. Thickness equals 0.200 inches,(5.08×10^{-3}M). Average maximum load, 128 lbs,(569N): average (W/A), 1.62 (in-lbs/in^2),(284J/M^2). Note stepped fracture surface.

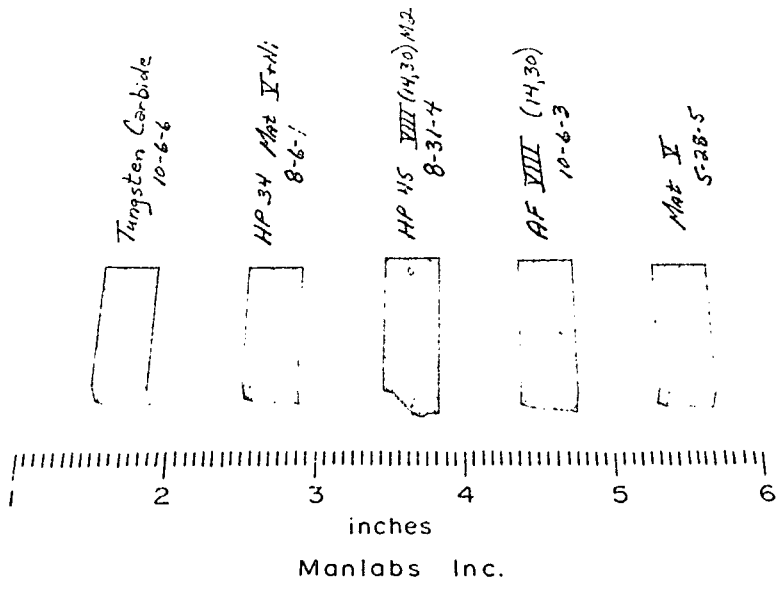

Plate No. 6083

Figure 45. Composite photograph of (from left to right): ($90^{v}/oWC$-$10^{v}/oCo$), ($70^{v}/oZrB_2$-$20^{v}/oSiC$-$10^{v}/oNi$), ($56^{v}/oZrB_2$-$14^{v}/oSiC$-$30^{v}/oC$) VIII-M2, ($56^{v}/oZrB_2$-$14^{v}/oSiC$-$30^{v}/oC$) VIII and ($80^{v}/oZrB_2$-$20^{v}/oSiC$)V. Note stepped fracture surface of Boride VIII-M2 composite as compared with smooth fracture surface of other bars.

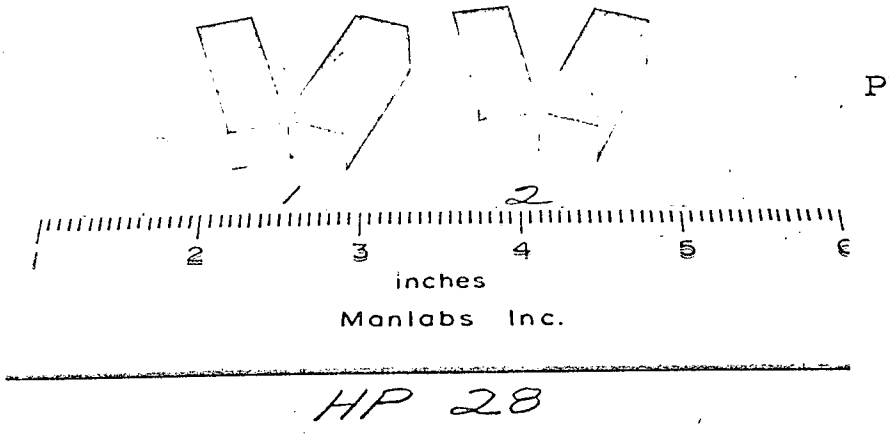

Figure 46. Photograph of Boride V (ZrB_2+20%SiC) Notched Charpy Bars run to fracture in Impact Test. Thickness equals 0.394 inches.

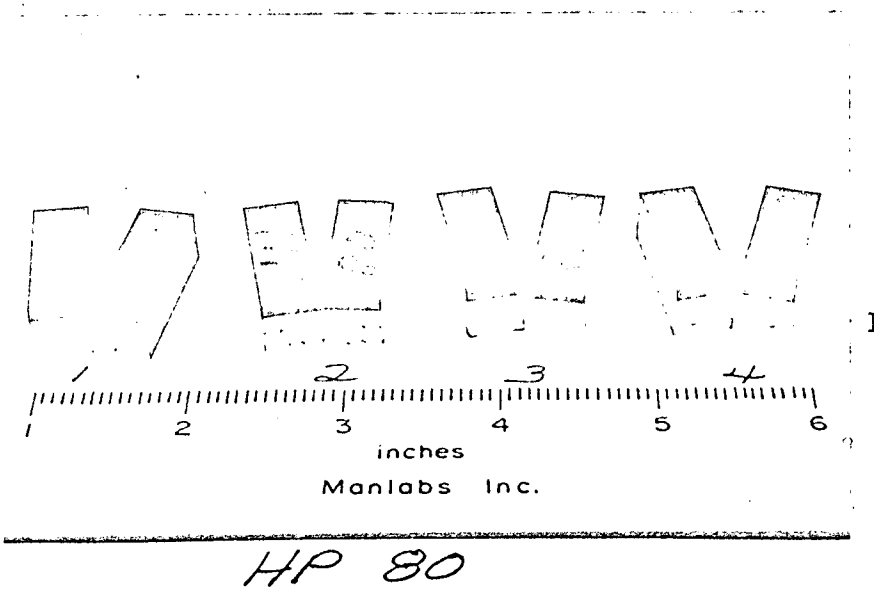

Figure 47. Photograph of Boride V reinforced with 1/8" layers of Graphite, Notched Charpy Bars run to fracture in Impact (1,2,3) and Slow Bend (4) Tests. Thickness equals 0.394 inches.

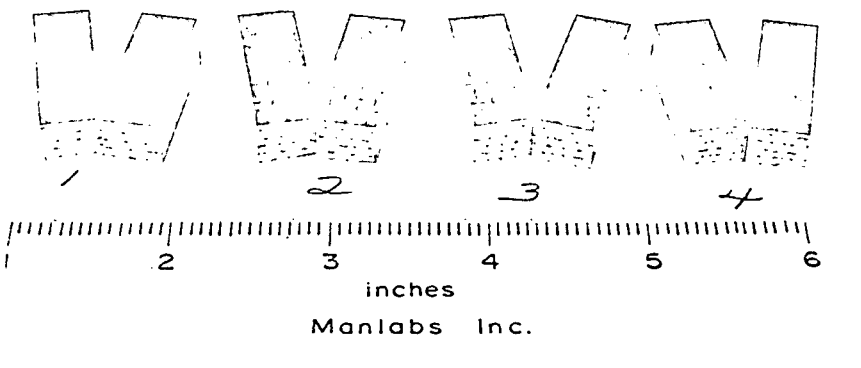

Plate No. 6163

HP 82

Figure 48. Photograph of Boride V reinforced with 1/16" layers of Graphite, Notched Charpy Bars run to fracture in Impact (1,2) and Slow Bend (3,4) Tests. Thickness equals 0.394 inches.

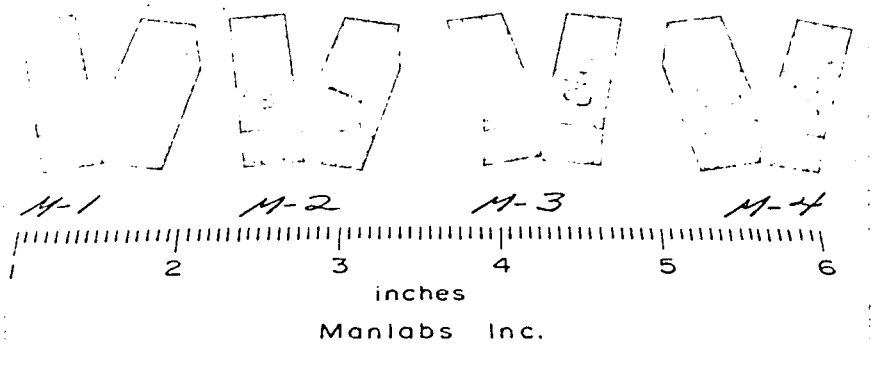

Plate No. 6159

D 201

Figure 49. Photograph of Boride VIII(14,30) Notched Charpy Bars run to fracture in Impact (1,2) and Slow Bend (3,4) Tests. Thickness equals 0.394".

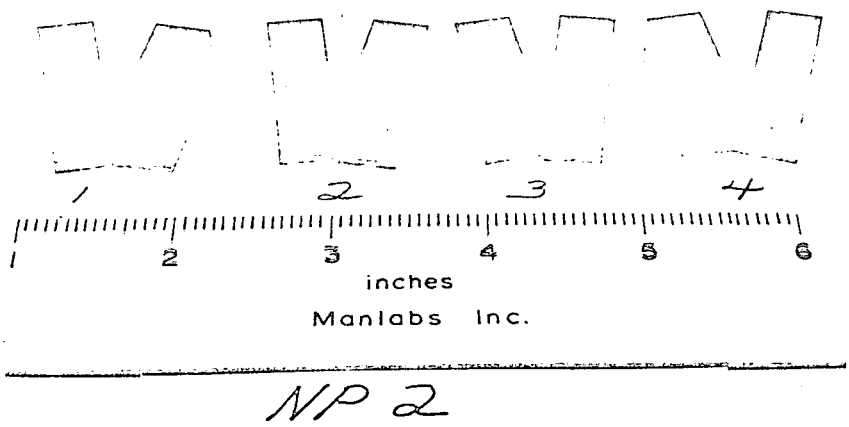

Figure 50. Photograph of Boride VIII(14,30)M2 Notched Charpy Bars run to fracture in Impact (1,2) and Slow Bend (3,4) Tests. Thickness equals 0.394 inches.

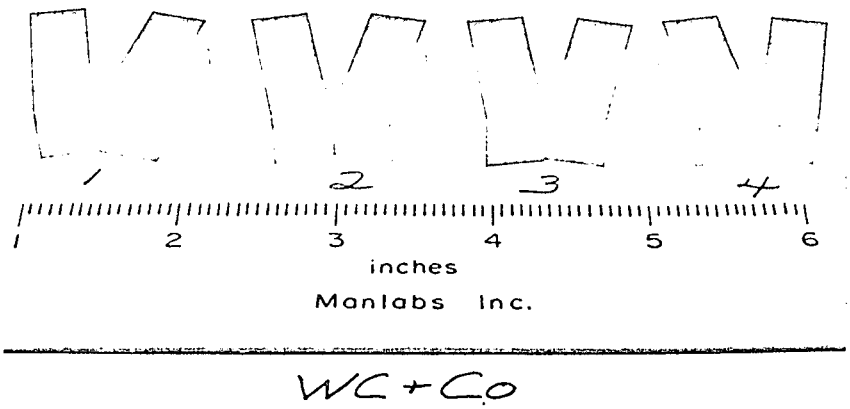

Figure 51. Photograph of Tungsten Carbide + $6^{W}/_{o}Co$ ($10^{V}/_{o}Co$) Notched Charpy Bars run to fracture in Impact (1,2,3) and Slow Bend (4) Tests. Thickness equals 0.394 inches.

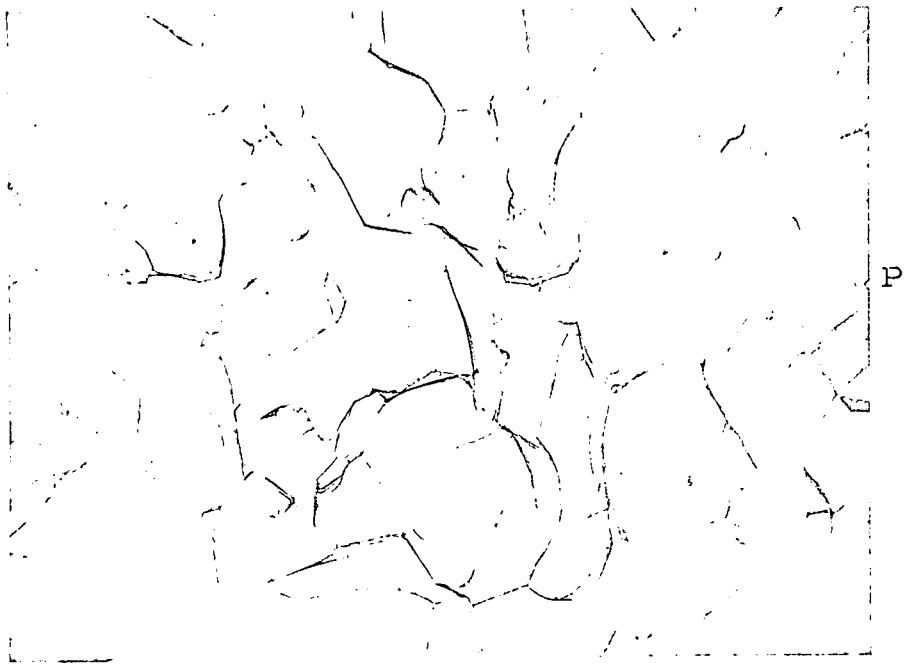

Plate No. 4210B

Two Stage Carbon replica shadowed with Chromium at 30°, Unetched X2750

Figure 52. Electron Fractograph of Boride V Sample 5-28-9 Fractured in Slow Bend Test. Note Smooth transgranular cleavage.

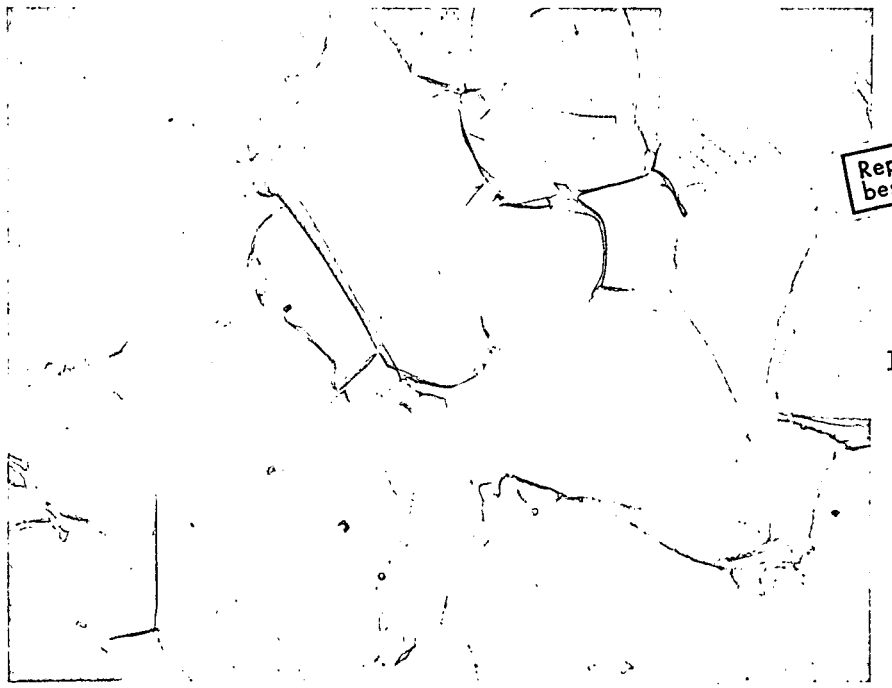

Plate No. 4210E

Two Stage Carbon replica shadowed with Chromium at 30°, Unetched X7750

Figure 53. Electron Fractograph of Boride V Sample 5-28-9 Fractured in Slow Bend Test. Note Smooth transgranular cleavage.

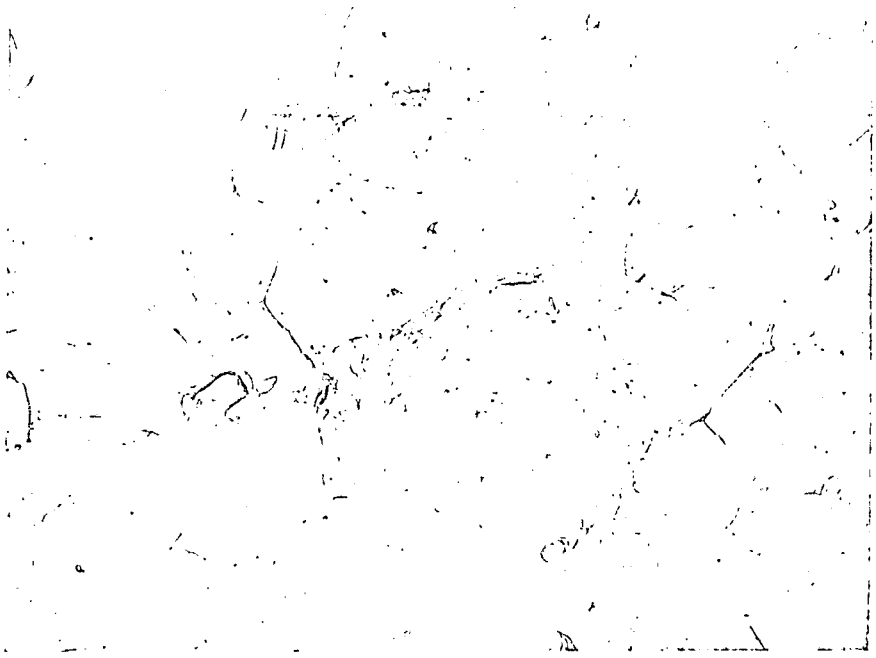

Plate No. 4262E

Two Stage Carbon Replica shadowed with Chromium at 30°, Unetched X2750

Figure 54. Electron Fractograph of Boride V Sample HP28-2 Fractured in Impact Test. Note Smooth transgranular cleavage.

Plate No. 4262C

Two Stage Carbon replica Shadowed with Chromium at 30°, Unetched X7750

Figure 55. Electron Fractograph of Boride V Sample HP28-2 Fractured in Impact test. Note smooth transgranular cleavage.

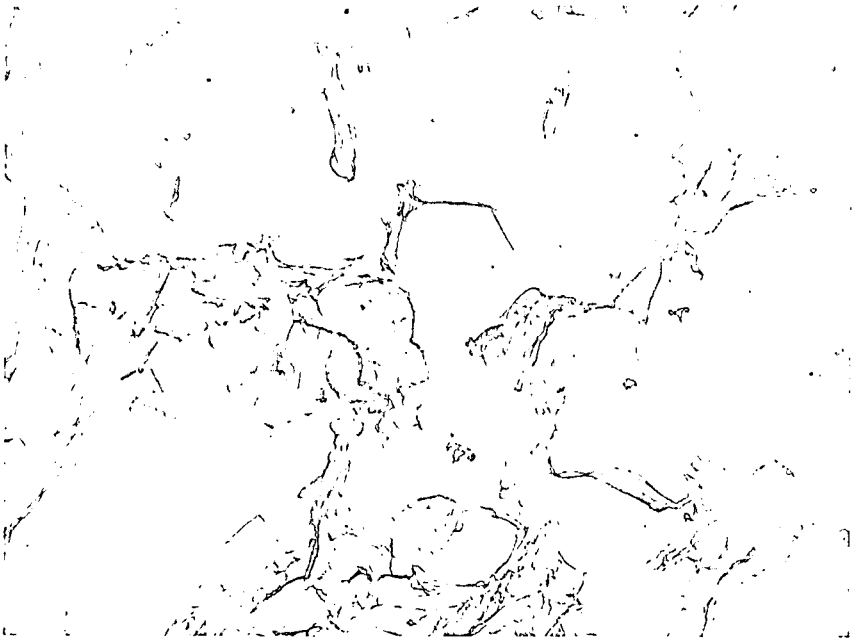

Plate No. 4211B

Two Stage Carbon replica shadowed with Chromium at 30°, Unetched X2750

Figure 56. Electron Fractograph of Boride V plus Nickel ($70^{v}/oZrB_2$-$20^{v}/oSiC$-$10^{v}/oNi$) Sample 8-6-3. Note relatively smooth intergranular surface cleavage.

Plate No. 4211C

Two Stage Carbon replica shadowed with Chromium at 30°, Unetched X7750

Figure 57. Electron Fractograph of Boride V plus Nickel ($70^{v}/oZrB_2$-$20^{v}/oSiC$-$10^{v}/oNi$) Sample 8-6-3. Note relatively smooth intergranular surface cleavage.

Plate No. 4268D

Two Stage Carbon replica shadowed with Chromium at 30°, Unetched X2750

Figure 58. Electron Fractograph of Boride V reinforced with 1/16" Graphite Layers Fractured in Slow Bend Test. Note Smooth Transgranular Cleavage. Sample HP82-3.

Plate No. 4268C

Two Stage Carbon replica shadowed with Chromium at 30°, Unetched X7750

Figure 59. Electron Fractograph of Boride V reinforced with 1/16" Graphite Layers Fractured in Slow Bend Test. Note Smooth Transgranular Cleavage. Sample HP82-3.

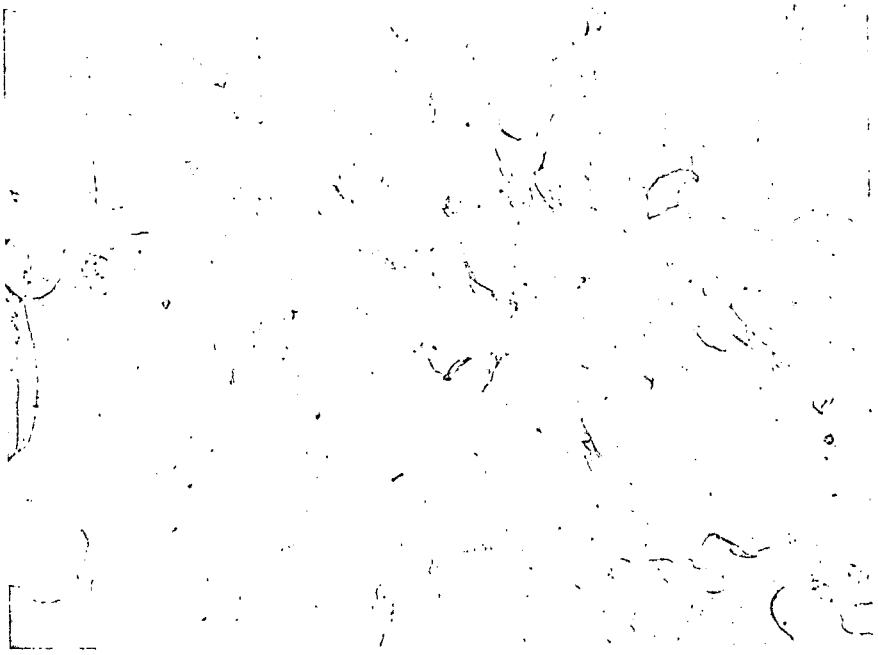

Plate No. 4266D

Two Stage Carbon replica shadowed with Chromium at 30°, Unetched X2750

Figure 60. Electron Fractograph of Boride V reinforced with 1/16" Graphite Layers, Fractured in Impact Test. Note Smooth transgranular Cleavage. Sample HP82-2.

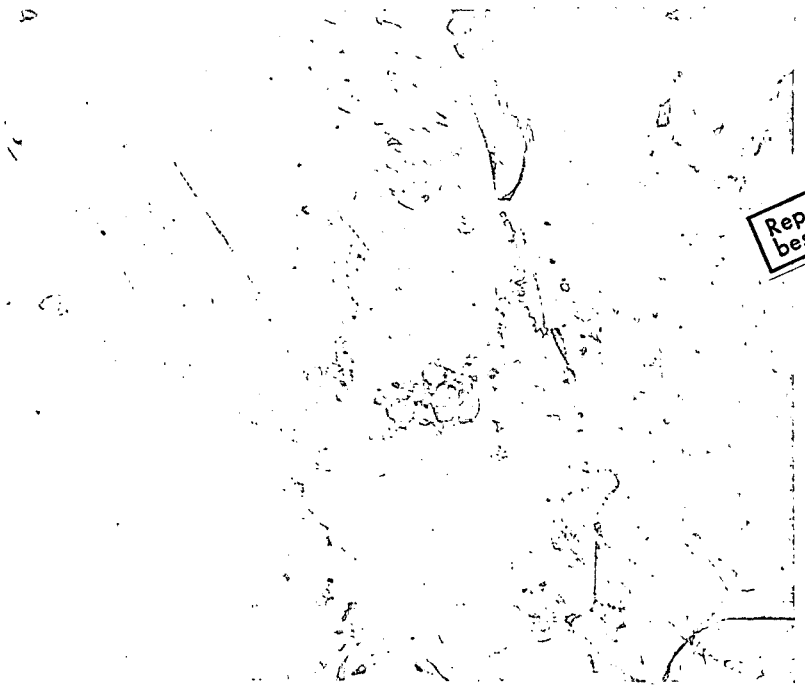

Plate No. 4266A

Two Stage Carbon replica shadowed with Chromium at 30°, Unetched X7750

Figure 61. Electron Fractograph of Boride V reinforced with 1/16" Graphite Layers Fractured in Impact Test. Note Smooth transgranular Cleavage. Sample HP82-2.

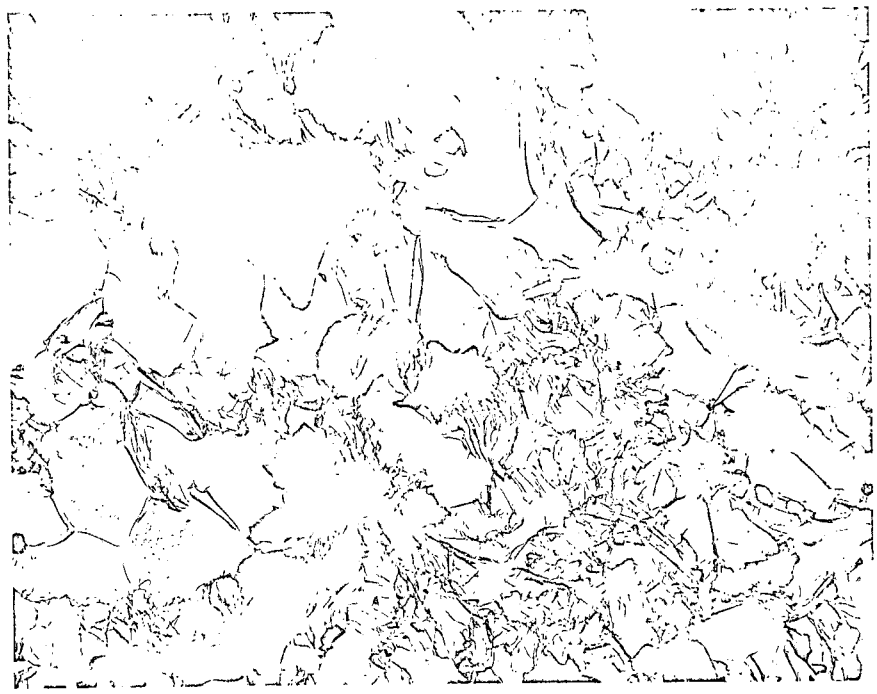

Plate No. 4260A

Two Stage Carbon replica shadowed with Chromium at 30°, Unetched X2750

Figure 62. Electron Fractograph of Boride VIII(14,30) Fractured in Slow Bend Test. Note rumpled quasi cleavage Surfaces. Sample D201M-3.

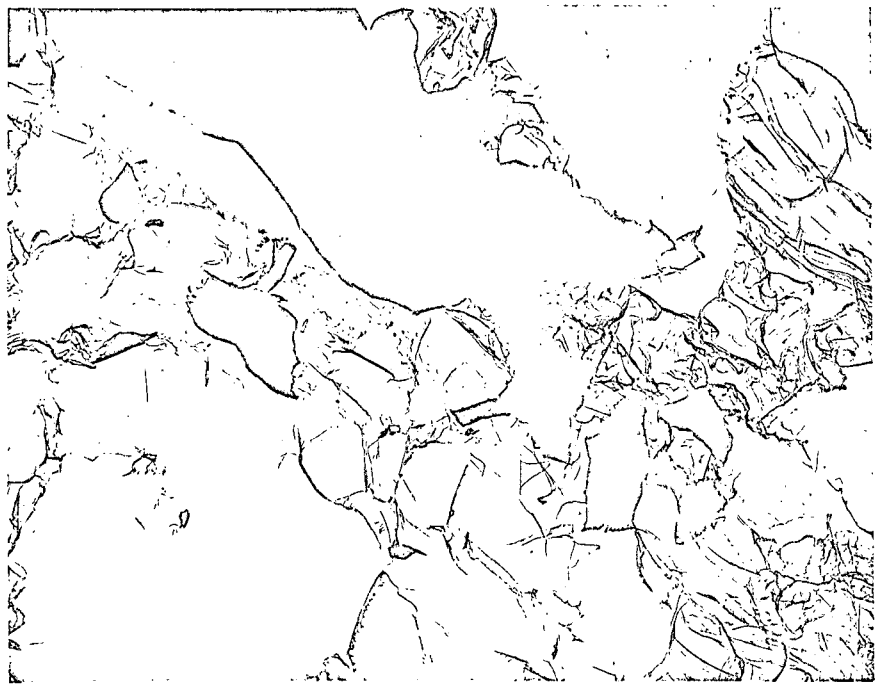

Plate No. 4260C

Two Stage Carbon replica shadowed with Chromium at 30°, Unetched X7750

Figure 63. Electron Fractograph of Boride VIII(14,30) Fractured in Slow Bend Test. Note rumpled quasi cleavage Surfaces. Sample D201M-3.

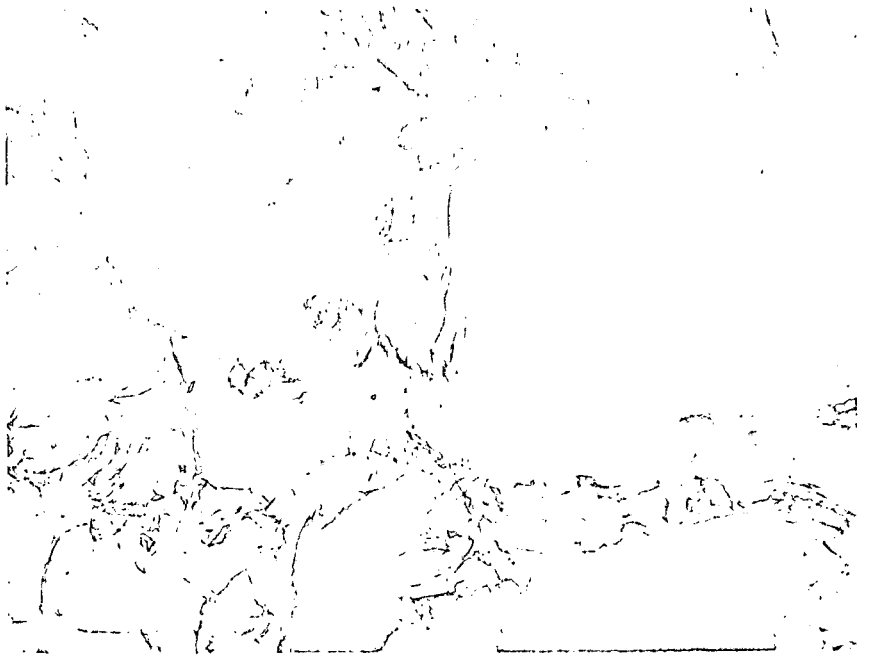

Plate No. 4263C

Two Stage Carbon replica shadowed with Chromium at 30°, Unetched X2750

Figure 64. Electron Fractograph of Boride VIII (14,30) Fractured in Impact Test. Note rumpled quasi cleavage Surfaces, Sample D201M-1.

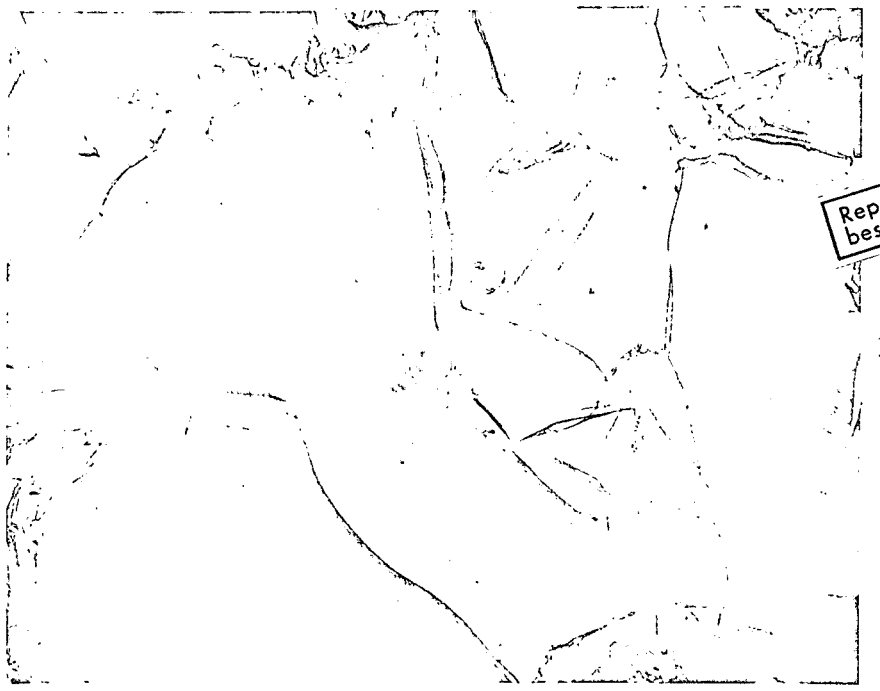

Plate No. 4263A

Two Stage Carbon replica shadowed with Chromium at 30°, Unetched X7750

Figure 65. Electron Fractograph of Boride VIII(14,30) Fractured in Impact Test. Note rumpled quasi cleavage Surfaces. Sample D201M-1.

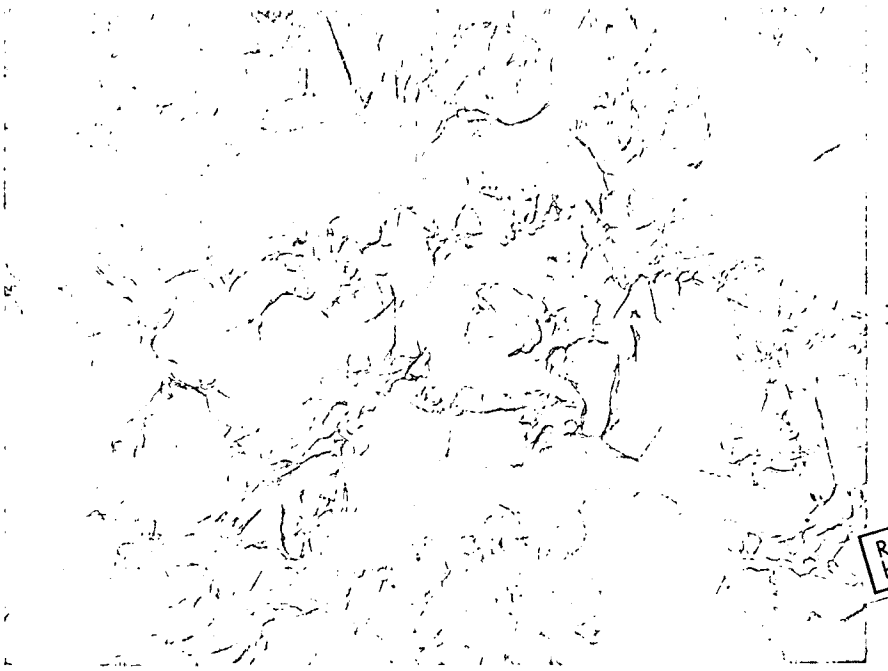

Plate No. 4218A

Two Stage Carbon replica shadowed with Chromium at 30°, Unetched X2750

Figure 66. Electron Fractograph of Boride VIII-M2 ($56^{v}/oZrB_2$-$14^{v}/o$ SiC -$30^{v}/oC$) Sample 8-31-3. Note rumpled quasi cleavage surfaces indicating irregular crack propagation.

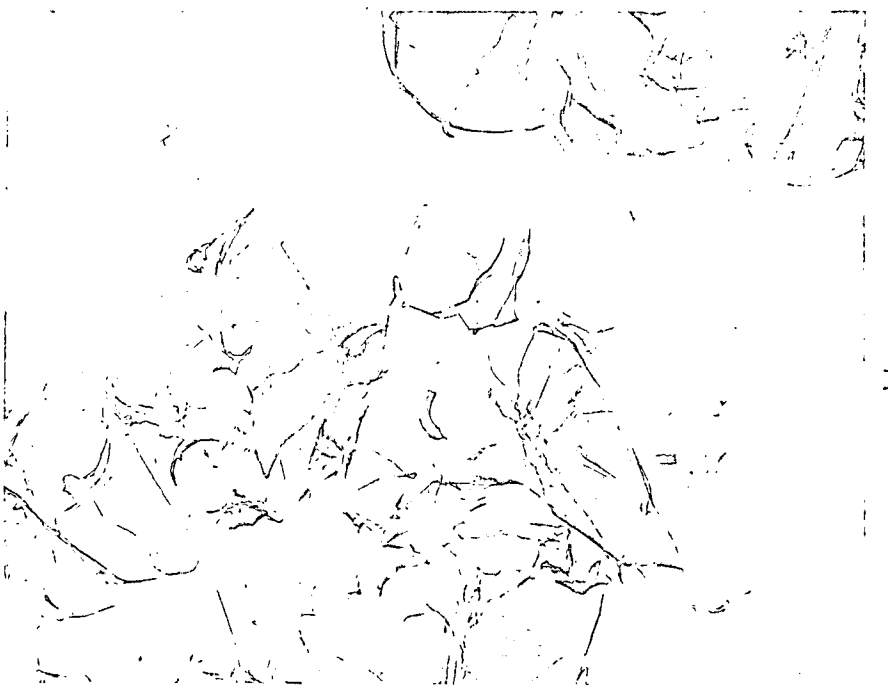

Plate No. 4218D

Two Stage Carbon replica shadowed with Chromium at 30°, unetched X7750

Figure 67. Electron Fractograph of Boride VIII-M2 ($56^{v}/oZrB_2$-$14^{v}/oSiC$ -$30^{v}/oC$) Sample 8-31-3. Note rumpled quasi cleavage surfaces indicating irregular crack propagation.

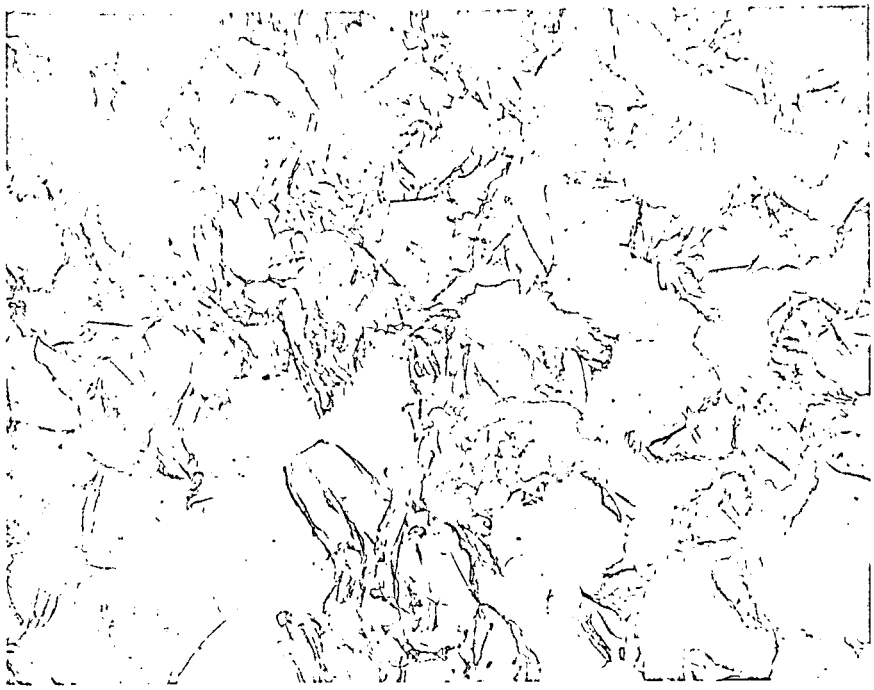

Plate No. 4264D

Two Stage Carbon replica shadowed with Chromium at 30°, Unetched X2750

Figure 68. Electron Fractograph of Boride VIII(14,30)M2 Fractured in Slow Bend Test. Note rumpled quasi cleavage Surfaces. Sample NP2-3.

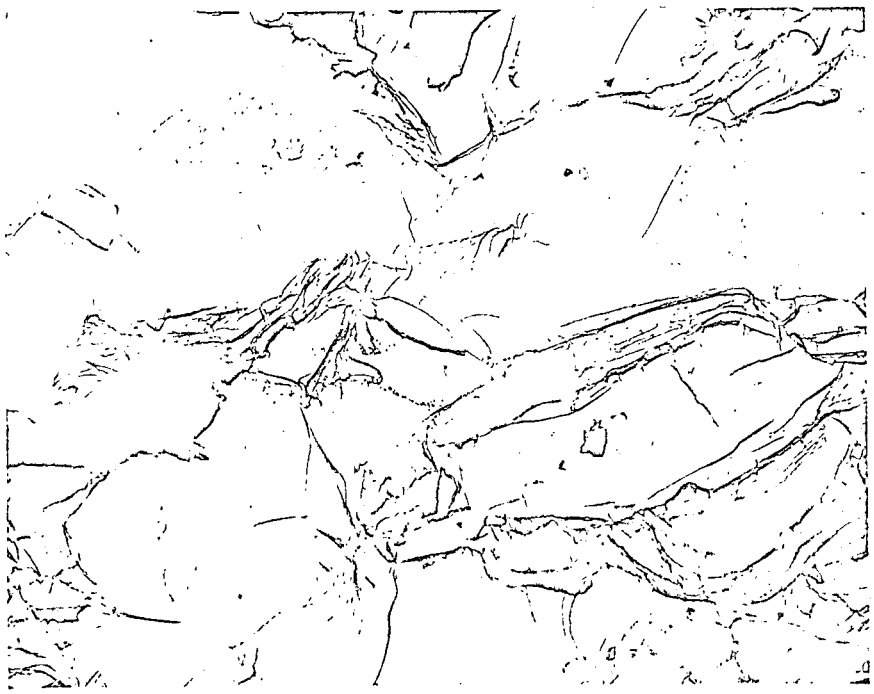

Plate No. 4264E

Two Stage Carbon replica shadowed with Chromium at 30°, Unetched X7750

Figure 69. Electron Fractograph of Boride VIII(14,30)M2 Fractured in Slow Bend Test. Note rumpled quasi cleavage Surfaces. Sample NP2-3.

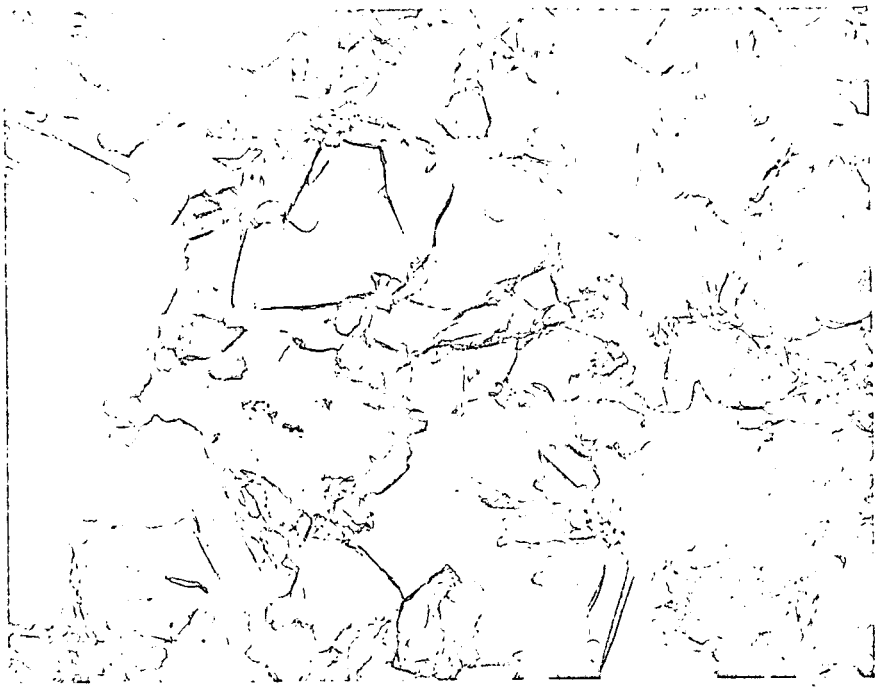

Plate No. 4260D

Two Stage Carbon replica shadowed with Chromium at 30°, Unetched X2750

Figure 70. Electron Fractograph of Boride VIII(14,30)M2 Fractured in Impact Test. Note rumpled quasi cleavage Surfaces. Sample NP2-2.

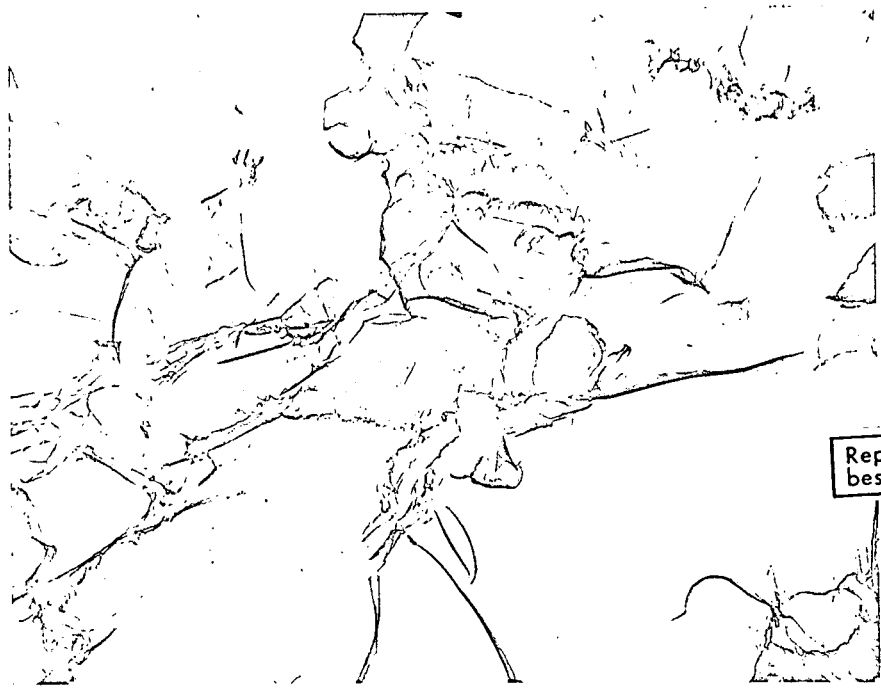

Plate No. 4260E

Two Stage Carbon replica shadowed with Chromium at 30°, Unetched X7750

Figure 71. Electron Fractograph of Boride VIII(14,30)M2 Fractured in Impact Test. Note rumpled quasi cleavage Surfaces. Sample NP2-2.

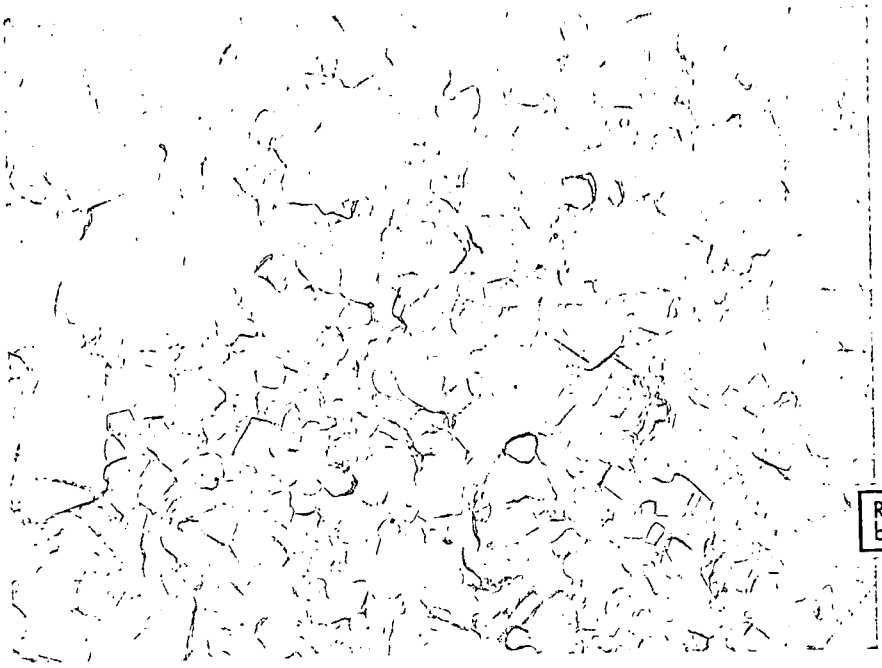

Plate No. 4215A

Two Stage Carbon replica shadowed with Chromium at 30°, Unetched X2750

Figure 72. Electron Fractograph of Tungsten Carbide + 6 $^{W}/_{o}$Co Fractured in Slow Bend Test. Note Smooth transgranular cleavage. Sample 10-6-5.

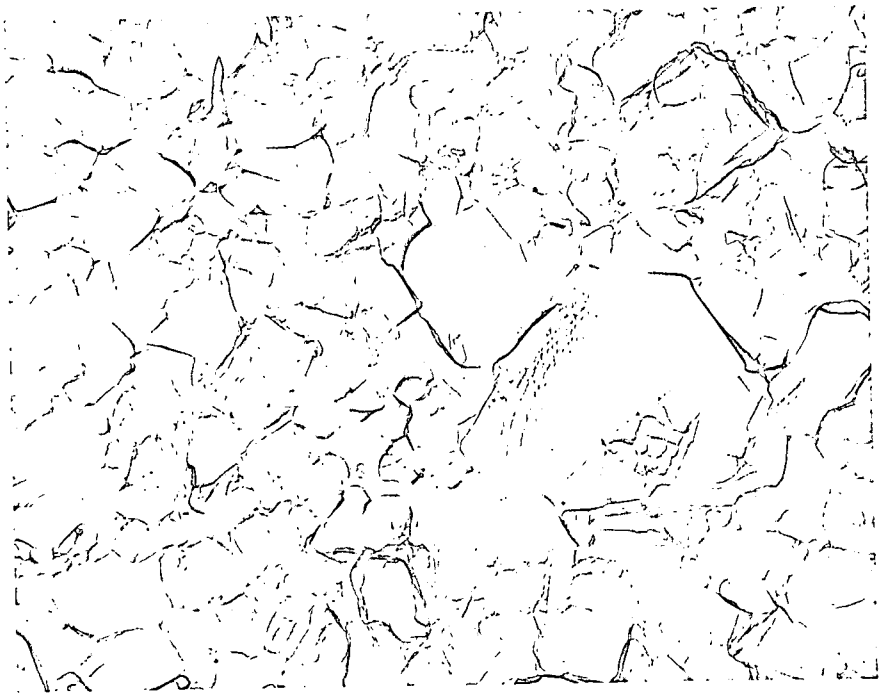

Plate No. 4215C

Two Stage Carbon replica shadowed with Chromium at 30°, Unetched X7750

Figure 73. Electron Fractograph of Tungsten Carbide + 6 $^{W}/_{o}$Co Fractured in Slow Bend Test. Note smooth transgranular cleavage. Sample 10-6-5.

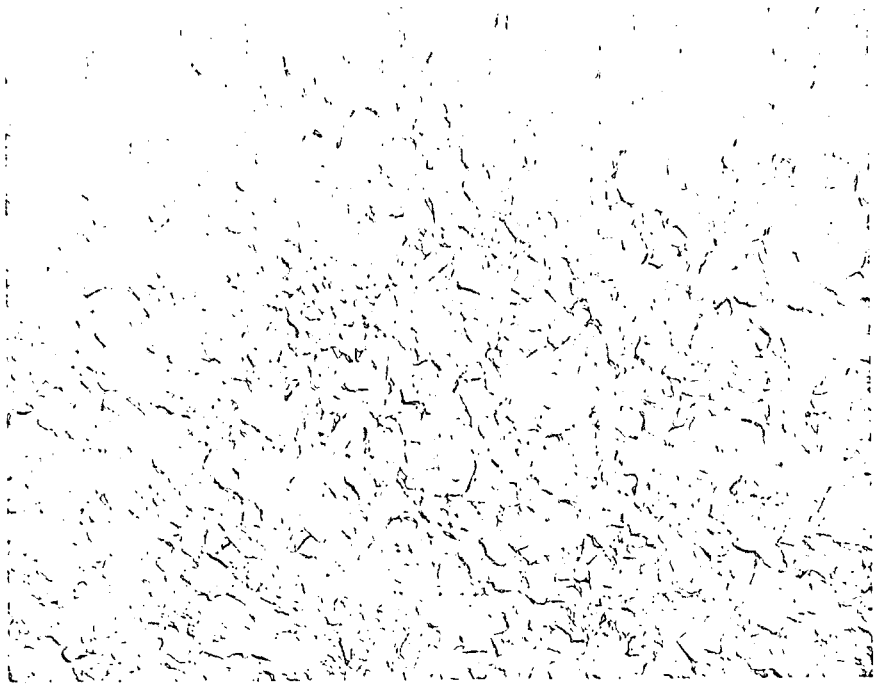

Plate No. 4261C

Two Stage Carbon replica shadowed with Chromium at 30°, Unetched X2750

Figure 74. Electron Fractograph of Tungsten Carbide + 6^{W}/oCo Fractured in Impact Test. Note intergranular failure and dimples on Surfaces. Sample WC-6Co-2.

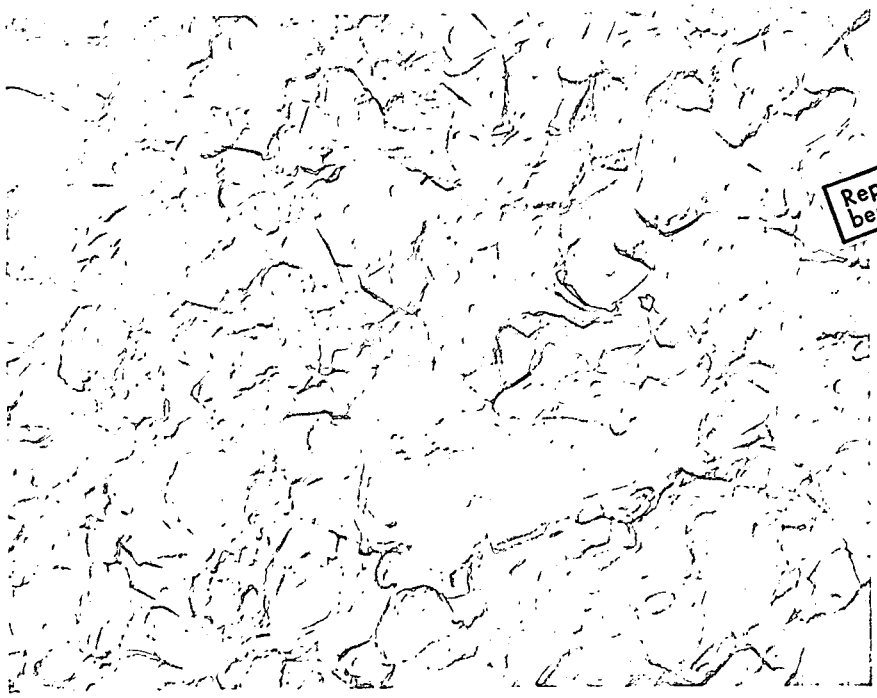

Plate No. 4261E

Two Stage Carbon replica shadowed with Chromium at 30°, Unetched X7750

Figure 75. Electron Fractograph of Tungsten Carbide + 6^{W}/oCo Fractured in Impact Test. Note intergranular failure and dimples on Surfaces. Sample WC-6Co-2.